NOTE TO USERS

Effect of Cryogenic Treatment on the Mechanical Properties of Steel and Aluminum Alloys

Saeed Zhirafar

A Thesis

in

The Department

of

Mechanical and Industrial Engineering

Presented in Partial Fulfillment of the Requirements
for the Degree of Master of Applied Science (Mechanical Engineering) at
Concordia University
Montreal, Quebec, Canada.

May 2005

Your file Votre référence
ISBN: 0-494-10278-0
Our file Notre référence
ISBN: 0-494-10278-0

ABSTRACT

Effect of Cryogenic Treatment on the Mechanical Properties of Steel and Aluminum Alloys

Saeed Zhirafar

This experimental program investigated the effects of cryogenic treatment on the mechanical properties and microstructures of AISI 4340 steel and aluminum alloy 7075. Mechanical tests including fatigue resistance, impact energy and hardness were carried out on both alloys, after they had undergone various heat treating conditions and the results were compared.

Experimental results showed that the hardness and fatigue resistance of the cryogenically treated 4340 steel, in general, were a little higher than those of the conventionally treated steel. However, the toughness of the cryogenically treated steel was lower when compared to that of the conventionally treated steel. The quantitative assessment of retained austenite using neutron diffraction technique was also explored. It is concluded that the transformation of retained austenite to martensite is the determining factor which improved hardness and fatigue resistance of the cryogenically treated 4340 steel. In aluminum alloy 7075, the results indicated that after cryogenic processing the fatigue resistance was lower than for conventionally solution and precipitation heat-treated samples. However, the hardness and toughness of the cryogenically treated samples were slightly higher in comparison to the conventional T6 treated specimens. The quantitative optical and electron microscopy has shown an increase in second phases after cryogenic treatment which was in agreement with x-ray diffraction results and electron dispersive spectroscopy (EDS).

ACKNOWLEDGEMENTS

The author wishes to express his gratitude and appreciation to his supervisor, Dr. Martin Pugh who provided guidance and encouragement throughout this research project. Special thanks go to Dr. H. Vali from McGill University who gave advice and access concerning secondary electron microscopy (SEM) for this work. The author acknowledges Dr. J. Root and Dr. R. Donaberger of the NRU reactor at Chalk River Laboratories, Ontario for helping in neutron diffraction tests. He would also grateful to Dr. F. Zarandian, A. Rezaean, F. Jalilian, Z. Albadavi and A. Zabiholla, for their helpful discussion and valuable comments during this research. Sincere thanks go to technical staff of the Department of Mechanical and Industrial Engineering, especially R. Oliver, J. Elliot and B. Cooper for their help in specimen fabrication and instrument preparation. Further, he would like to thank to secretaries of the Department, Charlene Wald and Sophie Merineau who were very kind and helpful in every aspect.

To my parents, I say thank you for your endless love and support.

TABLE OF CONTENTS

LIST OF FIGURES

LIST OF TABLES

Chapter 1. INTRODUCTION

1.1. Introducing AISI 4340 Steel and Aluminum alloy 7075

In this work, two well-known metallic alloys were investigated, which are introduced briefly as follows. AISI 4340 steel is one of the most popularly used steels for demanding applications. It has a combination of properties such as deep hardenability, good ductility and toughness, high strength, and high fatigue and creep resistance. It is often used in severe service applications and where high strength in heavy sections is required. Typical applications include bolts, screws, and other fasteners; gears, pinions, driveshafts, and similar machinery components; crankshafts and piston rods for engines; and landing gear and other critical structural members for aircraft. The 4340 steel products are available in the form of billets, bars, forgings, sheet, tubing, welding wire, light plate, and castings [1].

Aluminum alloy 7075 belongs to the 7xxx series of wrought aluminum alloys and has the highest strength in commercial heat treatable aluminum alloys and is also the strongest of the forging alloys. Furthermore, it has fair corrosion resistance. This alloy is in high demand by aircraft production companies for structural parts and also for other highly stressed applications [2].

1.2. Cryogenic Treatment

Ambient temperature mechanical property improvement of metals by different heat-treating techniques has been established for many years. The performance of well-known metals, regarding effective heat treatments, has been categorized in different handbooks. Cryogenic treatment of metals to develop their mechanical properties and wear characteristics is a relatively new engineering field. A little information about this treatment in tool steels has been reported but there is a dirth of information on how the technique operates and the degree of effectiveness of its application.

The idea of improving the properties of steel by exposure to low temperature is very old. Some industries have taken advantage of a subzero cold treatment for improving the serviceability of parts or tools for a long time. It is believed that old Swiss watchmakers were improving their watch components by burying them in snow during harsh winter temperatures. Toolmakers also stored the raw materials in freezer cabinets before using them for the same purpose [3]. However, because of the unpredictable behavior experienced by many when using this treatment and a lack of understanding in its working principle, it did not find a main place in the production line, unlike conventional heat treatments [4].

The cryogenic process typically involves slowly cooling a mass of parts to -196°C, holding them at this temperature for a period of time, and later tempering them. The idea for steels is to rid the structure of austenite, the soft, ductile phase in steels. Generally, the complete transformation from austenite to martensite is desired. Martensite resists plastic deformation much better than the austenitic structure.

The cryogenic treatment does not affect just the surface. It penetrates all the way through the mass of the item [5]. A wide range of improvements in industrial applications have been mentioned in a variety of non-academic reports and advertisements. Steels, aluminum, copper, carbides, and even plastics are reported to respond to cryogenic processing. However, tool steels seem to show particularly impressive property improvements from cryogenic processing [3]. Several investigators [6,7,8] have focused their attention on studying this process and trying to raise the efficiency of tool steels through cryogenics. More researchers [9,10] agree that the cryogenic treatment can improve the performance of tools. They found that the retained austenite of some tool steels transformed to martensite during this treatment.

There is very little information in the scientific literature regarding the understanding of the cryogenic effect on aluminum alloys and medium carbon steels such as AISI 4340. Therefore, this project was aimed at determining the mechanical properties and microstructural characteristics of aluminum alloy 7075 and 4340 steel after cryogenic processing.

Cryogenic treatment is not, as it is often mistaken for, a substitute for good heat treating. Rather it is a supplemental treatment that further improves performance. The immersion in liquid nitrogen might also help to overcome minor heat treating and tempering errors [5]. Even with the all potential benefits advertised, cryogenic processing is quite controversial. The fact that results of cryogenic applications are not always predictable is a major cause of arguments between scientists.

The National Aeronautics and Space Administration, NASA, in many of its specifications for parts, utilize cryogenic treatments at -196°C. They also use repeated

treatments to insure a high degree of stability in the part. The list of companies using cryogenic treatments includes Hughes Aircraft, General Dynamics, Northrop Corp., North America Rockwell, General Motors, Garrett Turbine, Steelcase, Motorola, IBM, Benedix, Continental Can, ITT Cannon, and others [5].

1.3. Research Objective

The objective of this experimental program was to evaluate the effects of cryogenic treatment on the properties of AISI 4340 steel and aluminum alloy 7075. The samples were subjected to mechanical tests (fatigue, impact energy and hardness) and microstructural characterization by optical and scanning electron microscopy, neutron and x-ray diffraction, and electron dispersive spectroscopy (EDS), giving some interesting indications of the changes in the properties resulting from the cryogenic processing. The mechanical properties showen by the materials (4340 steel and 7075 aluminum) subjected to conventional heat treatments were compared with those resulting from cryogenic treatments. The differences for 4340 steel are discussed on the basis of the effect of tempering temperature and the various sequences of conventional and cryogenic processing.

In particular, the resistance to fatigue, hardness and toughness were measured and compared for conventionally treated and unconventionally treated (cryo) specimens for 4340 steel and 7075 aluminum.

In the investigation of 7075 aluminum, quantitative optical microscopy, x-ray diffraction method and EDS were used to characterize the microstructure. A quantitative study of retained austenite in 4340 steel was performed using the neutron diffraction method. The lack of information in the scientific literature regarding the understanding of the cryogenic effect on 4340 steel and 7075 aluminum was the prime reason for this project.

Chapter 2

2.1. Conventional heat treatment

2.1.1. Conventional heat treatment of Steel

One of the mechanisms to strengthen and harden most steels such as carbon, low-alloy, and tool steels is *heat treatment* in which controlled amounts of martensite are produced in the microstructure. Heat treatments in steels may alter mechanical properties such as strength, hardness, fatigue resistance and toughness. In this regard, control of microstructures or phase structure of a specific alloy system is normally defined by the phase diagram. Many microstructures develop from phase transformations: the changes that happen between phases upon subsequent cooling. Heat treatment of steel begins with heating up the steel, according to the Iron-Carbon diagram, to usually above the eutectoid temperature, where austenite is produced and is stable, held there for a while, followed by cooling down to a suitable temperature. The selection of a heat treatment process often depends on the desired microstructures and steel composition. In addition the resultant structure and properties depend on the subsequent cooling rate [11]. The next discussion is about slow and fast cooling which result in pearlite and martensite structures, respectively.

2.1.1.1. Hardening and tempering processes

After cooling the austenite to below its critical temperature it becomes unstable and will transform to different products according to the cooling conditions, which can

range from slow to very fast. In the case of slow cooling rates, the transformation is usually controlled by diffusion; in plain carbon steels, structures like pearlite or bainite are formed, through a so called "diffusional transformation". In this kind of transformation, diffusion (especially that of carbon) plays the main role in the nucleation and growth stages, which in turn is controlled by temperature and time. By slow cooling of austenite to the temperature range 600-700 °C, two phases, ferrite and cementite, start to nucleate on the existing austenite grain boundaries. If in the same temperature range, time is given to the steel, these nuclei grow to form a special microstructure called pearlite, as indicated schematically in Figure 2.1.

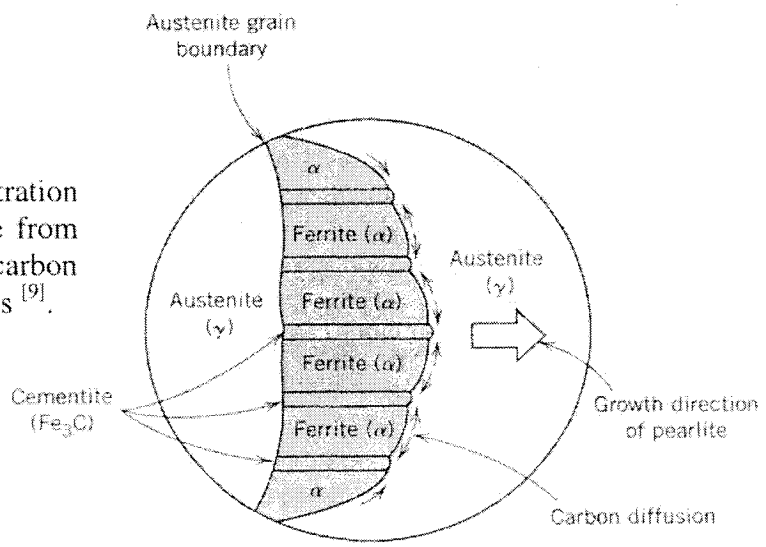

Figure 2.1 Schematic illustration of the formation of pearlite from austenite; direction of carbon diffusion indicated by arrows [9].

On the other hand, if the austenite is cooled rapidly from the austenitizing temperature, martensite phase will be formed through a so called "athermal or diffiusionless transformation" [12]. Martensite start (Ms) and martensite finish (Mf) temperatures, are the two main temperatures in the martensite transformation. In fact below Ms, the free energy of the metal is lowered if the metal changes its phase from that

stable at high temperatures to that stable at low temperature. This free-energy difference is a primary driving force for a martensitic reaction [13].

If the final temperature falls down to a temperature between Ms and Mf, the structure formed is the martensite phase. The martensite phase transformation occurs by a cooperative atomic re-arrangement. In this way atoms in the parent austenite lattice are re-aligned into the lattice of the martensite phase. [12]. In carbon steels the martensitic transformation involves a structure change from a face centered cubic crystal lattice (FCC austenite) to a body-centered tetragonal (BCT martensite) or highly distorted BCC crystal structure. The atomic re-arrangement associated with the martensite reaction produces a shape deformation, as shown schematically in Figure 2.2. The habit plane, or plane on which martensite plates form, is assumed to be the undistorted plane. The strain of this deformation is known as the invariant-plane strain [13]. In the mechanism of martensite formation, there are considerable controversies and several theories.

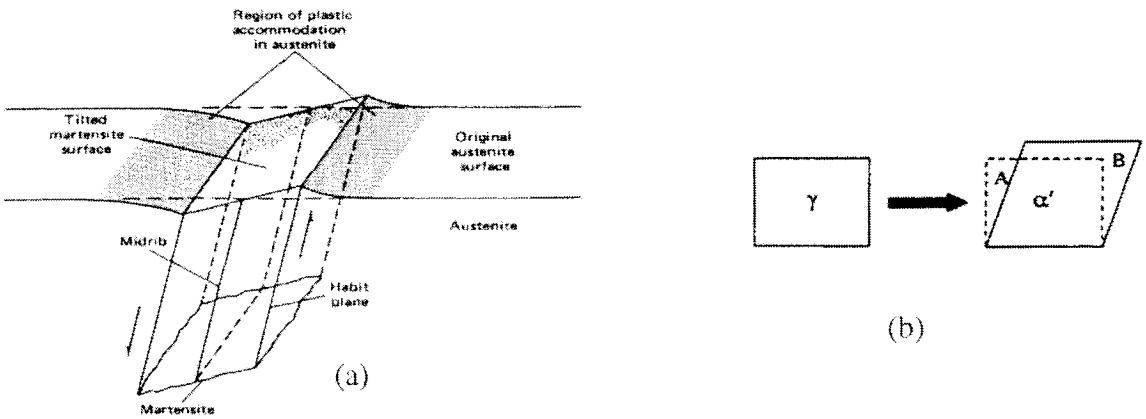

Figure 2.2 (a) Surface relief [1] and (b) Shape change during martensitic transformation.

A simple model of martensite transformation suggested by Bain [14] is shown in Figure 2.3. The carbon atoms situated on the edges of the martensite unit cube cause the unit cell to increase in one direction, which results in a tetragonal lattice. The progress of martensite formation can be seen in Figure 2.4.

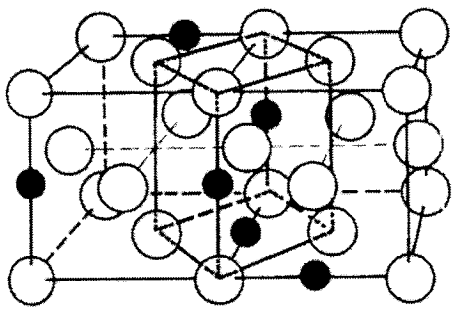

Figure 2.3 Simple model for transformation of austenite to martensite [14].

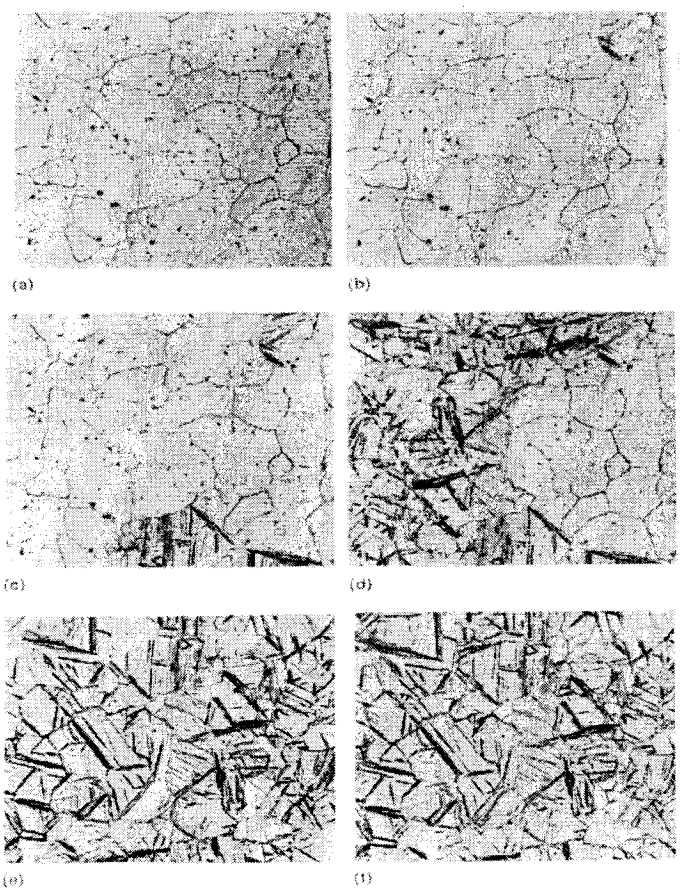

Figure 2.4 Transformation of austenite to martensite at successively lower temperatures. (a) 280; (b) 220; (c) 200; (d) 195; (e) 180 and (f) 175°C[14].

As mentioned before, by fast cooling down to a temperature below Ms, there is very little opportunity for carbon to diffuse out of the austenite lattice. Thus, the carbon atoms remain in the Fe solid solution. Since the space available for the carbon atoms is not sufficient, they expand the lattice to BCT. One of the major characteristics of martensite is the existence of many defects in the lattice. In low carbon steels, for instance, hardness results from the high dislocation density, whereas at higher carbon level, carbon interstitial solid solution strengthening is dominant [15,16]. Figure 2.5 shows the dependence of hardness on martensite volume fraction and carbon content of steel.

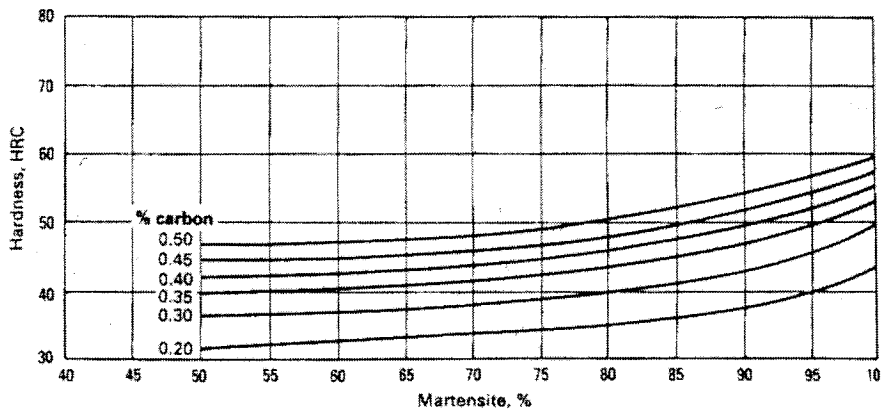

Figure 2.5 Dependence of as-quenched hardness on percentage of martensite and carbon [11].

It should be noted that improving the hardness of steel by means of martensite formation is accompanied by sacrifying toughness. This could be the result of the dramatic increase in the amount of internal energy due to the defects.

Increasing the carbon and alloy content of the austenite, such as by increasing the austenitising temperature or holding time, results in harder martensite, but lowers the Ms

and Mf temperatures. This is mainly due to the fact that by increasing the amount of dissolved alloying elements as well as carbon, the strength of the austenite lattice is increased. Therefore, transformation of such a strengthened matrix to martensite is accompanied by more deformation strain stored in the martensite lattice, leading to more lattice defects and harder martensite. In addition, martensite is harder due to more solid solution effects of carbon and alloying elements [17].

Quenching is the second part of the hardening stage. The most common quenchants are in the form of liquid or gas although molten salts can be used. The liquid quenchants are oil, water, aqueous polymer solutions, and water that may contain salt; the gaseous quenchants are air, and inert gases including helium, argon, and nitrogen. As mentioned before, the cooling rate from the austenite region to room temperature defines the final microstructure and can be shown by continuous-cooling- transformation (CCT) diagrams [18]. The CCT diagram for AISI 4340 steel is shown in Figure 2.6. It can be seen that a fully martensitic microstructure in this alloy requires a cooling rate faster than 8.3 °C/s from the austenitizing temperature [19].

Tempering is the next process to solve the problem of brittleness, in which the steel is heated up to some temperature between 160°C and 650°C for times from 30 min to 4 h. The definition of tempering of steel can be described as the process whereby hardened or normalized steel is heated to a temperature below the critical temperature, and then cooled at a suitable rate, mostly to increase ductility and toughness, moreover to obtain the desired mechanical properties, relieve quenching stresses, and to ensure dimensional stability. Other uses of a tempering process are to relieve stresses and reduce

the hardness resulting from welding and also to relieve stresses due to forming and machining.

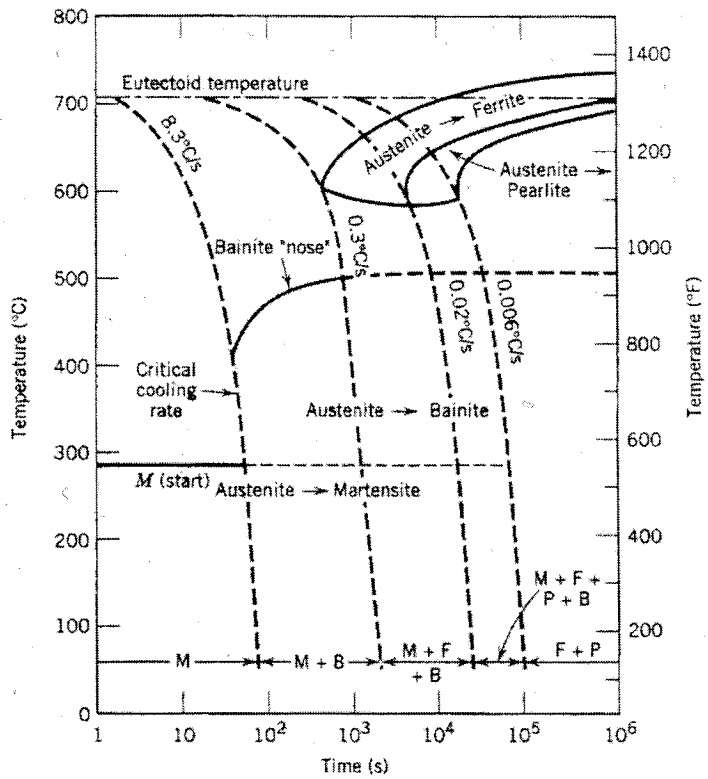

Figure 2.6 Continuous cooling transformation diagram for AISI 4340 [19]

In steels with a martensitic microstructure, the iron lattice is strained by the interstitial carbon atoms so hardness is greatly increased. By heating during tempering, the carbon atoms diffuse and form, through some steps, Fe_3C or an alloy carbide in a ferrite matrix, leading to a gradual decrease in the above-mentioned lattice strain. The properties of the final products after tempering, depend on the size, shape, composition, and distribution of the carbides that form. These changes in microstructure decrease hardness, tensile strength, and yield strength but increase ductility and toughness. Tempering of hardened steel at very low tempering temperatures may cause no significant change in hardness but may increase the yield strength [20,21].

2.1.1.2. Effect of austenitising temperature and time

For each grade of steel, according to practical experience, a range of temperatures has been recommended for austenitizing before hardening. In this temperature range all or part of the carbon and alloying elements are dissolved. As the temperature increases, grain growth takes place and also the amount of retained austenite after quenching is increased. This fact can be shown in Figure 2.7. At 920°C and 970°C the retained austenite may be distinguished as light angular areas [14].

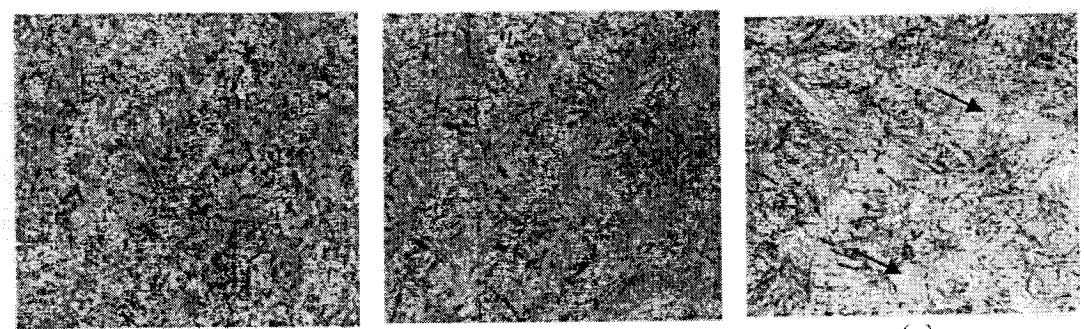

(a) (b) (c)

Figure2.7 Microstructure of steel SS2092 after hardening from (a) 870 (b) 920 (c) 970 °C followed by tempering at 200°C [14]

When the steel has reached the austenitizing temperature, the phase is austenite. The time of holding at this temperature depends on the desired amount of carbide dissolution and acceptable grain size. Since the amount of carbide is different for different types of steel, the holding time is also varied according to the grade of steel. For

example, a few minutes holding time is enough for plain-carbon and low-alloy structural steels as they contain easily dissolved carbides. In these steels, to ensure sufficient carbide dissolution, a holding time of 5-15 min is sufficient, whereas for medium-alloy structural steels a holding time of 15-25 min is recommended [14].

2.1.1.3. Effect of tempering temperature and time

Temperature and time are related variables in the tempering process. However, temperature changes have a greater effect than time changes in typical tempering operations. Figure 2.8 shows the effect of tempering temperature on hardness, tensile and yield strengths, elongation, and reduction in area of plain carbon steel which has 0.52% carbon. It can be seen that both hardness and strength decrease as the tempering temperature is increased. Also, ductility increases with tempering temperature. Most medium-alloy steels are affected by tempering almost in the same manner as this carbon steel [20,21]. When carbon steels are tempered at incorrect tempering temperatures, a loss in toughness occurs compared to the normal tempering cycle and it should be avoided. This phenomenon, temper embrittlement, can be shown in Figure 2.9 for a type of Cr-Ni-Mo steel (SS2550) by the drop in impact strength, which is very similar to toughness [14].

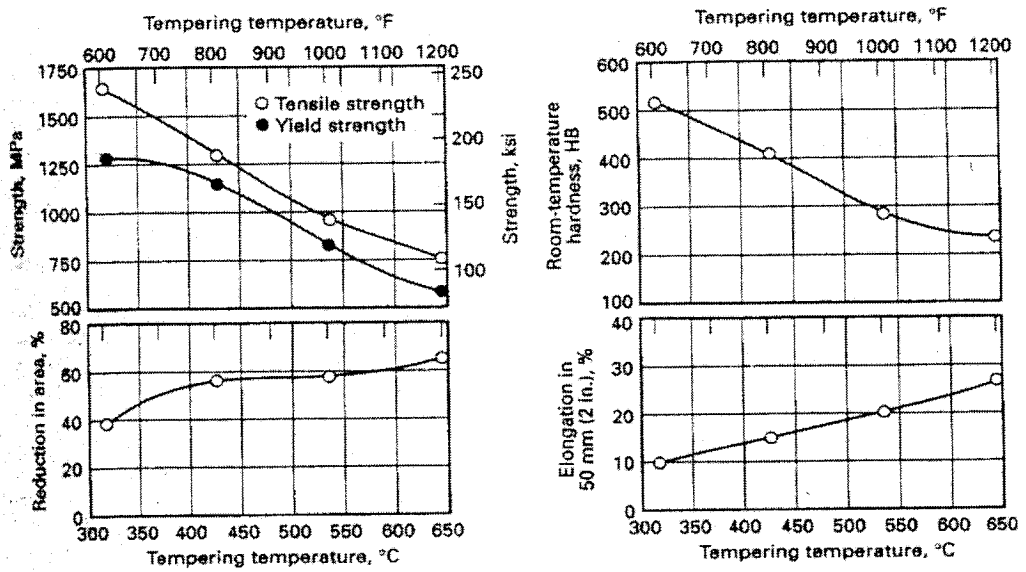

Figure 2.8 Effect of tempering temperature on mechanical properties of 1050 steel [20]

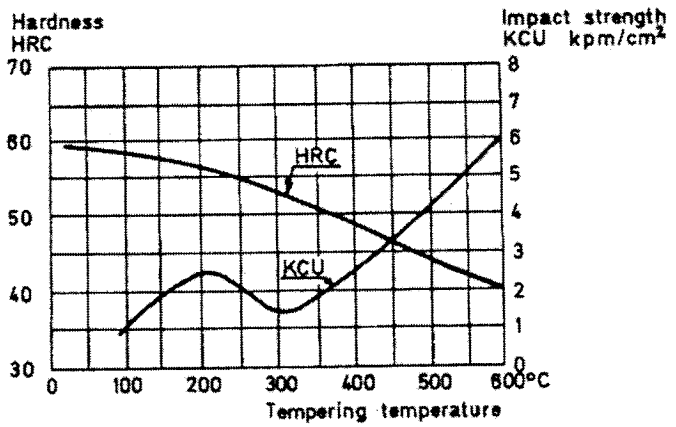

Figure 2.9 Hardness and impact strength as function of tempering for Cr-Ni-Mo steel [14]

The change in mechanical properties with tempering temperature for AISI 4340 steel is shown in Figure 2.10. As explained before, by increasing the tempering temperature, tensile and yield strengths decrease against the increase in reduction area as a measure of ductility [19].

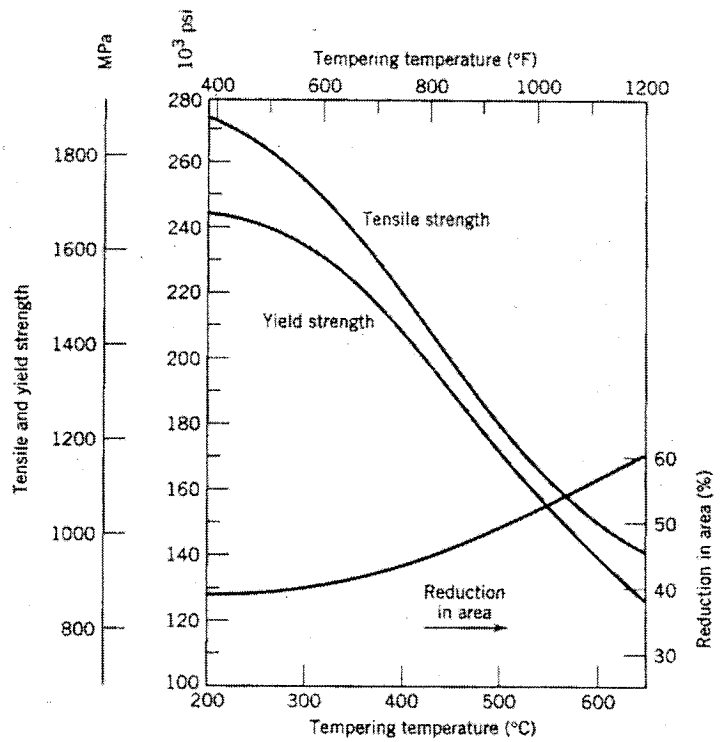

Figure 2.10 Tensile and yield strengths and ductility versus tempering temperature for AISI 4340 steel [19]

Time is also another parameter in the tempering process. The diffusion of carbon and necessary alloying elements for the formation of carbides depends on both temperature and time. The effect of tempering time on the hardness of a carbon steel at various temperatures is shown in Figure 2.11. It can be seen that the changes in hardness

are approximately linear over a large part of the time range if the time is presented on a logarithmic scale [20].

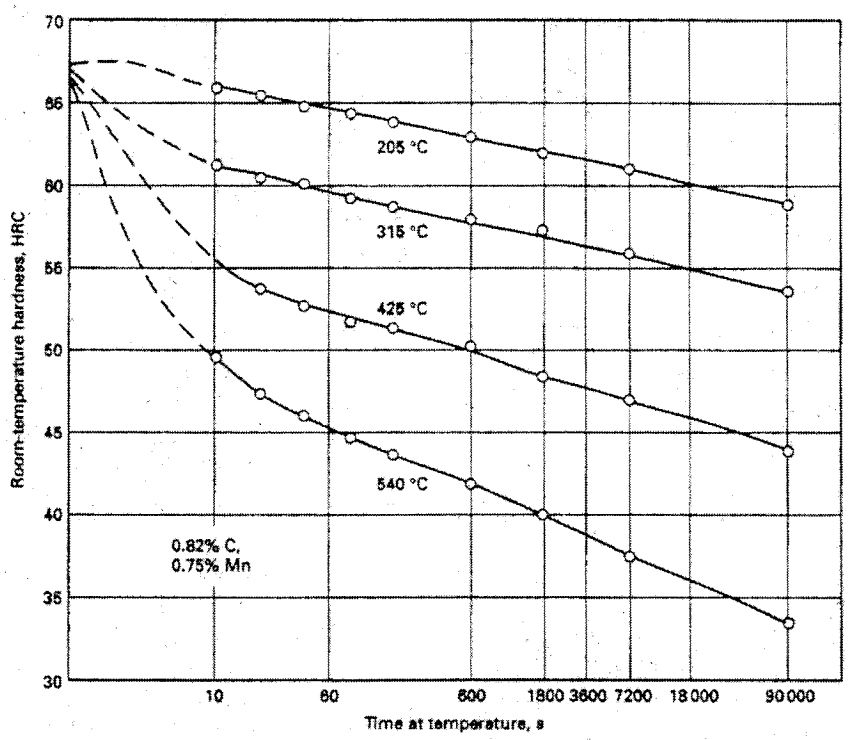

Figure 2.11 Effect of time at four tempering temperatures on hardness of a 0.82% carbon steel [20]

2.1.2 Conventional heat treatment of Aluminum

The important attributes of aluminum and its alloys are low density, high electrical and thermal conductivity, corrosion resistance, good malleability and formability [22]. The strengthening mechanisms of some aluminum alloys is the formation of very small uniformly distributed particles of a second phase within the original phase matrix, known as precipitation hardening, by suitable heat treatment of

particular alloys [23]. The process is named precipitation hardening since the second phase is due to the precipitation of small particles. The precipitation hardening includes two different heat treatments: solution heat treatment and precipitation heat treatment [24]. It should be mentioned that precipitation hardening in aluminum alloys and the hardening process of steel which was explained before in section 2.1.1 are different phenomena because the mechanisms in the quenching stage of the process are totally different, although the profiles of the heat treatments are similar to each other [19].

2.1.2.1. Precipitation hardening

Heat treatment of aluminum alloys is usually limited to solution and precipitation heat treatments, which can affect the strength and hardness of alloys. The mechanical properties of aluminum may also be improved by alloying or cold working. Aluminum alloys can be classified as heat-treatable, which means reacting to solution heat-treating, and nonheat-treatable, the strength of which can be improved by cold working; aluminum alloys are also classified as cast or wrought [24]. Since aluminum 7075, used in this research is a heat-treatable alloy, some explanation about this heat treatment is given here. Heat treating aluminum alloys to increase strength and hardness has three steps:

- Solution heat treatment: to dissolve soluble phases and form a solid solution
- Quenching: to make a supersaturated solid solution
- Precipitation heat treatment: to precipitate a second phase from solid solution, this can be done either by natural aging or artificial aging and is known as "age" or "precipitation" hardening.

Different alloying elements, for example copper, magnesium, silicon, manganese and zinc, can affect the response of aluminum alloys to heat-treatment [24]. In a number of these alloys, precipitation of two elements forms an intermetallic compound such as $MgZn_2$ [2].

The most important aluminum alloy systems with precipitation hardening include:

- Aluminum-zinc-magnesium systems ($MgZn_2$)
- Aluminum-zinc-magnesium-copper systems
- Aluminum-copper systems ($CuAl_2$)
- Aluminum-copper-magnesium systems
- Aluminum-magnesium-silicon systems (Mg_2Si) [2,25]

Solution heat treatment consists of heating up a heat-treatable alloy to a specific range, holding for the necessary time and finally quenching quickly. Since many heat treatable aluminum alloys like 7075 include more than two alloying elements (Al-Zn-Mg-Cu), the metallurgical theory of heat-treating is complicated, but for better understanding of solution heat treatment, a brief explanation of a binary system mechanism is given here. Two metals are considered that are melted together or alloyed, and the mixture is allowed to solidify. One of the metals may be totally or partially dissolved in the other, resulting in crystals of any undissolved metal and the solid solution to form a mixture. Solubility of one metal in another usually depends on temperature. For example copper has 0.5 percent solubility in aluminum at room temperature and 4.5 percent at 520°C. Figures 2.12 and 2.13 show the solubility of copper in aluminum. Considering an aluminum alloy with 4.5

percent copper as it is gradually cooled to room temperature from almost 550°C, a certain amount of copper will precipitate or come out of solution (about 4 percent). On the other hand, if the same alloy is cooled fast, for example by quenching in water to room temperature, a supersaturated solution of copper in aluminum will be formed as insufficient time at elevated temperature is available for diffusion of the copper atoms through the aluminum structure.

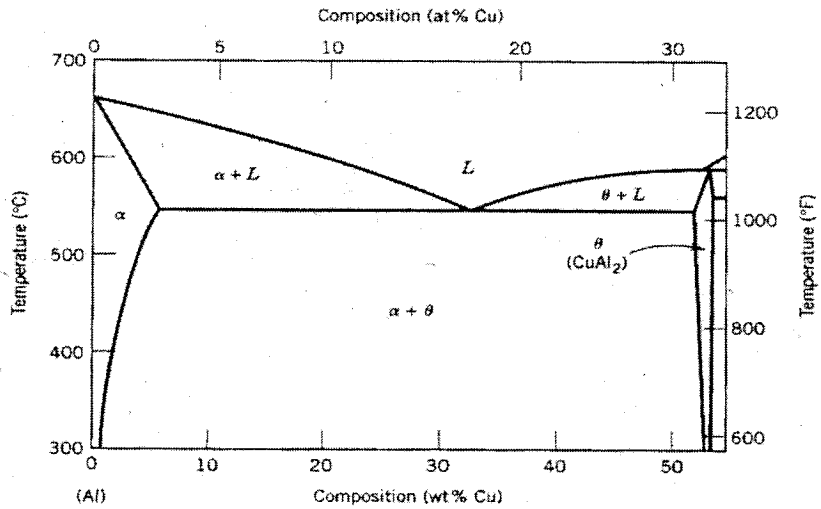

Figure 2.12 A part of aluminum-copper phase diagram [19]

This supersaturated state is unstable and a heat treatment can be conducted to produce the desired distribution of the precipitate in the matrix. This **precipitation heat treatment** or artificial ageing allows the copper aluminide precipitate phase to form as finely dispersed particles. This process is completed by heating in the range of 120 to 200°C for several hours and is known as the "T6" process [2.24].

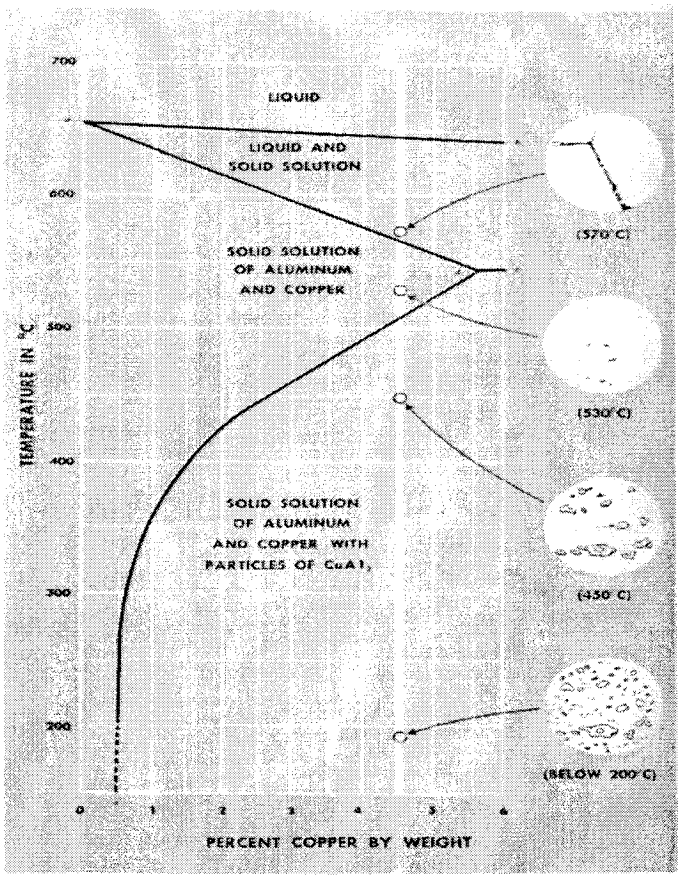

Figure 2.13 Example of solid solution: solubility of copper in aluminum [24]

Figure 2.14 shows both solution and precipitation heat treatments on a schematic time-temperature plot and Table 2.1 indicates recommended temperatures and times for some wrought aluminum alloys.

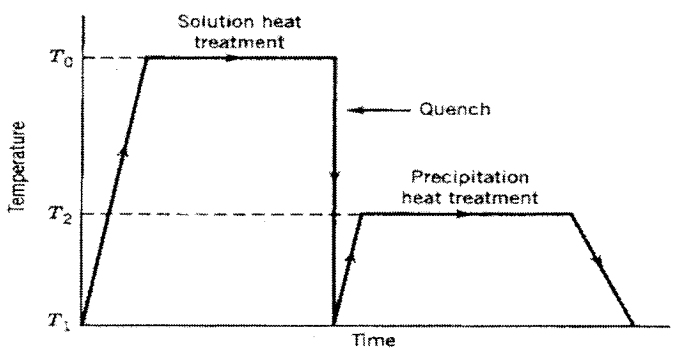

Figure 2.14 Schematic time-temperature plot of solution and precipitation heat treatments [19]

Table 2.1 Wrought Aluminum Alloys – Heat Treatment Data [24]

ALCAN ALLOY	ANNEALING				SOLUTION HEAT-TREATMENT				PRECIPITATION HEAT-TREATMENT (AGEING)			
	Temperature Range °C. ± 3	Temperature Range °F. ± 5	Approximate time at Temperature, hours	Temper Symbol	Temperature Range °C. ± 3	Temperature Range °F. ± 5	Approximate time at Temperature, hours	Temper Symbol	Temperature Range °C. ± 3	Temperature Range °F. ± 5	Approximate time at Temperature ③	Temper Symbol
1S	350	660	④	–O	—	—	—	—	—	—	—	—
2S	350	660	④	–O	—	—	—	—	—	—	—	—
3S	400	750	④	–O	—	—	—	—	—	—	—	—
16S	425⑤	800⑤	2–3	–O	490	915	①②	—	room	room	5 days	–T4
17S	425⑤	800⑤	2–3	–O	500	930	①②	—	room	room	5 days	–T4
24S⑦	425⑤	800⑤	2–3	–O	495	920	①②	—	room	room	5 days	–T4
26S⑦	425⑤	800⑤	2–3	–O	505	940	①②	–T4	170	340	8-12 hrs	–T6
28S	425⑤	800⑤	2–3	–O	520	965	①②	–T4	180	355	8-12 hrs	–T6
50S	425⑤	800⑤	2–3	–O	520	965	①②	–T4	170	340	8-12 hrs	–T6
C54S	—	—	—	–O	—	—	—	—	—	—	—	—
55S	425⑤	800⑤	2–3	O	520	965	①②	–T4	170	340	10-14 hrs	–T6
	—	—	—	—	505	940	①②	—	177	350	6- 8 hrs	–T6A
56S	350	660	2–3	–O	—	—	—	—	—	—	—	—
57S	350	660	2–3	–O	—	—	—	—	—	—	—	—
61S	425⑤	800⑤	2–3	–O	515	960	①②	—	170	340	8-12 hrs	–T6
65S	425⑥	800⑤	2–3	–O	520	965	①②	–T4	180⑧	355⑧	4- 6 hrs	–T6
	—	—	—	—	—	—	—	—	170⑧	340⑧	8-12 hrs	–T6
	—	—	—	—	—	—	—	—	160⑧	320⑧	16 hours	–T6
75S⑦	425⑧	800⑧	2–3	–O	465⑨	870⑨	①②	—	120⑩	250⑩	22-26 hrs	–T6

2.2. Cryogenic Treatment ("unconventional heat treatment")

2.2.1. Cryogenic Treatment of Steel

The main procedure in cryogenic treatment is cooling the specimen down to very low temperatures, as low as –196 °C. In this stage the parts are not subjected directly to the liquid nitrogen (cryogenic fluid) but their temperature is reduced gradually in an airtight refrigeration chamber. In this way the risk of thermal shock damage is minimized. The parts are then soaked in a cryogenic atmosphere (–196°C) for 20 to 60 hours. The holding time is different in various works. Then they are slowly returned to room temperature and a tempering treatment is performed [3]. The schematic time-temperature plot for cryogenic processing is shown in Figure 2.15.

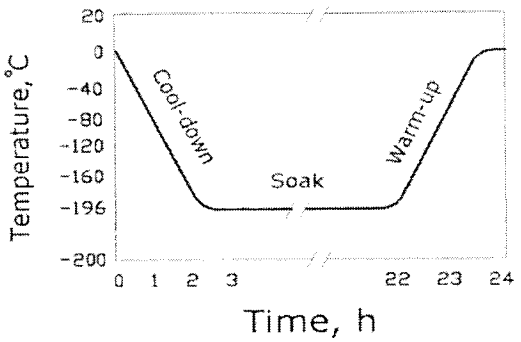

Figure 2.15 Temperature –Time plot for the Cryogenic treatment

2.2.1.1. The Definition of Cryogenic Treatment

Cryogenics can be defined as the knowledge that is attributed to the production of very low temperatures and their effects on the properties of materials. In the science of metallurgical engineering, cryogenic treatment can be used as a supplemental treatment to enhance the properties of parts, dies, or tools [26,27]. "Cryogenics" and the subsequent prefix "cryo" refers to all processes, techniques or apparatus used at temperatures below 123 °K (-150°C) [26].

Very low temperatures are required to create permanent changes in metal components, and cryogenic process effectively concerns taking the material to temperatures below -184°C [28].

2.2.1.2. The Cryogenic Treatment Process

In the 1950s and 60s, people tried to treat steel tools by directly immersing them in a media maintained at -84°C (189°K or -120°F). However, further research was discouraged since tool damage occurred due to the thermal shock [5].

According to some sources [29] a cryogenic treatment at -196°C optimizes the mechanical properties of steel. "There are also a few heat treaters who integrate deep cryogenics into the heat treat process, between austenitizing and first temper, as recommended in ASM International's Heat Treater's Guide: Practices and Procedures for Iron and Steels" [29].

The benefit of using deep cryogenics after quenching is that it increases the precipitation of fine carbides during the following temper and because of this homogeneouse carbide distribution, there are improvements in hardness, toughness, wear resistance and resistance to fatigue cracking in steel products [30].

Some investigators [31-33] have defined two sub-zero treatments as "cold treatment" (CT), in which the temperature is reduced down to -80°C and "deep cryogenic treatment" (DCT), in which the treatment is carried out in liquid nitrogen with a temperature of about -196°C.

In addition, the improvement in mechanical properties of some kind of steels such as high-speed steels can be varied according to the parameters of the DCT operation including austenitizing temperature, holding time at cryogenic temperature, etc as well as the possibility to combine the DCT process with conventional heat treatment as explained in the previous sections. Repeated cycles of DCT, for instance, have been reported [34] to improve the mechanical properties to their maximum. Also, DCT applied immediately after quenching, and before tempering, improves the mechanical properties of high-speed steels to a greater extent than does DCT performed after both quenching and tempering.

In other words, cryogenic processing is not a substitution for conventional treatment, it is a supplemental treatment as mentioned before.

Furthermore, it's been shown that tempering before cryo-treatment is not as desirable as compared to cryo-treatment directly after conventional quenching. This may be due to the stabilization of carbides and microstructural phases during the tempering process, which prevents further transformation during cryogenic treatment [35]. This will be explained in more detail in the section 2.3.

2.2.2 Cryogenic Treatment of Aluminum and its improvement

As was explained before, some work has been done to show the effects of cryogenic processing on tool steels, whereas only a few studies have been conducted on nonferrous alloys like copper and aluminum alloys, most of which were published in Chinese [36-39].

The only work found in the literature regarding the effect of cryogenic treatment on 7075 aluminum alloy was done by Lulay [40]. In that work, aluminum alloy 7075-T6 was examined with two different soaking times (2 and 48 hours) at cryogenic temperature (-196°C) and then at the room temperature they measured the strength, hardness and toughness of the samples. Samples with 2 hours soaking time at cryogenic temperature did not show a change in mechanical properties whereas there was a small change in those samples soaked for 48 hours. The observed changes were 11% increase of charpy impact toughness and a half point decrease in Rockwell B hardness.

Cryogenic treatment can affect the structure of aluminum alloys such as relieving residual stresses which leads to increasing dimensional stability. It was also shown that

cryogenic treatment can improve thin-walled aluminum castings. Finished parts show considerable improvements in both service life and machinability [7].

Investigators at Marshall Space Flight Center (MSFC) are studying the potential benefits of cryogenic treatment for aerospace Aluminum alloys. In this research, they have reported the effects of cryogenic treatment on some mechanical properties such as hardness and fatigue of a kind of aluminum alloy. There was no noticeable improvement of fatigue observed, but the average hardness increased for parent metal that was artificially aged and then subjected to cryogenic treatment [41].

2.3. Mechanisms of Cryogenic Treatment

2.3.1. Mechanisms of Cryogenic Treatment of Steel

Considerable work has been done on sub-zero treatments by different industries, but there are very few scientific papers. It has been reported in these investigations that there is a particular improvement in the life of cryogenically treated tools; however it was mentioned that there is a need for more studies on the phenomenon. The point of these publications is that, they indicate the existence of the phenomenon. Therefore, in this section the current explanations for the mechanisms of cryogenic treatment according to the limited sources and different contradictions will be outlined.

It should be also noted that researchers working on cryogenic treatments have not been able to explain the exact phenomena that takes place during the process mainly due to the fact that the process does not show apparent visible change in the material and also the mechanism is unpredictable [4]. In addition some investigators [9,10,42] mention contradictions and the unpredictable nature of cryogenic treatments. However a number

of aerospace, automotive and electronic industries in the USA, China and other developed countries have applied this process in their regular treatment line to improve wear resistance and dimensional stability of components [4].

The nature and the morphology of the transformations in the material in this process on the fine-scale microstructural level have been of interest recently. However, in the past, the efforts of research were concentrated on decomposition of retained austenite during tempering and/or sub-zero treatment, and effects of retained austenite upon mechanical properties [43]. In this regard, it has been suggested so far that two main different mechanisms are associated with the cryogenic treatments of steels; transformation of retained austenite and "low-temperature conditioning" of martensite. These mechanisms are briefly explained in the following sections [31,43,44,45].

2.3.1.1. Transformation of Retained Austenite to Martensite

One phenomenon reported by general investigators is the transformation of retained austenite to martensite [7,8,43,46]. Gulyaev et al [42,46] studied the martensitic transformation of R18 steel cooled in liquid oxygen at -183°C. In this work, it was found that the amount of retained austenite decreased 10% and transformed to martensite. In another work, Zablotskii et al [47] studied the microstructure of several steels and found that most of the retained austenite in steels was transformed during cooling to -80°C and a small portion (5-7%) during cooling to -196°C.

The above-mentioned transformation of retained austenite is complete for most steels in the temperature range of -70 to -110°C (CT), resulting in better dimensional

stability, higher hardness values, lower toughness and also improvement in wear resistance. It has been found that continuous cooling of martensite below the Mf temperature, e.g. to -196 °C (DCT) and holding in this temperature range for sufficient time results in the precipitation of very fine carbide particles in subsequent tempering [29,34,43,44].

Conversion of the retained austenite to martensite can be detected by the microstructural change during cryogenic treatment with an increase in the dislocation density. The fact that the number of dislocations is higher in quenched and cryo-treated samples can be evaluated by internal friction study. Kelker et al [48] plotted internal friction versus frequency for samples with different thermal processing sequences, as shown in Figure 2.16. As can be seen, the highest internal friction was found to be in the quenched and cryotreated sample with thermal history 4. This is an effect of the full transformation of retained austenite to martensite and the relative thermal contraction of the matrix as compared to the carbides during cryogenic treatment. These can both result in an increased dislocation density.

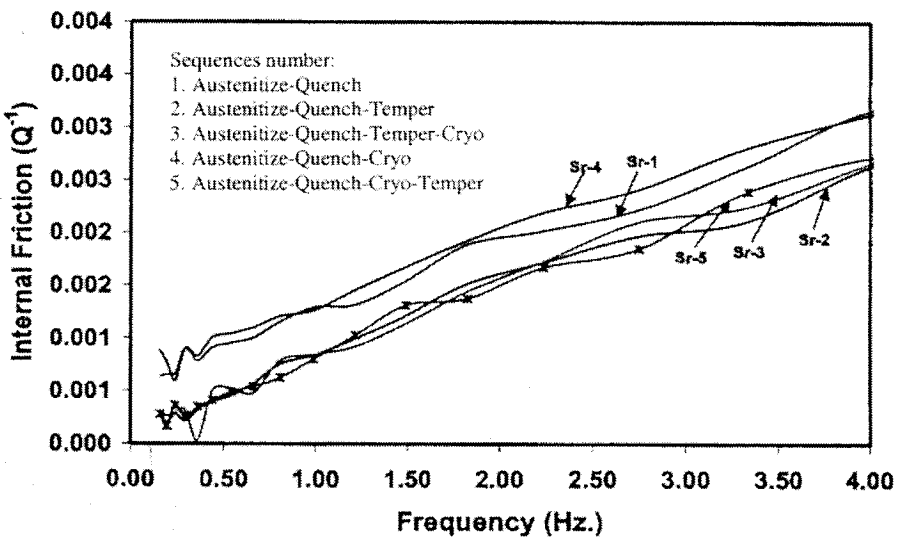

Figure 2.16 Internal Friction versus Frequency for each sequence for M2 steel [48]

In addition, some researchers have shown that fresh martensite which was formed during cryogenic treatment had an uncommon axial ratio of tetragonality (c/a ratio) at low temperature. Hayakawa monitored the c/a ratio of freshly formed martensite from 77K (-196 °C) to room temperature by means of x-ray diffraction analysis. He found that the c/a ratio of the freshly formed martensite was 1.0755, whereas that of the original martensite was 1.039. The c/a ratio decreased with increasing temperature. Once the specimens were heated to near room temperature, further cooling and heating did not change the c/a ratio, which was about 1.0655, showing that the cryogenic treatment process was irreversible [49].

2.3.1.2. Precipitation of Transient Carbides

In addition to martensitic transformation, some investigators indicated that transient carbides exist in the microstructure of cryogenically treated specimens by using different methods such as X-ray diffraction, electron microscopy and diffraction, Mossbauer spectroscopy, atom probe field ion micrscopy, electrical resistivity, dilatometric and calorimetric analysis. They found that transient carbides precipitate during the tempering process, which was performed after the cryogenic treatment. It was believed that this transient carbide, called η-carbide, precipitated from the decomposition of martensite. These fine carbide particles enhance the strength and toughness of the martensite matrix and also improve wear resistance [32,33,50].

In this regard, cryogenic treatment can cause carbon atom clustering, leading to the formation of fine carbide precipitation after some weeks at room temperature.

Clustering of carbon and alloying elements near the dislocations or some precipitation of small carbides may contribute to the higher yield strength for different thermal schedules, which is shown in Figure 2.17. The clustering effect can be detected by resistivity measurements in Figure 2.18. As can be seen, the highest resistivity is for the quench and cryotreated sample. More tempering reduces the carbon in solution because of precipitation and reduces the dislocation density and thus lowers the resistivity [48].

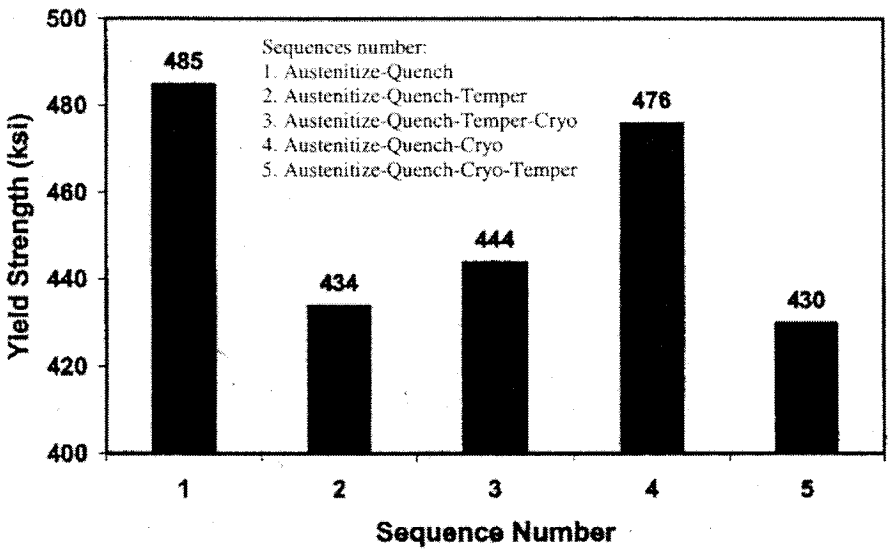

Figure 2.17 Yield Strength versus sequences of M2 steel [48]

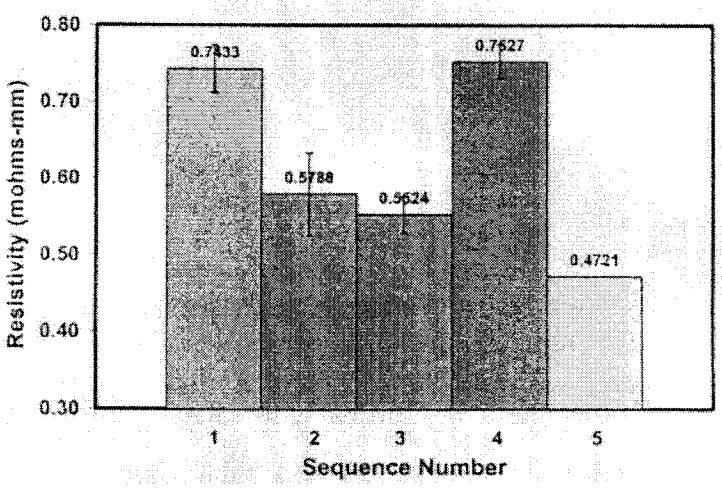

Figure 2.18 Resistivity measurements for each sequence of M2 steel [48]

In addition, the reduction in internal stresses in the martensite can be the proof of the submicroscopic carbide precipitations during cryogenic treatment. This may also reduce microcracking tendencies resulting from reduced internal stresses and therefore improving properties [27].

Meng et al [33] in their work suggested that the formation mechanism of η-carbide could be attributed to the fact that iron or substitutional atoms expand and contract, and carbon atoms shift slightly due to lattice deformation as a result of cryogenic treatment.

In another work, they found that the structure of the cryogenic treated alloy specimens exhibited a heavily tempered structure with little sign of original martensite structure. It also showed small spherical carbide particles, which were distributed more numerously and uniformly in the tempered matrix (Figure 2.19c) [32].

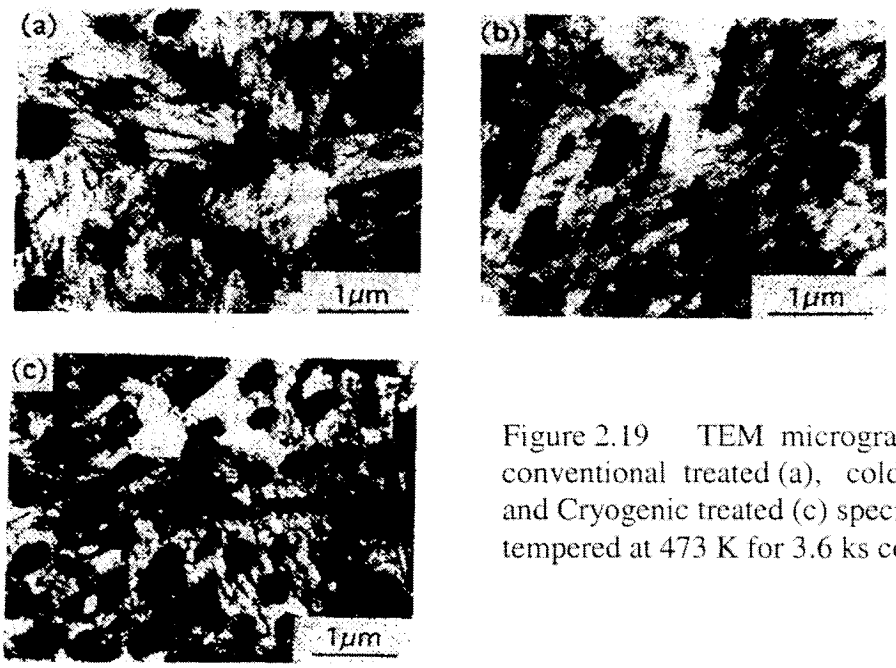

Figure 2.19 TEM micrographs of the conventional treated (a), cold treated (b) and Cryogenic treated (c) specimens in the tempered at 473 K for 3.6 ks conditions [32]

Moreover, J.Y. Huang et al [51] showed that cryogenic treatment not only aids the carbide formation and increases the carbide population and volume fraction in the martensite matrix, but also makes the carbide distribution more homogeneous.

The precipitation of transient carbides can be explained as follows: at cryogenic temperatures, crystallographic and microstructural changes take place in the martensite formed during the initial quench. It has been reported that there exists some changes in the lattice defects of the martensite lattice [9]. It is suggested that these defect sites may act as nucleation sites for the precipitation of fine carbides after warming up to or above ambient temperature. It should be noted that since the diffusion at these very low temperatures is slow, it takes a long time for these changes take place. This phenomenon has been named ***"Low-temperature conditioning"*** of martensite. For this, the temperature should be reduced to the ones lower than the martensite start temperature. Therefore, martensite that forms at or above ambient temperature becomes ***"conditioned"*** at liquid nitrogen temperatures, but it is interesting to note that this temperature is not low enough to condition martensite formed from retained austenite at about -80°C during cold treatment [44].

Some contradictions can be found about the effects of cryogenic treatment on material properties. This is possibly because of the fact that the mechanism responsible for the influence of this treatment on steels might be extremely complex Furthermore; differences in the tested materials as well as the variations in the cryogenic techniques are other possible reasons [31].

2.3.2. Mechanisms of Cryogenic Treatment of Aluminum

As was mentioned before, some limited speculations in Chinese journals [37,38] have been reported regarding the effect of cryogenic treatment on the properties of Aluminum alloys. Due to very cold temperatures of cryogenic treatment, the matrix of aluminum undergoes contraction which results in two effects; firstly it can close the internal defects of the structure such as microporosities and vacancies and also can reduce the lattice parameter, leading to expulsion of the solute atoms and so more volume fraction of the second phase. Both of these possibilities cause strength to be increased.

2.4. Improvement of Performance

2.4.1. Hardness

One of the mechanical properties, which can be influenced by cryogenic treatment, is hardness. As is known, hardness is a measure of a material's resistance to permanent deformation or scratching under specified loading. D.N. Collins [52] studied the effect of cryogenic processing on the hardness of different tool steels including AISI D2 and AISI H13. He stated that the hardness of D2 was dependent on the cryogenic temperature; hardness increased as retained austenite was transformed. However, no change in hardness with time of treatment was observed, whereas the hardness of HI3 was additionally dependent on holding time at cryogenic temperature due to possible isothermal martensite transformation.

In another work, the same author reported that cryogenic treatment can increase the hardness of D2 and decrease the toughness. It was found that the well-known effect of

transforming retained austenite to martensite resulted in hardness increases in the specific range of sub-zero temperatures from -80 to -110 °C [44].

In addition, R. Mahmudi studied the effect of cryogenic processing on the hardness of M2 tool steel. In this work, the hardness was increased after cryogenic processing compared to conventional treatment [43].

R. Kelkar [48] worked on the same steel and compared the effect of five different heat treatment sequences. He found that the hardness was 0.2 HRC lower for an austenitizing, quench, cryogenic and temper treatment than for the austenitizing, quench and tempered, which is the conventional treatment. This was explained as in the latter, secondary hardening took place whereas in the former, precipitation of carbides enhanced by cryogenic treatment has reduced the tetragonality of martensite and so reduced the martensite hardness. It should be mentioned that before tempering, the hardness of cryo-treated specimens was 1.5 HRC higher than those hardened conventionally, mainly due to transformation of retained austenite to martensite.

2.4.2. Toughness (Impact energy)

Toughness is a mechanical property of materials that is used to measure the ability of a material to absorb energy up to fracture. In toughness determinations, specimen geometry as well as the manner of load application is important. For high strain rate loading conditions and when a notch (or point of stress concentration) is used, the toughness is called ***notch toughness***.

R. Mahmudi studied the effect of cryogenic processing on impact toughness of M2 tool steel. In this work, the toughness decreased after cryogenic treatment compared to

conventional hardening. This was reported to be due to the short soaking times at cryogenic temperature. In this way, they suggested that the process of carbide precipitation, which was explained in the previous section, seemed to be incomplete and thus the expected improvement in toughness was not observed [43].

In another investigation on H13 steel, A. Molinari et al showed the same result, reduced toughness after a quenching – cryogenic- tempering cycle. However, by changing the sequence of treatment to quenching – tempering – tempering – cryogenic treatment, the toughness was improved slightly compared to the conventional hardening [53].

2.4.3. Fatigue (Life time)

Fatigue is one of the most common failure mechanisms of materials in structures subjected to dynamic and fluctuating stresses, such as bridges, aircraft and machine components. In repeated stress or strain cycling, the material may fracture at a stress level significantly lower than the tensile or yield strength for a static load. One method to measure fatigue is using a rotating-bending test. The compression and tensile stresses are applied on the specimen as it is bent and rotated at the same time. The results of such a test can be shown as a Stress-Cycle plot called an S-N curve. Fatigue life is defined as the number of cycles to fracture at a specific stress. It can be determined from the S-N plot. The process of fatigue failure contains three different steps: (1) crack initiation, (2) crack propagation, and (3) final failure [19].

In terms of the effect of cryogenic treatment on fatigue behavior, it has been reported by Dreger [3], that the fatigue strength of cryogenically processed spring-wire steel is improved. The process converted more than 75% austenite to martensite.

2.4.4. Wear Resistance

In the engineering industry, abrasive wear is another common cause of mechanical damage. It has been shown that the wear characteristics of materials can be improved by cryogenic treatment. For example, it has been reported that the wear resistance of tool steels used in the pulp and paper industry and also the lifetime of some machine elements, such as dies used in metal working have been increased by means of cryogenic treatment [5].

There are four main types of wear, adhesive wear, abrasive wear, fatigue wear, and corrosive wear. For wear resistance testing, abrasive wear tests are usually chosen. "Abrasive wear is defined as the removal of material caused by hard particles which indent the surface of a component and slide relative to it. It shows itself in several forms: in wear of equipment which deal with an abrasive medium, in wear of seals or machine parts between which abrasive particles can penetrate and wear by abrasives carried in fluids". Wear can be varied by the parameters related to the service conditions like properties of the abrasive, abrasive type and relative hardness, abrasive grit size, abrasive shape, speed, load, specimen size, frictional heating, and humidity or environment; or factors in relation to mechanical properties like hardness, and flow and fracture

properties; or variables related to metallurgical structure like grain size, dispersion of phases, size and shape of phases, and lamellae [54].

As was shown in the preceding section, cryogenic treatment can change the microstructure by changing the retained austenite content and carbide distribution. In a comparison between the two processes of conventional and unconventional treatment, Barron showed that the cryogenic treatment resulted in an improvement in the wear resistance by a factor of 2.4 for the AISI TB steel and by factor of 1.4 for the C1045 steel. In addition, the wear resistance of the steels was enhanced by the cryogenic treatment by a factor of approximately 2 for steels 52100, O2, A2, M2, and O1 respectively [45].

2.4.5. Corrosion

The cryogenic treatment may reduce the corrosion rate. Barron et al [55] studied several steel compositions and concluded that this treatment can improve corrosion resistance. The highest reported increase was by a factor of 1.786. It has been suggested that the cryogenic treatment results in some refinement of the grain boundaries, which is the region in which corrosion was most predominant. In this particular case, there would be a smaller microscopic area available for diffusion of the hydrogen sulfide the corroding species in this case, into the metal, leading to reduction of the corrosion rate.

2.5. Assessment of retained austenite in the steel microstructure

Retained austenite is a component that can have detrimental or beneficial effects, depending on the use of steel. It can occur in various steels such as tool steels, martensitic stainless steels, martensitic carbon steels, or carbon steel welds. The measurement of the amount of retained austenite in a structure is generally difficult. Several different techniques have been introduced for the measurement of retained austenite in martensitic and ferritic structures, which will be explained in brief below.

2.5.1. Neutron Diffraction

The diffraction of thermal neutrons is a distinctive survey of condensed matter that can be used in a broad range of applications. This costly tool can be used for determination of atomic arrangements (crystal structure, short and long-range order), especially for structures containing light atoms in the presence of heavier atoms or neighboring elements, determination of residual stress and texture in polycrystalline engineering materials, and quantitative analysis of multiphase materials; the final attribute can be employed to measure the retained austenite before and after cryogenic treatment [56].

In this technique, it is necessary to have a neutron source (e.g. a reactor), a target (the material to be studied), and a detector. The neutrons in the beam have kinetic energies which cover a wide range, but a monochromatic beam, i.e. a beam collected of neutrons with a single energy, can be achieved by diffraction from a single crystal. This diffracted beam can be used to reveal structural details of the specimen. The main

concept is to record the way in which neutrons are deflected [57]. Figure 2.20 illustrates a schematic of this experimental procedure.

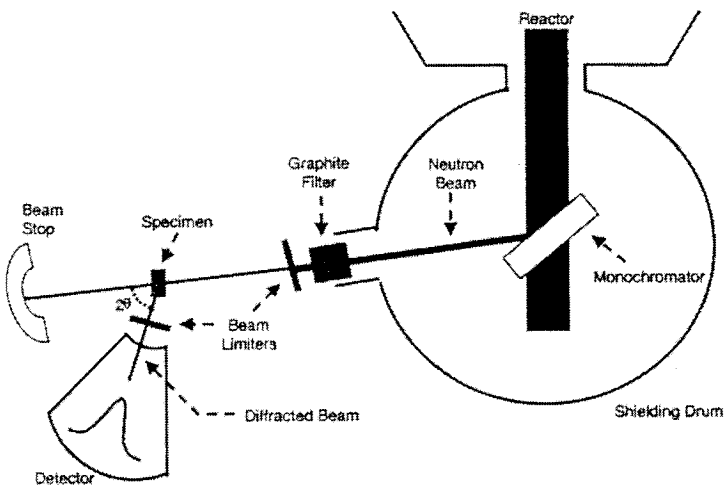

Figure 2.20 Schematic illustration of neutron diffractometer

There exist three difference sources for diffraction methods; x-ray, electrons, and neutrons. While all three are capable of distinguishing phases in specimens and many other applications, nonetheless, the nuclear reactor, needed to produce neutrons, is a significant limiting factor to widespread use of the neutron diffraction technique. The main difference between neutron diffraction and the others techniques such as x-ray and electron diffraction is the variation of the atomic scattering power [57].

It should be noted that the minimum measurable amount of austenite is limited in the x-ray technique while in the neutron technique it is possible to evaluate materials with phases of low volume fraction. Neutron diffraction has more penetration than x-ray, which shows the way to a bulk measurement, where it will bring a better statistical

representation of the specimen microstructure. Furthermore, for neutron diffraction there is no need to prepare special samples [56-58].

2.5.2. X-ray diffraction

The austenite and martensite phases in a steel can have similar chemical composition but not the same crystal structures. This is the basis of the significant work that has been done in the past on the application of x-ray techniques for recognizing and measuring retained austenite in hardened steels. The fundamental of X-ray techniques is the fact that the intensity of the diffracted radiation is proportional to the volume fraction of the diffracting phase. In this regard, there are two basic methods of measurement, which can be used with a diffractometer. These are the internal standard method and the direct comparison method; the former can be used for powder samples by mixing the sample with a substance whose diffraction pattern is known. Diffraction peaks from the unknown phase can be compared with reference peaks from the standard substance. On the other hand, in the direct comparison method, the ratio of intensities of selected diffraction peaks from the phases present are used to determine the amount of each phase present. This method can be used in polycrystalline solids [57,59,61]. Also the x-ray diffraction technique to measure retained austenite has been established by an ASTM standard [60].

2.5.3. Chemical and electrochemical etching

Metallographers prefer to use the optical methods due to their simplicity and quick implementation. However, they are limited and have not been compared in terms of

accuracy with the more commonly used quantitative techniques mentioned above. At the beginning, to obtain meaningful data, representative samples must be selected and prepared. Polishing and etching must reveal the true microstructure without distortion. It is possible to achieve the development of structure without introducing any changes in the surface of the section by oblique illumination, polarization and phase or interface contrast.

2.5.4. Magnetic etching

The fundamental of this method dates back to the time when the magnetic patterns were seen by sprinkling magnetic powder on the surface of a material in a magnetic field and observing the distribution of the particles. Although the basic concept is the same many changes have been made. For instance, microscope techniques were improved for the observation of magnetic patterns by replacement of magnetic powders with colloidal magnetic fluids. The particles, preferentially gather together at the domain boundaries, which appear as dark lines in visible light. The separation between two dark lines is roughly equal to the size of a domain, and the width of the dark line is the width of the wall or transition zone [62]. In this method, the observations of microscopic phases depend on the resolution of the optical microscope. It has been reported [63] that by using the magnetic etching technique, one can recognize delta ferrite or martensite that makes up as little as 0.5% of the microstructure in an austenitic matrix.

CHAPTER 3

EXPERIMENTAL METHODOLOGY

3.1 Overview

This chapter explains the experimental approach for the ferrous and also the non-ferrous alloy. Experiments were designed in this study in order to investigate the effect of cryogenic processing on mechanical properties of the steel and aluminum alloy by comparing with those subjected to conventional hardening treatments. For the steel, the procedures of cryogenic and conventional hardening treatments were considered separately and then different tempering temperatures were examined. Mechanical tests including hardness, toughness and fatigue for both materials were performed. Microstructural examinations, including measurement of the amount of retained austenite in the steel using neutron diffraction technique, and X-ray diffraction (XRD) for the aluminum alloy were employed to identify the phases. Scanning Electron Microscopy (SEM) was used to characterize the microstructure as well as for fractography of the specimens.

3.2 Experimental Approach

In the previous sections, the two different types of heat treatments for the materials used (steel and aluminum) were explained. In this study, eight different heat treatment sequences were designed to evaluate the response of the steel. Mechanical

testing involved impact energy and hardness tests for the specimens in all sequences, whereas fatigue testing, microstructural examination, Neutron diffraction, and XRD were carried out on selected specimens with critical sequences. The eight sequences used for steel are as follows:

1) Austenitising- Quench

2) Austenitising- Quench- Temper (200°C)

3) Austenitising- Quench- Temper (300°C)

4) Austenitising- Quench- Temper (455°C)

5) Austenitising- Quench- Cryo

6) Austenitising- Quench- Cryo- Temper (200°C)

7) Austenitising- Quench- Cryo- Temper (300°C)

8) Austenitising- Quench- Cryo- Temper (455°C)

For the Aluminum alloy, two different series of heat treatment were chosen. The two schedules used for the aluminum alloy were:

1) Solution - Quench- precipitation

2) solution- Quench- Cryo- precipitation

The composition of materials, specimen preparation, and thermal cycles for both conventional and cryogenic processes adopted in this work are described in the following section.

3.3 Experimental Materials

3.3.1 Steel– AISI 4340

The steel chosen for the study was AISI 4340 steel which is used in high performance vehicle and aircraft components where high strength and toughness are fundamental design requirements [64]. Hence it is employed in the production of mechanical components with complex shapes and close dimensional tolerances such as aircraft landing gear and drive shafts. In addition, very little work has been done on this type of steel regarding the effect of cryogenic treatment. The chemical composition is shown in Table 3.1: as can be seen, the principal alloying elements for this steel are nickel, chromium and molybdenum.

Table 3.1 Composition of AISI 4340 steel

Element	Amount (%)
C	0.38 to 0.43%
Mn	0.6 to 0.8%
Si	0.15 to 0.3%
Cr	0.7 to 0.9%
Ni	1.65 to 2.00%
Mo	0.2 to 0.3%
P	Max 0.035 %
S	Max 0.04 %
Fe	Bal.

3.3.2 Aluminum Alloy 7075

The other material for this study was an aluminum alloy, 7075. This kind of Al-alloy is employed in production of structural components in the aerospace industry, where high strength and lightness are design requirements. Similar to the steel, very little information has been reported about the effect of cryogenic treatment on the properties of this alloy. The chemical composition of the studied material can be seen in Table 3.2, with the principal alloying elements being zinc, magnesium and copper with minor additions of iron and chromium [25].

Table 3.2 The composition of the Aluminum alloy 7075

Element	**Amount (%)**
Cu	2%
Si	0.3%
Fe	0.202%
Mn	0.3%
Mg	2.9%
Zn	6.1%
Cr	0.184 %
Ti	0.2 %
Al	Bal.

3.3.3 Steel Sample Preparation

The AISI 4340 steel was supplied in the normalized condition, as bar in two forms; round and square (Vaudreuil Steel Company). The material with round section, with 9.5 mm (3/8 inch) diameter was used for making fatigue specimens whilst the square material, with (12.7x12.7mm) cross section was used for the Charpy impact specimens. The round diameter was machined to form one inch reduced section length samples as shown in Figure 3.1. The dimensions for preparation of this sample were according to ASTM standard E466 [66]. Charpy specimens were also made according to ASTM E23 [65], Figure 3.2.

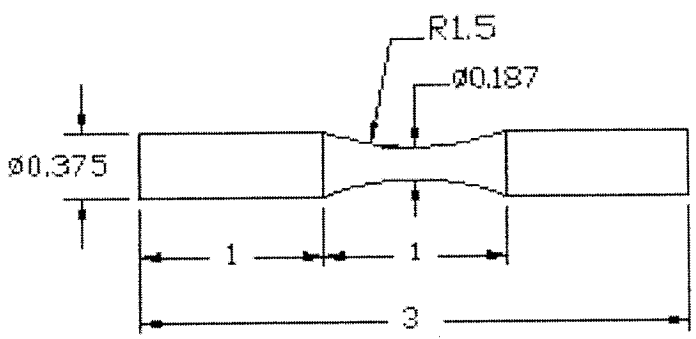

Figure 3.1 Schematic illustration of AISI 4340 steel fatigue specimen (inch)

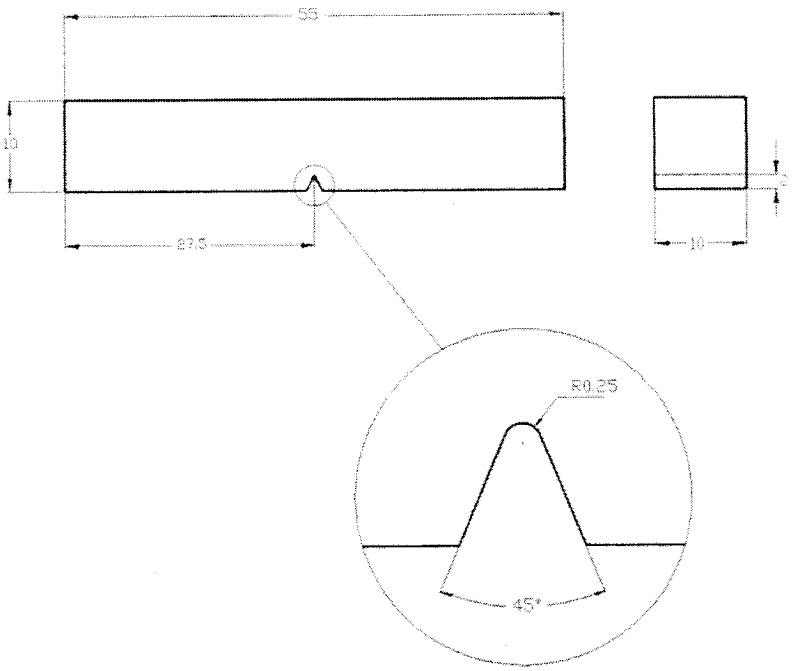

Figure 3.2 Schematic illustration of AISI 4340 steel Charpy sample (mm)

3.3.4 Aluminum Sample Preparation

Aluminum alloy 7075 bar was received in two forms of cross section, round and square. In order to make the fatigue and charpy specimens, the round material with 12.7 mm (1/2in) diameter and the square bar (12.7x12.7mm) were used, according to ASTM E466 [66]. Figure 3.3.

Charpy specimens were made according to ASTM E23, with the similar dimensions as the steel samples, as shown in Figure 3.2 [65].

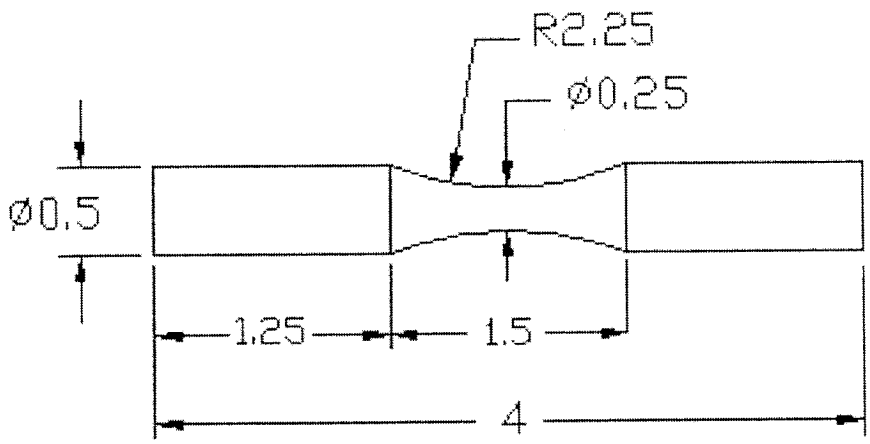

Figure 3.3 Schematic illustration of Aluminum alloy 7075 fatigue specimen (inch)

3.4 Hardening - Conventional Heat Treatment

3.4.1 Conventional Heat Treatment for AISI 4340

A group of specimens were subjected to conventional heat treatment including, austenitizing at a temperature of 845°C for 15 minutes in a tube furnace under argon flowing atmosphere. The specimens were then quenched in oil with a temperature of 20°C followed by 2 hours tempering. A schematic thermal cycle for this process is shown in Figure 3.4. The tube furnace was used for all heat-treating in this study (HTF 55000 produced by Lindberg Blue Inc). The chamber of this furnace is covered by two semi-

cylindrical heating parts, with refractory ceramic fiber and firebrick (silica) insulation. The furnace is heated by heating elements placed symmetrically above and below the chamber. The furnace programming and data acquisition system were fully automatic for different thermal cycle schedules, allowing accurate time and temperature control. Austenitizing treatments were carried out in the tube furnace in which a continuous flow of argon was directed into the hot zone to minimize the amount of oxidation, contamination with air, and decarburization throughout the treatment. Different tempering temperatures of 200°C, 300°C, and 450°C were similarly conducted on the specimens using the same protective argon atmosphere, with 2 hours holding time for each specific group of samples. The hardness measurements of samples indicated fairly uniform temperature distribution in the furnace. Also, the microhardness measurements performed on the cross section of hardened specimens did not indicate significant decarburization taking place during the heat treatment.

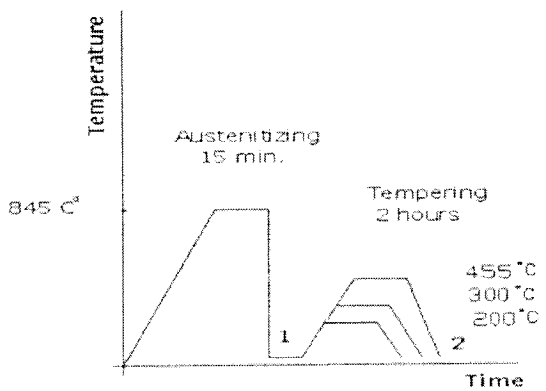

Figure 3.4 Conventional thermal cycle for AISI 4340 steel

3.4.2 Precipitation Hardening of Aluminum Alloy 7075

Solution heat-treating consisted of heating up the specimens as quickly as possible to 465°C, soaking for 2 hours, and then rapidly quenching in water from that temperature. As mentioned before, the quenching must be performed from the solution heat treatment temperature as fast as possible, therefore the quench tank was placed very closed to the furnace. Once the specimens were taken out of the furnace, they were dropped immediately into the water tank. The precipitation heat treatment or "artificial ageing" was the next step, to be performed immediately after solution treatment, by heating to 120°C temperature and holding for 24 hours, followed by air-cooling at the end. This process is called the "T6" treatment and the material after this process is known as aluminum alloy 7075-T6. A schematic thermal cycle of this complete process is shown in Figure 3.5.

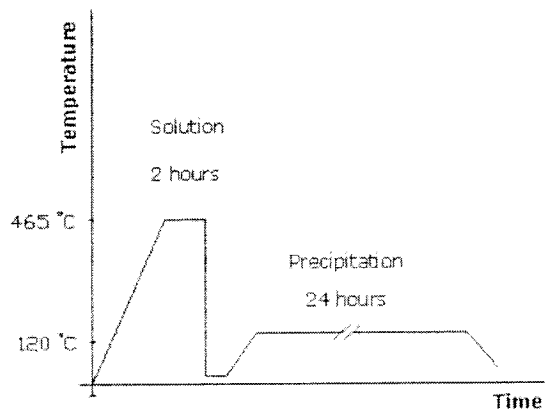

Figure 3.5 Precipitation hardening cycle for Aluminum alloy 7075

3.5 Cryogenics - Unconventional Heat Treatment

3.5.1 Cryogenic Treatment for AISI 4340 Steel

Cryogenic, or subzero treatment, consisted of slowly cooling the specimens to approximately -196°C and holding at this low temperature for 24 hours and gradually heating the specimens back to room temperature. This single cryogenic treatment was used directly after oil quenching from the austenitising temperature and was followed by tempering, as shown in Figure 3.6.

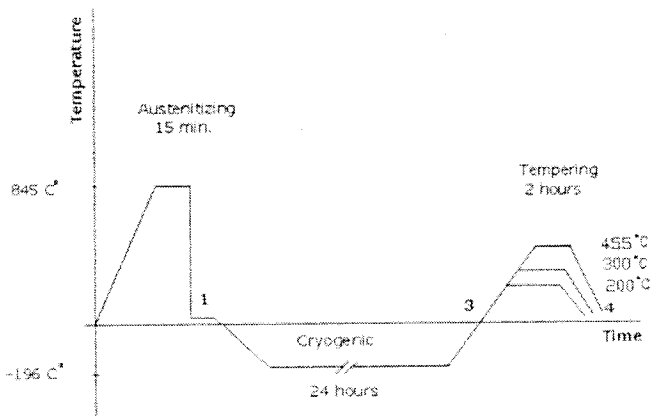

Figure 3.6 Cryogenic thermal cycle for AISI 4340 steel

The conditions for austenitising, quenching and tempering, such as time and temperature, were similar to those in the conventional treatment, explained in section 3.4.1. The slow cool-down process was done from room temperature to liquid nitrogen temperature through gaseous nitrogen. This means that the cool-down rate is achieved by

immersing the specimens in gaseous nitrogen above the liquid nitrogen and then going into the liquid nitrogen in the same tank. The temperature of samples was monitored during the cool-down and soak period by means of a thermocouple attached to the samples. The specimens (and thermocouple) are fed together into the nitrogen tank very slowly. After the sample temperature reached approximately -196°C, they were soaked in liquid nitrogen for 24 hours, as shown schematically in Figure 3.7.

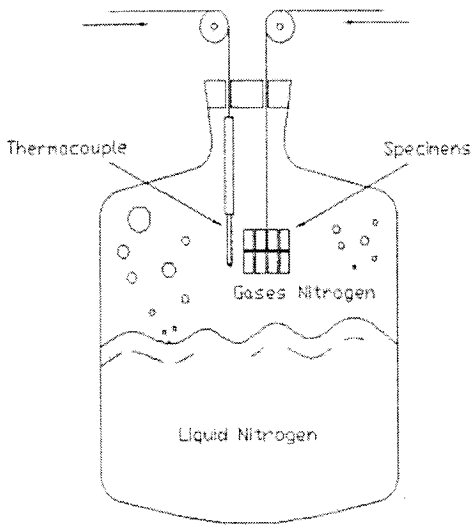

Figure 3.7 Schematically illustration of the Cryogenic process set-up

It should be noted that thermal shock must be avoided. Marder [67] showed that microcrack sensitivity is related to tetragonality of the martensite. Larger tetragonality (as a result of higher carbon content) shows a greater tendency for microcracking. The effects of other alloying elements (Ni, Cr and Mo) are negligible. The critical carbon content for microcraking susceptibility is 1.4 wt percent [67]. The amount of carbon in AISI 4340 steel is 0.4 wt percent, which is lower than the critical value, however

provisions were made to obtain a steady and very slow cooling rate to prevent thermal shock during the cryogenic process. Table 3.3 shows the experimental sequences performed on AISI 4340 in this work.

Table 3.3 Heat treatment schedule

Designation	Heat Treatment
Sequence 1	Austenitise at 845°C, oil quench
Sequence 2	Austenitise at 845°C, oil quench, temper at 200°C
Sequence 3	Austenitise at 845°C, oil quench, temper at 300°C
Sequence 4	Austenitise at 845°C, oil quench, temper at 455°C
Sequence 5	Austenitise at 845°C, oil quench, cryo
Sequence 6	Austenitise at 845°C, oil quench, cryo, temper at 200°C
Sequence 7	Austenitise at 845°C, oil quench, cryo, temper at 300°C
Sequence 8	Austenitise at 845°C, oil quench, cryo, temper at 455°C

3.5.2. Cryogenic Treatment for Aluminum Alloy 7075

The specimens were solution-treated at 465°C for 2 hours, followed by quenching into water. After quenching the specimens were immediately transferred to the liquid nitrogen tank for immersion at a temperature of -196°C for 24 hours. Then they were warmed up to room temperature in ambient atmosphere and the precipitation hardening

treatment was finally performed by heating to 120°C for 24 hours followed by air cooling to room temperature. This thermal cycle is shown schematically in Figure 3.8.

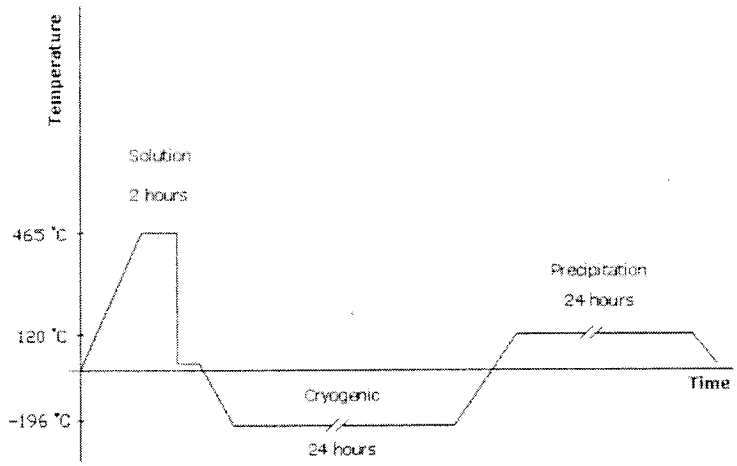

Figure 3.8 Cryogenic thermal cycle for aluminum alloy 7075

3.6 Mechanical Properties Tests

3.6.1 Mechanical Tests of AISI 4340

3.6.1.1 Hardness of Steel

Hardness measurements were determined using a Rockwell hardness machine on the "Rockwell C" (HRC) scale for all the heat-treated specimens with the conical diamond penetrator and 150Kg major load. Hardness measurements were done on Charpy samples with an average of ten measurements for each specimen. Prior to tests a

calibration of the tester was carried out using standard calibration blocks. Also for reducing the risk of decarburization, the microhardness of the cross sections of specimens was measured. . The latter was done using a LECO M400-G2 microhardness tester which has a load capacity ranging from 50 gr to 2 Kg with a diamond indentor. The measurements were made in terms of Vickers hardness (HV), which can be converted to the Rockwell C values with the use of conversion charts.

3.6.1.2. Charpy Testing of Steel

Impact fracture testing is commonly used to measure the toughness of low and high strength materials. In this work for AISI 4340 steel, a Tinius Tolsen impact test machine was used (Willow Grove, PA, USA). The machine has the Charpy impact energy range between zero and 264 ft-lbs.

According to ASTM E23 [65] V-notched Charpy specimens were made as shown in Figure 3.2 and then subjected to the various heat treatments and finally tested on the impact testing machine. For performing the test, the hammer was released from a fixed level and hit the specimen exactly behind the notch and led to specimen fracture. The energy absorbed during fracture is shown by the instrument (related to the difference of the maximum level of hammer heights before and after the fracture). Eight sequences in Table 3.3 were chosen in order to compare the effect of cryogenic and conventional processing as well as tempering temperature on the impact energy of AISI 4340 steel at room temperature. For each sequence, four samples were tested.

3.6.1.3. Fatigue Testing of steel

The fatigue experiments were performed in a rotating-bending configuration by means of a fatigue test machine, which is shown in Figure 3.9. The fatigue machine was a compact, bench-mounted unit designed to apply reversed bending loading to unthreaded, straight-shank, specimen bars. The machine is produced by the Instruments Budd Division Company in Phoenixville, PA, USA. Samples were made from 4340 steel according to Figure 3.1. The specimens were subjected to rotation at different levels of load until complete fracture. Reversed bending loading gives a variation of stress with time, that causes fatigue failure, in which the stress alternates from a maximum tensile stress to a maximum compressive stress of equal magnitude of a type typically found in shafts or axles. Generally, rotating bending fatigue tests are conducted using a sinusoidal load with load ratio of R=-1 at room temperature. In this method, either complete fracture of the specimen or 10^8 load cycles are considered as the end of the test [66]. The collet size for this test is 3/8 inch diameter, which is matched to the specimen grip diameter as shown in Figure 3.9.

Since the fatigue data is affected by manufacturing procedures and heat treatments, which result in surface roughness, decarburization and residual stresses [1], in this work all specimens were ground longitudinally in the reduced section before testing with 400, 600 and 1200 grit papers. Four sequences (2, 4, 6 and 8) were chosen in order to determine S-N curves, before and after, the cryogenic process. Also, some individual sequences, like 1 and 5, were subjected to fatigue testing to show the effect of martensite

amount on fatigue life. According to experimental design standards for fatigue testing [68] four samples were tested for each point, or 12 to 16 specimens were tested to produce the S-N curve for each thermal sequence.

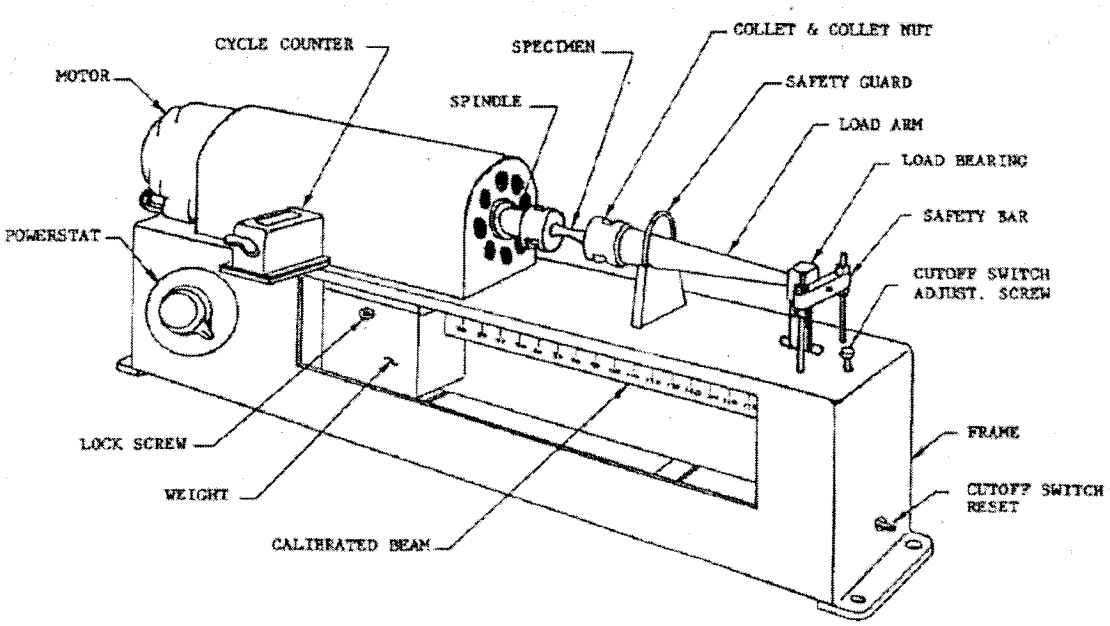

Figure3.9. Fatigue machine [69]

3.6.2. Mechanical tests of Aluminum alloy 7075

3.6.2.1. Hardness of Aluminum

The same hardness apparatus that was used for steel was also used for the aluminum samples except that the Rockwell B (HRB) scale, using a 1/16 inch ball penetrator and 100Kg major load, was used. Hardness measurements were performed on

Charpy and fatigue samples with an average of ten measurements on each specimen. Prior to tests a calibration of the tester was carried out using standard calibration blocks.

3.6.2.2. Charpy Testing of Aluminum 7075

As the toughness level of aluminum alloys is generally lower than that of steels, a machine with a lower range for measuring softer material was used to achieve more accurate results. The Charpy test apparatus that was employed for aluminum samples was the SI-1B model produced by SATEC SYSTEM INCO. The V-notched Charpy specimens were prepared according to ASTM E23 [67] as shown in Figure 3.2 and then subjected to the various heat treatments and finally tested exactly with the same procedure as explained for steel. For the aluminum, two sequences were examined, as mentioned in section 3.2, to compare the effect of cryogenic and conventional treatments (T6) on the impact energies of aluminum alloy 7075 at room temperature. For each sequence four samples were tested.

3.6.2.3. Fatigue Testing of Aluminum 7075

The same apparatus and procedure, as explained in section 3.6.1.3, was used for the aluminum specimens, except that different grips were used for the aluminum samples. Specimens were categorized in two major groups as mentioned in section 3.2 to compare the fatigue resistance before and after cryogenic processing.

3.7. Microstructural Investigation

There are three main categories of metallography: optical microscopy, scanning electron microscopy (SEM), and transmission electron microscopy (TEM). All examination of microstructures should begin with optical microscopy [56,70]. Both optical microscopy and SEM are used in this research to characterize the structure by revealing microstructure, second phases, microhardness, volume fraction and evidence from fracture surfaces.

3.7.1 Steel Characterization

3.7.1.1 Optical Microscopy of Steel

Specimens were cut transversely and were mounted in an epoxy resin and ground using silicon carbide abrasive papers with 120, 240, 400, and 600 grit, respectively. Polishing was performed with a 9 μm, 3μm, and 1μm diamond suspension. The microstructures were revealed with a 2% nital etchant. Finally, the microstructures were viewed and photographed using an optical microscope.

3.7.1.2 Scanning Electron Microscopy (SEM) of Steel

The fracture surfaces, which were cleaned ultrasonically in an ethanol bath, were examined in a Hitachi S4700 cold Field Emission Gun Scanning Electron Microscope (FEGSEM) that operates at low and medium accelerating voltage, ranging from 1 to 10 kV, at a working distance of 12 mm.

3.7.2 Aluminum Characterization

3.7.2.1 Optical Microscopy of Aluminum

Grinding and polishing of aluminum samples was almost the same as was explained in section 3.7.1.1. However, the etchant was totally different and for this purpose, Keller's reagent was used [2 mL HF, 3 mL HCL, 5 mL HNO3, 175 mL H2O]. An optical microscope associated with an image analyzer was used to take photographs and measure the second phase volume fraction, as will be explained in the next section.

3.7.2.2 Image Analysis

The volume fraction of second phase structure in aluminum alloy 7075 was determined by image analysis using the "Image Analyzer" LECO image analyzer. Volume fraction measurements were based on area percent, which is the ratio of the total detected phase area to the image frame area. In order to obtain a good representation of the microstructure, a magnification of 100 times was chosen and 10 different fields of the specimens were examined.

3.7.2.3 Scanning Electron Microscopy (SEM) of Aluminum

The SEM was used as the most efficient way to characterize the type of second phase particles in aluminum alloy 7075 where the phases have been identified in terms of composition, morphology, size, and distribution. Also fracture surfaces were investigated by SEM before and after cryogenic treatment.

The FEGSEM apparatus (Hitachi S4700) was used. It is equipped with two secondary electron detectors (below the lens and above the lens detectors) and a Robinson backscattered electron detector. The Robinson detector, which is utilized for backscattered imaging was needed. For chemical analysis, the Oxford INCA system (EDS) was employed in this microscope.

3.8. Neutron Diffraction Experiments

Neutron diffraction was used for measuring the retained austenite and martensite contents of the AISI 4340 steel specimens before and after cryogenic processing. Four samples were tested in different sequences (1, 4, 5, and 8).

3.8.1 Instrumentation and Experimental Setup

The instrument used for the measurements was the C2 DUALSPEC diffractometer located in the NRU reactor at Chalk River Laboratories, Ontario. The diffractometer detector consists of 800 individual wires separated by an angular spacing of approximate 0.1 degrees, which allows a diffraction pattern up to 80 degrees for 2θ to be measured at a single detector position. The measurements were taken with a monochromatic neutron beam of wavelength 0.132877 nm. At this wavelength the diffraction pattern of each sample was measured from 35 to 115 degrees. The specimens were continuously rotated in order to minimize the effects of texture on the diffraction pattern.

The reactor provides a Maxwellian distribution of thermal neutrons, which scatter from the reactor core through a collimator with a monochromatic wavelength of about 1.33 Angstroms (0.133 nm). A diffracted beam monitor is mounted in the neutron beam before the sample table in order to measure the neutron flux incident on the sample. Neutrons diffract off the sample and through an oscillating collimator to the 800 wire BF3 detector. The schematic illustration of the neutron diffraction process is shown in Figure 3.10 [71].

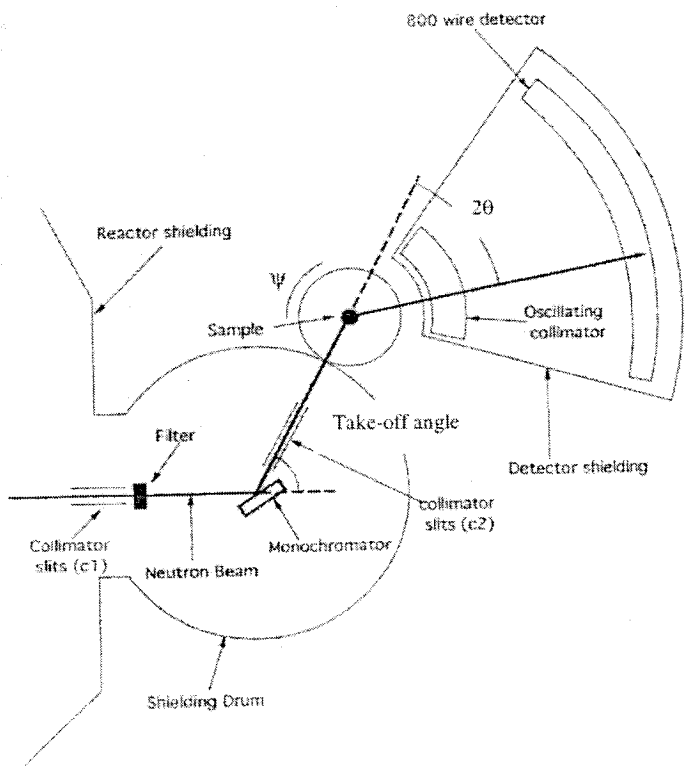

Figure 3.10 Schematic diagram of experimental setup

3.8.2 Experimental Procedure

The Bragg peaks correspond to crystallographic lattice planes of the crystallites that form the material. Thermal neutrons with characteristic wavelength λ, will diffract off these planes at a scattering angle 2θ governed by Bragg's Law [$\lambda=2d \sin(\theta)$], where d is the spacing between the lattice planes. The reflection positions have to be indexed with reflection positions from the expected phases.

A least squares refinement program such as GSAS, (General Structure Analysis System), which uses the Rietveld refinement method to fit the diffraction patterns, is used to determine the phase fractions. The least-squares refinements are performed on the entire pattern until the best fit can be obtained between the experimental data pattern and a calculated pattern based on models for the crystal structure of each phase. GSAS calculates the phase fraction per unit cell of each phase (austenite, and martensite). Using the lattice parameters for each phase the volume per unit cell can be calculated. The phase fraction can then be expressed in terms of % volume fraction for each phase.

$$\text{Volume fraction phase(i)} = \frac{\text{unit cell fraction phase(i)} * \text{unit cell volume phase(i)}}{\Sigma\text{unit cell fraction phase(i)} * \text{unit cell volume phase(i)}}$$

3.9. X-ray Diffraction Experiments

Two aluminum alloy 7075 specimens from each sequence were tested using an APD 1700, Philips, X-ray diffractometer to identify the phases formed before and after cryogenic process. Specimens were exposed to an accelerating voltage 40 kV and a beam current of 20 mA with a scanning rate of 0.02 degree. The intensity and 2θ data were acquired and stored using a personal computer. Secondary phases were identified using JCPDS-XRD pattern data as an internal reference standard. In order to quantify the secondary phases, the collected data were further analyzed using Oxford Instruments INCA, which was employed in an SEM, as explained before.

Chapter 4

RESULTS AND DISCUSSIONS

In this chapter, the results of the experiments described in Chapter 3 are presented and discussed with references to the literature review in Chapter 2. As in this work two alloys, steel AISI 4340 and Aluminum 7075 alloy, have been studied, each alloy is discussed separately since the relevant mechanisms are different. The steel section (4.1) starts with the effect of cryogenic treatment on the amount of retained austenite as measured by neutron diffraction analysis. In the following sections, the effect on the mechanical properties of the studied steel, such as hardness, impact energy, and fatigue are presented and discussed. In each section, the aim is to compare the effect of cryo-treatment with the conventional treatment. The Aluminum section (4.2) will start with a discussion of the microstructure which includes optical and electron microscopy followed by XRD results and discussion. The mechanical properties along with the fractography results of Al alloy 7075 will be explained at the end of this chapter.

4.1. AISI 4340 Steel

4.1.1. Measurement of Retained Austenite

The typical experimental neutron diffraction profiles of selected samples, sequences 1, 4, 5, and 8 in Table 3.3, are shown in Figures 4.1 to 4.4, respectively. In these neutron patterns, intensity is plotted versus scattering angle (2θ), with each peak related to a particular phase. The height of the peaks corresponds to the amount of the phase being measured.

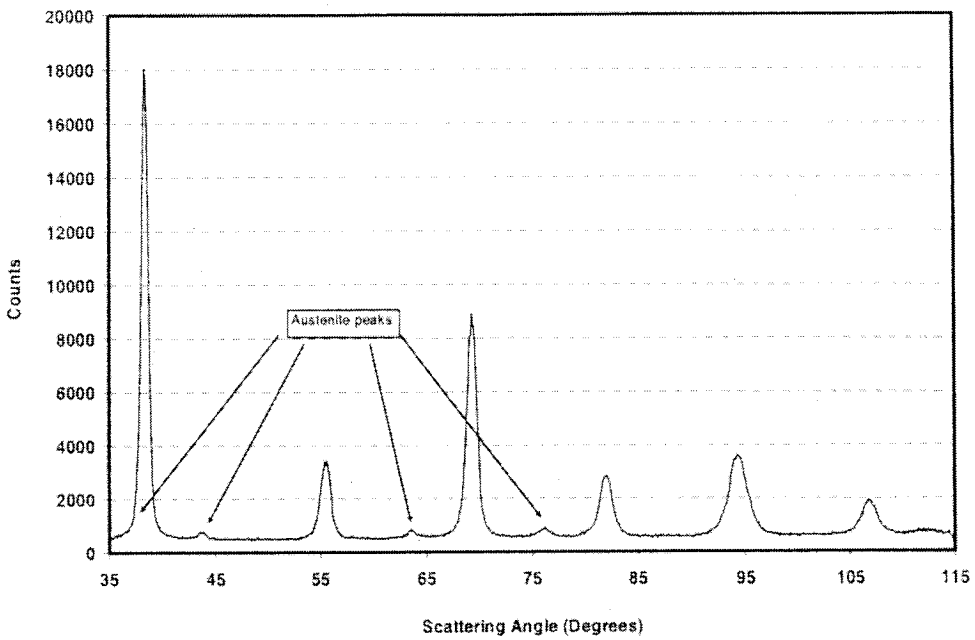

Figure 4.1 The experimental neutron diffraction profile of 4340 steel (Conventional- seq.1)

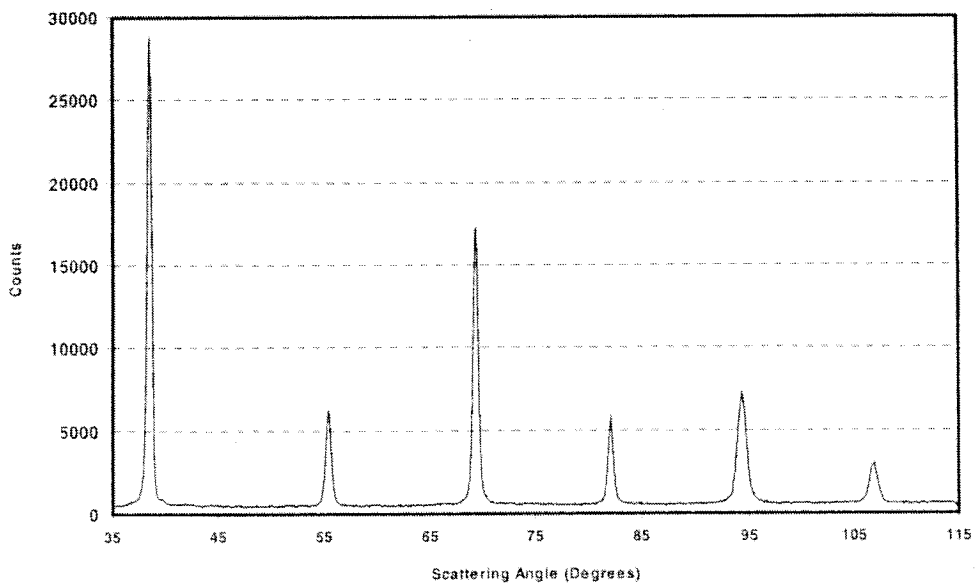

Figure 4.2 The experimental neutron diffraction profile of 4340 steel (Conventional- seq.4)

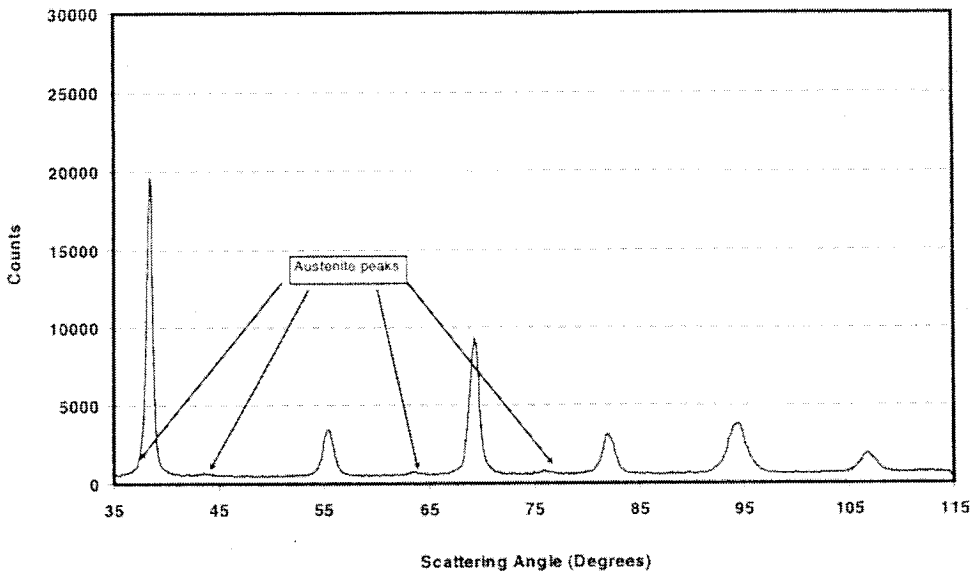

Figure 4.3 The experimental neutron diffraction profile of 4340 steel (Cryo- seq.5)

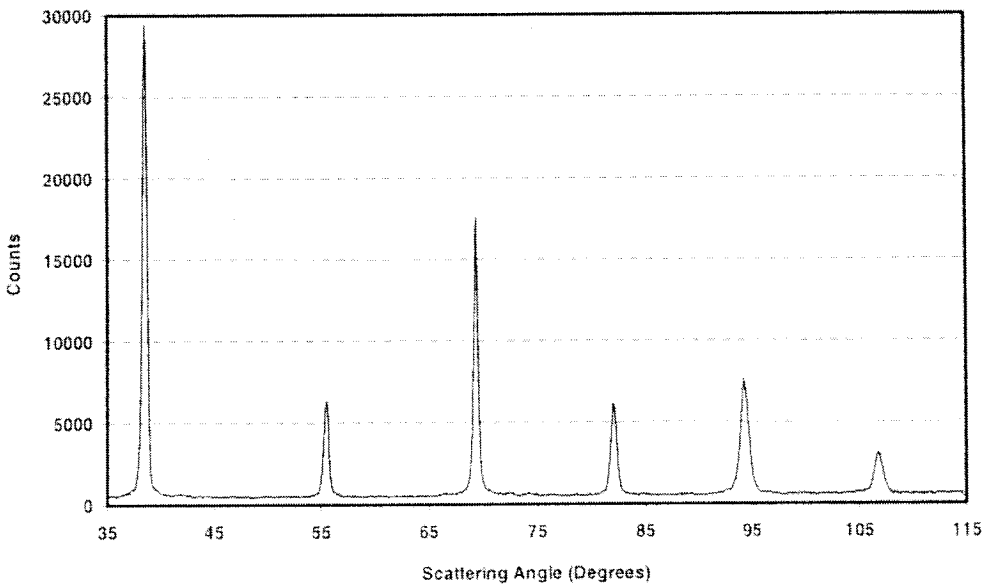

Figure 4.4 The experimental neutron diffraction profile of 4340 steel (Cryo- seq.8)

In the above Figures the peaks corresponding to the retained austenite have been indicated and the rest are the martensite phase peaks. The position of the peaks has to be considered with the positions from the expected phases. For a wavelength of about 1.328 Angstroms; approximate diffraction positions for austenite and martensite are shown in Tables 4.1 and 4.2.

Table 4.1.Austenite

2θ (deg)	Relative Intensity	Plane
36.755	0.6012	1 1 1
42.698	0.3446	2 0 0
61.973	0.3743	2 2 0
74.271	0.5855	3 1 1
78.181	0.1838	2 2 2
93.454	0.117	4 0 0
105.013	0.444	3 3 1
108.984	0.442	4 2 0

Table 4.2.Martensite

2θ (deg)	Relative Intensity	Plane
38.378	0.608	1 0 1
38.576	0.3012	1 1 0
55.1	0.0818	0 0 2
55.697	0.1608	2 0 0
69.272	0.2334	1 1 2
69.666	0.4633	2 1 1
82.2	0.1905	2 0 2
82.696	0.0947	2 2 0
94.115	0.1699	1 0 3
95.102	0.1688	3 0 1
95.226	0.1687	3 1 0
107.5	0.1613	2 2 2

A least squares refinement program such as GSAS, (General Structure Analysis System), which uses the Rietveld refinement method to fit the diffraction patterns [71], is used to determine the phase fractions. The least-squares refinements are performed on the entire pattern until the best fit can be obtained between the experimental data pattern and a calculated pattern based on models for the crystal structure of each phase. These refinement plots for samples with seq. 1 and 5 are shown in Figures 4.5 and 4.6, respectively. The second plot for each sample (Figures 4.5b and 4.6b) has a higher

magnification of the austenite (2 0 0) reflection. In Figures 4.5(a) and 4.6(a), the crosses are the neutron data points and the lines are the calculated model results. The closer the lines match with the crosses (i.e. the calculated model matches the data points), the better the fit. There is another plot below the calculated curve with higher magnification which is a difference between the data points and the calculated model. Ideally this should be a straight line. This can show the good level of agreement between the said data. Eventually, GSAS software, as described in section 3.8.2, calculates the phase fraction per unit cell of each phase (austenite, martensite), and these are shown in Table 4.3 in terms of % volume fraction for each phase.

Table 4.3 The % volume phase fraction of 4340 steel by Neutron diffraction and GSAS program.

Phase	**% volume phase fraction after**	
	Conventional treatment (Seq.1)	**Cryogenic treatment (Seq.5)**
Martensite	94.3 ±0.4	95.7 ±0.4
Austenite	5.7 ±0.3	4.2 ±0.3

As can be seen from Table 4.3, the volume fraction of austenite decreased from 5.7 to 4.2 % due to cryogenic treatment. This corresponds to the decrease of austenite peaks, which is shown in the neutron patterns of the same samples in Figures 4.1 and 4.3. The by-product of the GSAS refinement method corresponding to the phases can be found in Table 4.4.

Table 4.4. The Neutron diffraction results by GSAS refinement for tested samples.

Phase	Lattice spacing (Angstroms)	Unit cell Volume (Angstroms^3)	Unit Cell Weight	Unit Cell Density (gm/cm^3)
Martensite	a=2.8626(2) c=2.8890(3)	23.67	111.69	7.84
Austenite	a=3.587(1)	46.16	223.39	8.04

In terms of the effect of tempering on the patterns by comparing Figures 4.1 and 4.3, specimens without tempering show the existence of small amounts of retained austenite, whereas in the specimens that have undergone a tempering process, Figures 4.2 and 4.4, there is almost no evidence of the retained austenite peaks. This can be attributed to the typical effect of tempering which is decomposition of retained austenite to martensite or other products such as ferrite and cementite during tempering at 455 °C. This can be seen by comparing the area under the peaks in Figures 4.1 and 4.3 with those in 4.2 and 4.4, indicating that the disappearance of retained austenite resulted in an increase in the amount of other phases like martensite.

The effect of cryogenic treatment on the amount of phases, especially the retained austenite, can be shown by comparing the volume fraction obtained by GSAS (Table 4.3). That is, in the latter the amount of retained austenite was decreased due to more transformation to martensite, called freshly formed martensite, as was explained in section 2.3. This is the most important purpose of cryogenic treatment which is in

agreement with the literature as explained in Chapter 2. There is not a huge amount of retained austenite in this steel (as compared to the tool steels normally discussed) in either case – this is due to several factors including the lower carbon content of this alloy plus the presence of alloying elements. However, the cryogenic process has reduced the percentage of retained austenite by a small amount.

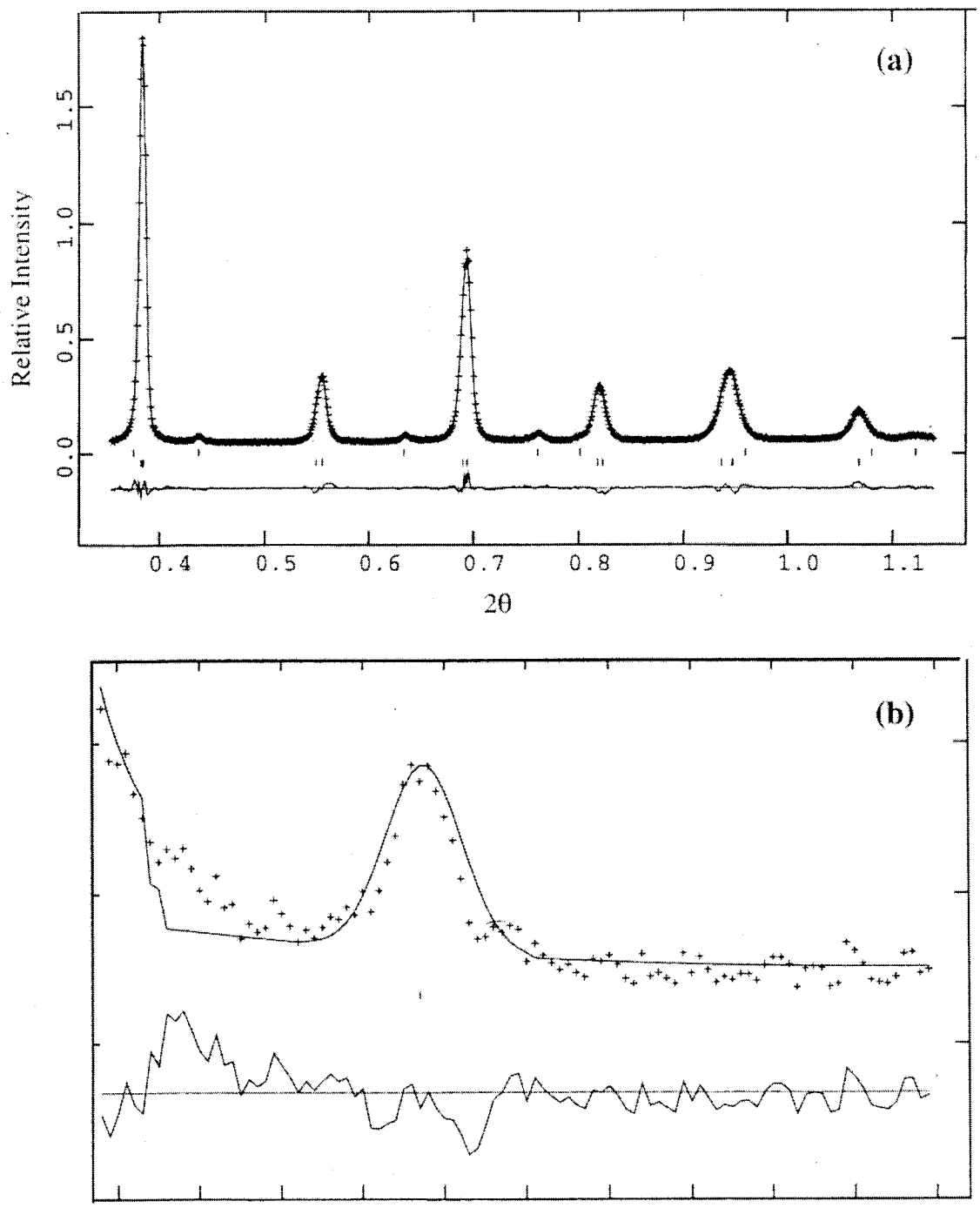

Figure 4.5 The experimental neutron diffraction profiles of 4340 steel specimen in sequence 1 (a) Crosses show neutron data points, lines show GSAS refinement (b) higher magnification view of the first austenite peak with conventional process

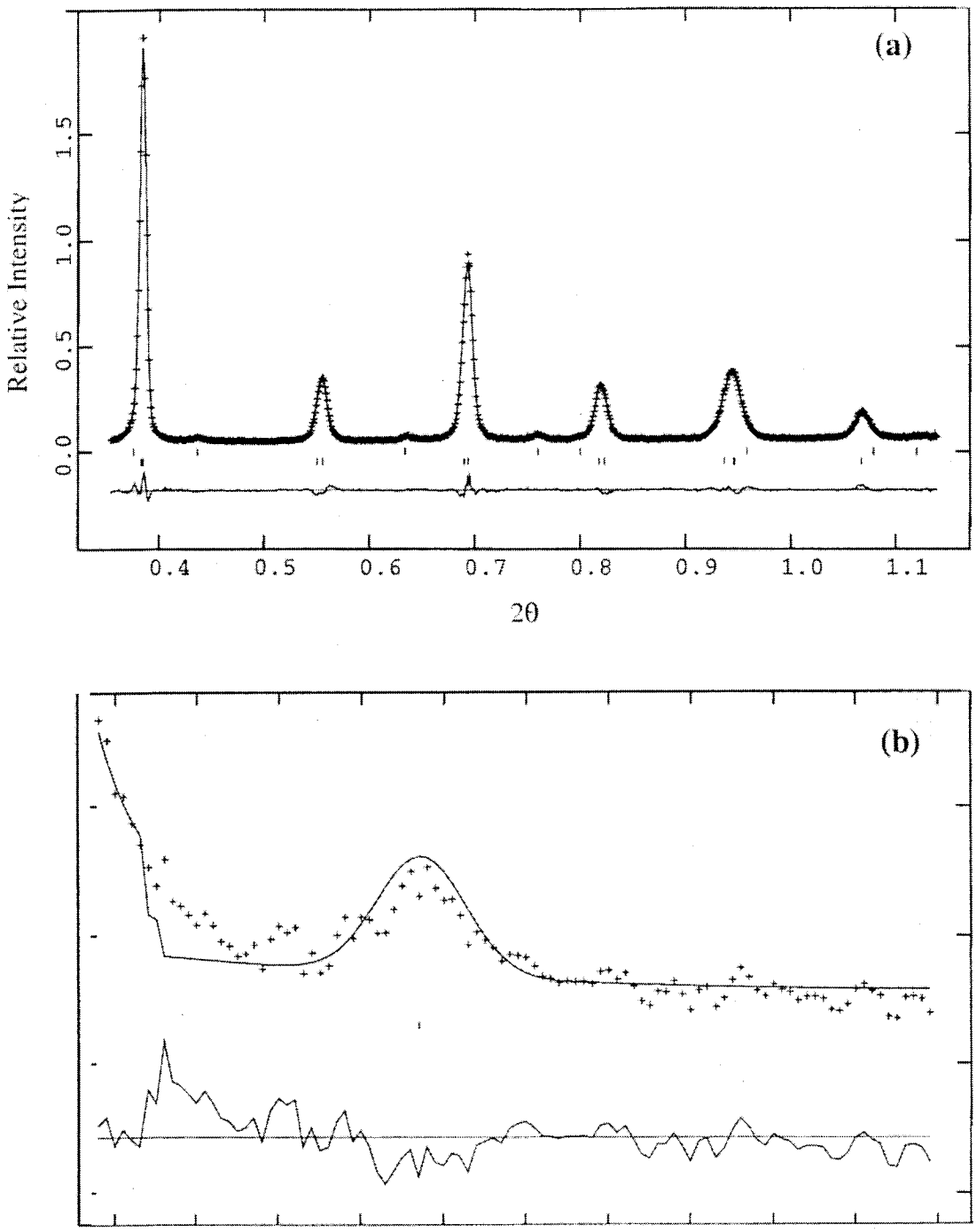

Figure 4.6 The experimental neutron diffraction profiles of 4340 steel specimen in sequence 5 (a) Crosses show neutron data points, lines show GSAS refinement (b) higher magnification view of the first austenite peak after cryogenic process

4.1.2. Hardness

Figure 4.7 shows a plot of hardness as a function of the different thermal processing sequences, 1 and 5, in which the effect of cryogenic treatment can be seen without being affected by the subsequent tempering process. As shown, performing the cryogenic treatment directly after quenching caused a slight increase in the average hardness from 54.5 HRC in sequence 1 to 55.3 in sequence 5 (before tempering). As these hardness values were obtained before tempering, the slight improvement can be attributed to the transformation of a small amount of the retained austenite to martensite. This is in agreement with the result, of the neutron diffraction experiment in which the small amount of retained austenite was reduced after cryogenic treatment.

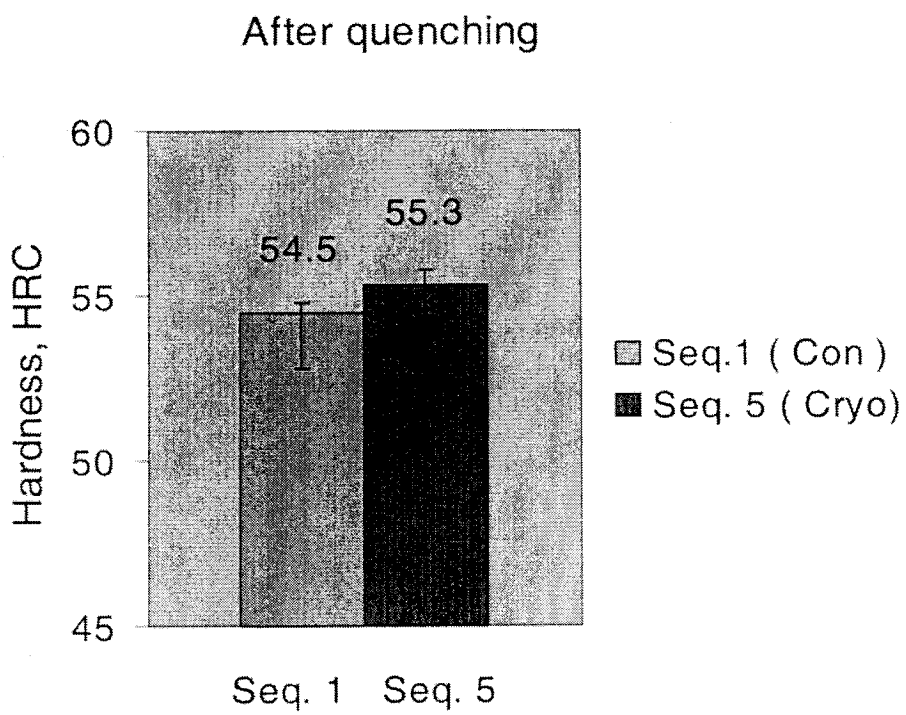

Figure 4.7 Hardness results of 4340 steel after quenching (seq. 1 and 5)

It should be noted that many researchers [42-46,7,8] have reported slight hardness improvements due to cryogenic treatment even in tool steels, in which the amount of retained austenite is much higher than the one in the present steel. In addition, some researchers [50,54] have mentioned those specimens that have undergone cryo-treatment showed almost the same, or an even lower level, of hardness compared to the conventionally quenched and tempered specimens, but other properties like wear resistance were improved. This is one discrepancy that has been observed in terms of cryogenic treatment which needs more investigation.

The effect of tempering temperature on both conventional and unconventional treatments is exhibited in Figures 4.8 and 4.9. As expected, increasing the tempering temperature decreased the hardness for those sequences, which include the tempering process (seq. 2,3,4,6,7, and 8). This is as expected as the energy supplied during tempering is sufficient to decompose the martensite to ferrite and cementite as discussed in the literature review, Chapter 2 and Figure 2.8.

When hardness is plotted as a function of tempering temperature (Figure 4.9), it can be seen that the cryogenically treated samples show a slightly higher level of hardness over the tempering temperature range compared to the conventional heat treatment (seq. 2, 3, and 4).

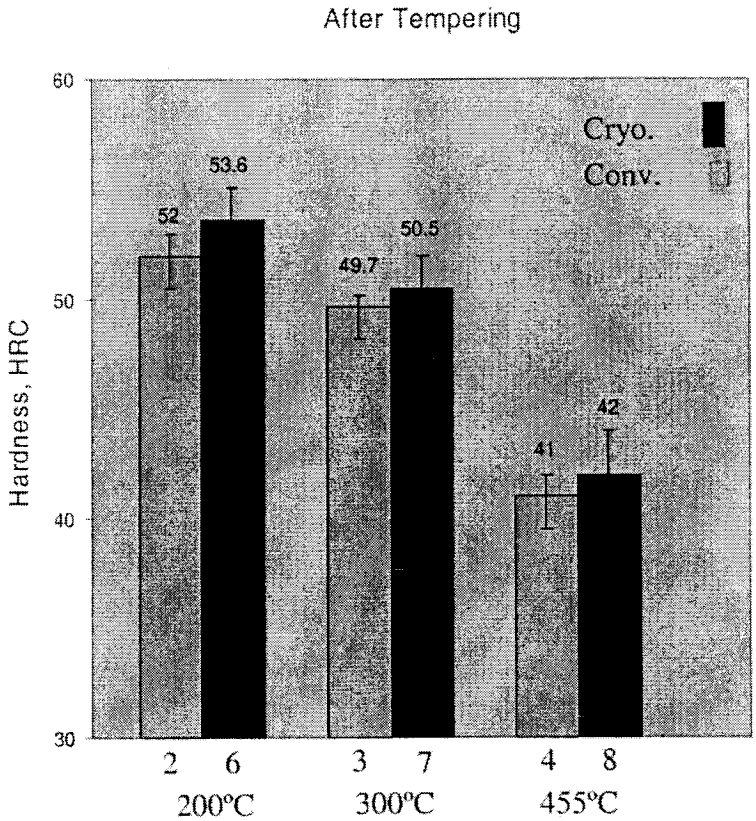

Sequences: 2, 6,3,7,4, and 8
Tempering Temperature : 200,300, and 455°C

Figure 4.8 Hardness results of 4340 steel after different tempering temperatures before and after cryogenic

As discussed in Section 2.3, two main mechanisms might have contributed to this slightly higher hardness level for the specimens with cryogenic treatment. The first is transformation of retained austenite to martensite during the sub-zero treatment. This was previously discussed as the explanation for the slightly higher hardness (seq. 1 and 5), before tempering in cryogenically hardened samples than those that had undergone conventional hardening. This increase in martensite volume fraction may also be

responsible for the increased hardness after tempering. This can be seen by comparing the neutron patterns Figures 4.1 to 4.4, based on their heat treatment sequences. It can be seen that the small peaks of retained austenite in the former have disappeared in the latter specimens due to the tempering process. Furthermore, cryogenic treatment could have encouraged carbide formation during tempering, which led to increased hardness. This needs further study comparing the volume fraction of carbides in the specimens with and without cryogenic treatment, in which microanalysis using Transmission Electron Microscopy (TEM) would be used. The task was beyond on the scope of this research.

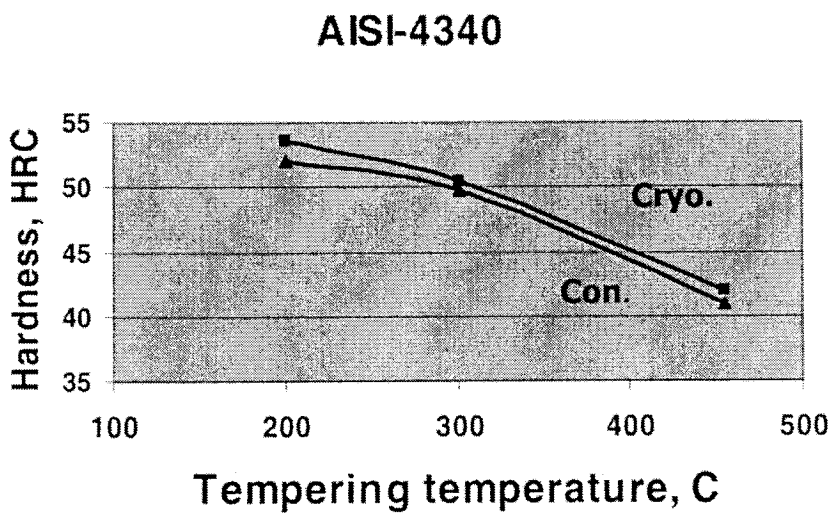

Figure 4.9 Hardness 4340 steel for different tempering temperatures after cryogenic and conventional treatments

4.1.3. Impact Energy

Figure 4.10 compares the toughness based on Charpy impact tests, of 4340 steel after being tested in two sequences (1 and 5). Similar to the effect of cryogenic treatment on hardness, an attempt was made to isolate the effect of tempering from the cryogenic process. It can be seen that the toughness of for Seq. 5, (cryogenic treatment) was 7.7 J whereas that for Seq. 1 was 10.8 J. This decrease in toughness after cryogenic treatment can be attributed to an increase in the amount of martensite that transformed from the retained austenite. In fact, the harder and so more brittle matrix, leads to the lower toughness values obtained. As was explained in the literature survey (section 4.1.2) such an increase in the amount of martensite is responsible for the higher hardness.

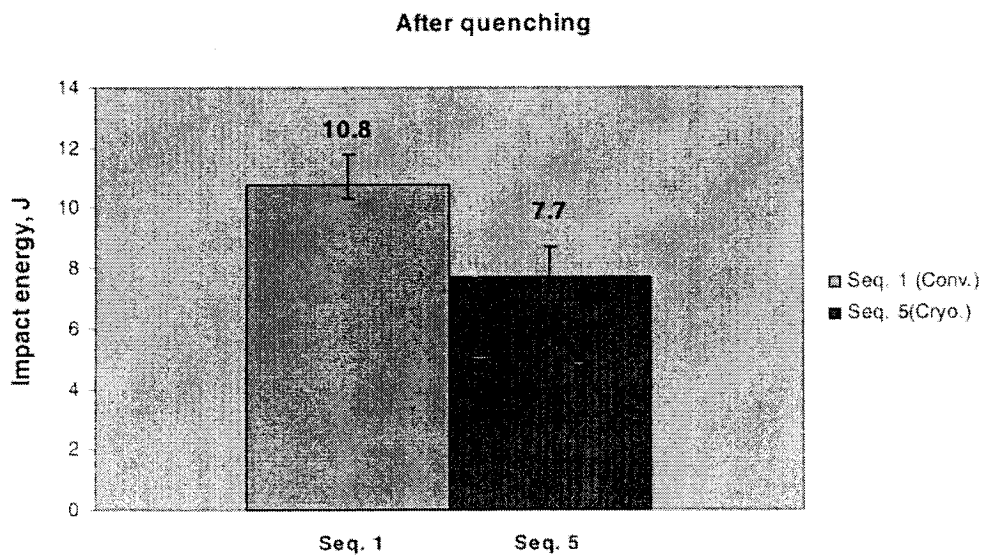

Figure 4.10 Impact Energy of 4340 steel without tempering

The effect of tempering on the toughness of specimens subjected to cryogenic as well as conventional treatments is illustrated in Figure 4.11. It is observed that for both conditions (cryo- and conv.) by increasing the tempering temperature, toughness first decreased to around 11 J at 300°C, and then increased to higher values at 455°C. This behavior is the well-known "temper embrittlement" of steel when tempered in the temperature range between 250 to 400 °C [14]. This behavior of 4340 steel with conventional treatment is in agreement with the one that has been reported in the Metals Handbook [20]. Such decomposition of retained austenite can be traced by the neutron diffraction experiments, Figures 4.1 to 4.4, in which the peaks corresponding to retained austenite disappeared after the tempering process.

Furthermore, the increase in toughness above the temper embrittlement range is due to decomposition of the secondary martensite by reducing the super-saturation of martensite, which is the main objective of the tempering process.

In addition, the results in Figure 4.11 show the effect of cryogenic treatment followed by tempering. It can be seen that toughness of the specimens subjected to cryogenic process show the same overall trend as those for conventional hardening and tempering.

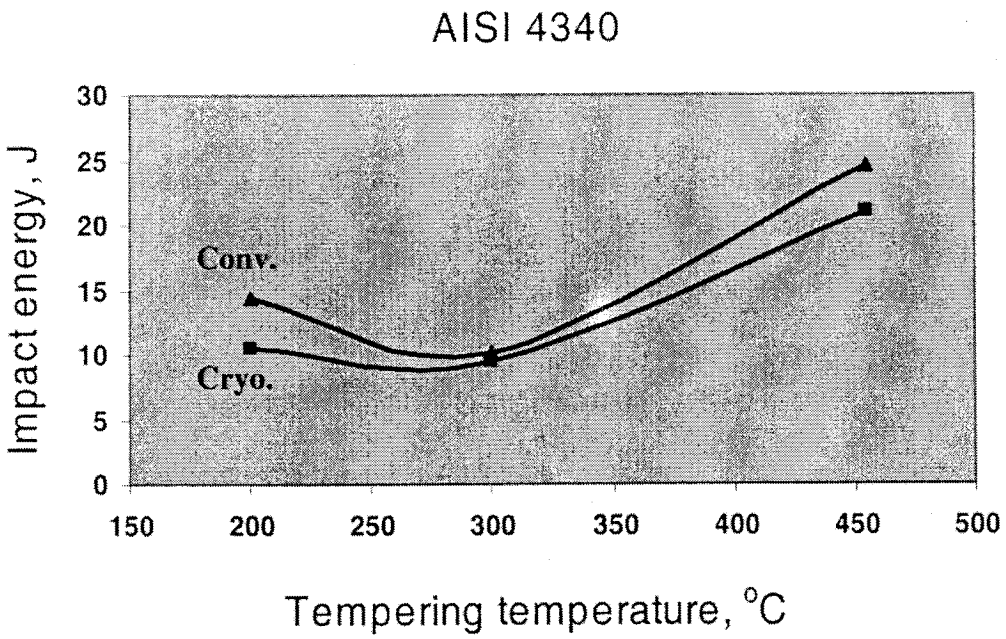

Figure 4.11 Comparison of Impact Energy of AISI 4340 Steel before and after Cryogenic processing

However, the former show slightly lower toughness than the latter over all tempering temperatures tested in this work. At the tempering brittleness temperature, around 300°C, it seems that the above-mentioned mechanism is common and also dominant for both cases, with and without cryogenic treatment. The larger differences between the two treatments happened mainly at temperatures of 200 and 455°C. At 455°C, it might be that precipitation of carbides resulted in a higher hardness in the cryogenic process which could have contributed to the lower toughness. The tempering

temperature chosen depends on the desired strength or hardness; according to tempering results in this work and other sources [20], 455°C is recommended to optimize the hardness and impact properties of 4340 steel, and this study indicates that for this tempering treatment, cryo-treatment produces a slight increase in hardness (% 2.4) at the expense of a higher % (14.3) drop in toughness.

4.1.4. Fatigue

The typical S-N curves (Stress-Cycle plots) of the 4340 steel, with and without cryogenic treatment, and tempered at 455°C and 200 have been plotted from the experimental results and can be seen in Figures 4.12 and 4.13, respectively.

Normally, the S-N curve is the mean curve drawn of the data points [19, 72]. After applying a load (stress) below the static strength, the specimens require a significant number of loading cycles until failure. The S-N curves are expressed in terms of values of σ_N, the fatigue strength at N cycles. There was some scatter in fatigue data, which is a difference in the measured N values for a number of specimens that were tested at the same stress level. The scatter in results is due to the fatigue sensitivity to a number of test and material factors that are very difficult to control precisely. These factors consist of specimen manufacturing and surface preparation, specimen alignment in the apparatus, mean stress and metallurgical variables such as strength level, ductility, residual stress and cleanliness [19, 72].

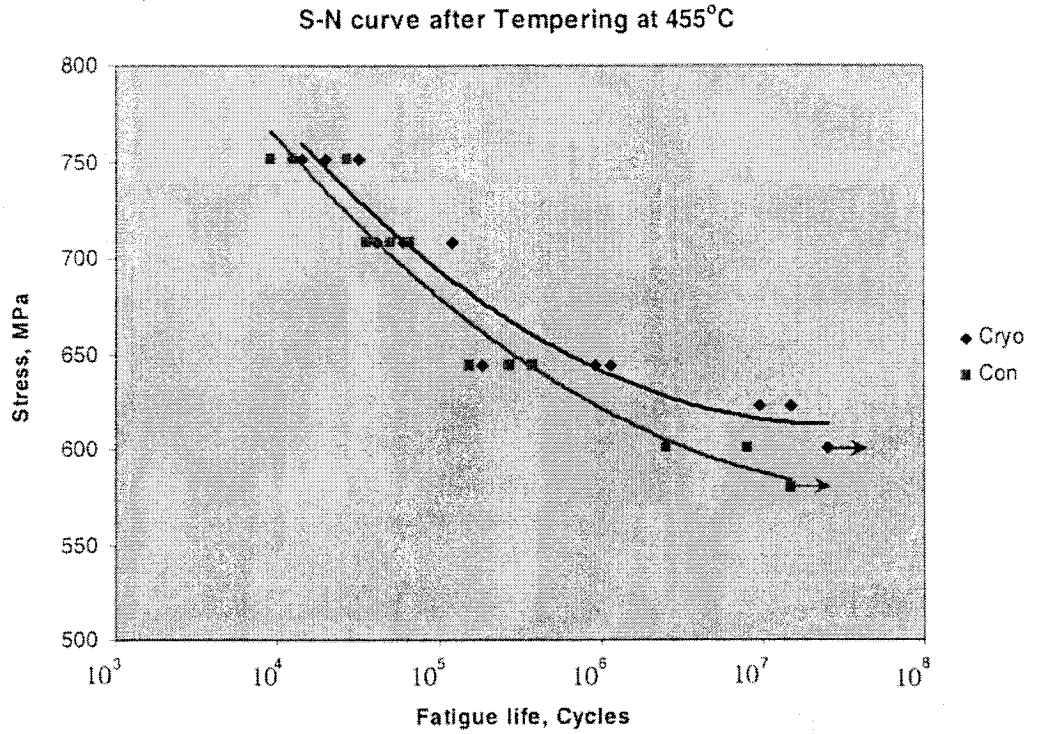

Figure 4.12 S-N curves with and without Cryogenic treatment with tempering at 455°C

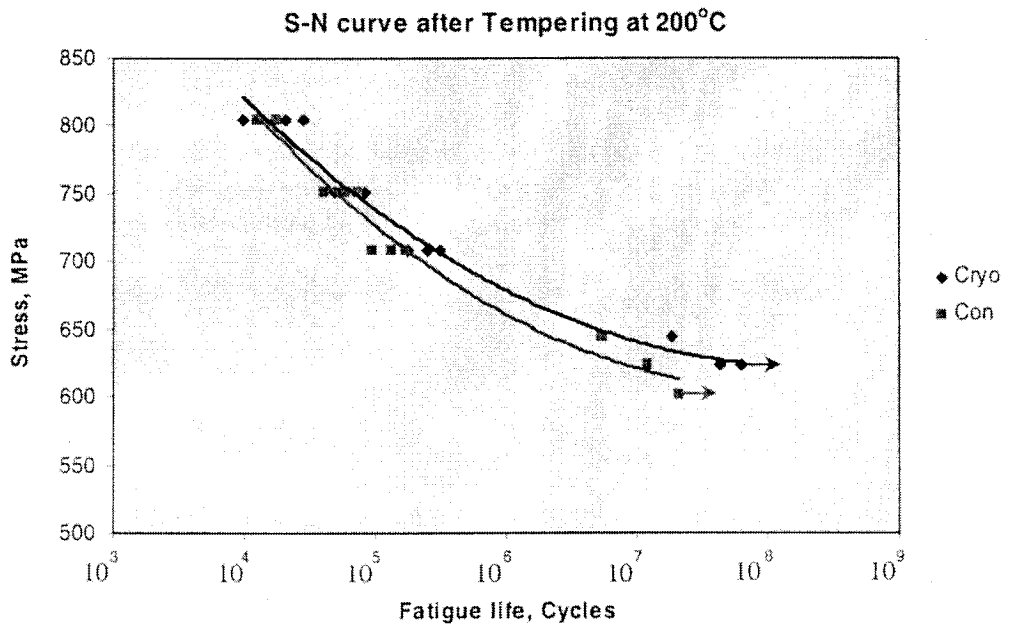

Figure 4.13 S-N curves with and without Cryogenic treatment with tempering at 200°C

The curves, as expected, show that by decreasing the stress, the number of cycles to failure is increased. However the data points of the fatigue test of 4340 steel indicate the presence of an endurance limit or fatigue limit as can be seen by arrows in above figures. It is generally thought [19] that for ferrous alloys (iron-based), the S-N curve becomes horizontal at higher N values. A part which is never stressed above this level should have infinite life (assuming no stress concentrations, defects etc exist). In addition, in both plots, the specimens that underwent cryogenic treatment showed slightly higher fatigue stress levels than those without this treatment.

This behavior of the steel should be related to the variables, which affect the fatigue behavior of engineering materials. Some of these factors as reviewed in the literature [19, 72] include mean stress level, geometrical design, surface effects, and metallurgical variables. All the above – mentioned variables were the same for all specimens, however the difference between the cryo-treated specimens and the conventional quenched - tempered ones, can be attributed to the primary metallurgical conditions of these two types of specimens. It has been reported so far that increasing the strength of steel due to any heat treatment or alloying addition, can lead to an increase in the fatigue life [73]. It was discussed in the previous sections that specimens subjected to the cryo-treatment showed slightly higher hardness, most probably because of transformation of retained austenite to martensite. The improvement of fatigue life can also be related to this metallurgical factor, i.e. that the hardness of cryo-treated specimens is higher than that of those conventionally treated.

As mentioned in the literature review, fatigue failure consists of three stages, with the first one being initiation of a crack in the metal. In this regard, it seems that by

increasing the strength of the steel under study by the cryogenic treatment, initiation of fatigue cracks is more difficult and crack grown is also hindered. The small amount of retained austenite, as measured by neutron diffraction experiments, in the conventionally treated specimens, can also lead to inhomogenites of microstructure on the surface, which may have resulted in a lower fatigue stress level for this set of specimens.

On the other hand, it has been reported that strength and ductility have different effects on the fatigue behavior of medium carbon steel. At cycles less than 10^3, the ductility effect is dominant in such a way that the higher ductility gives higher fatigue life, whereas at higher cycles than 10^3, higher hardness and strength can lead to higher fatigue life, i.e. hardness effect is dominant [73]. As exhibited in Figure 4.12, at increasing numbers of cycles, the difference between cryo-treated and conventional quenched and tempered specimens is higher. It should be noted that all fatigue experiments have been carried out at stress levels giving at least 10^3 cycles to failure.

In addition, the effect of tempering temperature on the fatigue resistance can be seen by comparing Figures 4.12 and 4.13. It can be seen that by increasing the tempering temperature from 200 °C to 455 °C, the fatigue resistance has been decreased. It has been reported [73] that the fatigue resistance of steels is generally proportional to hardness and tensile strength, and the results support this.

Another factor affecting fatigue resistance between cryogenic and conventional treatments is the percentage of martensite for the same strength. It has been reported that "For specimens having comparable strength levels, resistance to fatigue depends somewhat on microstructure. A tempered martensite structure provides the highest fatigue limit. However, if the structure as-quenched is not fully martensitic, the fatigue

limit will be lower (Figure 4.14)" [73]. In this regard some fatigue tests were carried out following the schedule shown in Table 4.5 for different sequences (1 and 5) which are in agreement of above mentioned survey. Quenched-cryo specimens (Seq. 5) had significantly higher fatigue resistance than those specimens that has been quenched conventionally (Seq. 1).

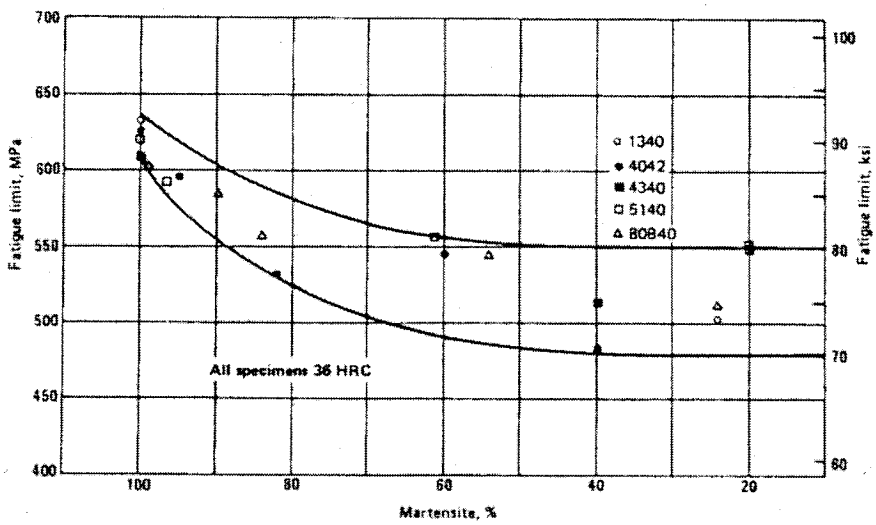

Figure 4.14 Effect of martensite content on fatigue limit. Data are based on standard rotating-beam fatigue specimens of alloy steels. [73]

Table 4.5. Results of individual fatigue tests of 4340 steel

	Load=708 MPa	Load=687 MPa	Martensite %
Cryo. (Seq.5)	6,880,000 cycles	50,182,100 cycles	95.7
Con. (Seq.1)	3,125,000 cycles	8,984.500 cycles	94.3

Overall, the mechanical tests showed that the hardness and fatigue resistance of the cryogenically treated 4340 steel, in general, were a little higher than those of conventionally treated steel. However, the toughness of the cryogenic treated steel was lower when compared to that of the conventionally treated steel.

4.1.5 Microstructure

4.1.5.1. Decarburizing test

As most of the experiments performed were dependant on the surface condition of the specimen (as explained in Chapter 3), provisions were made to avoid such variations in the specimen surface. In this regard, before starting the tests, trial experiments were made to ensure that in the hardening treatment, and especially during heating of specimens in the furnace, no decarburization had taken place. Figure 4.15 shows the microstructure of the cross section of a specimen austenitized and oil-quenched under argon protective gas. The whole structure showed a typical martensite structure with no apparent sign of decarburization close to the edge of specimen, as no ferrite or pearlite were observed. According to ASTM standard [74] for estimation of the depth of decarburization of steel, occurrence of this phenomenon up to a limited level is acceptable in terms of mechanical properties. However, Figure 4.15 shows that the heating process successfully prohibited this detrimental phenomenon. In addition, the microhardness profile starting from the edge toward the center of the cross section area showed only small variations, implying that a uniform microstructure (which was mostly martensite) extended from the edge to the center of the specimens.

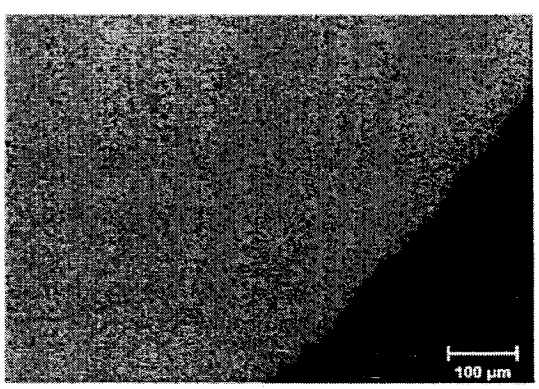

Figure 4.15 Heat-treated 4340 steel microstructure (Fully Martensitic) with no apparent decarburization

4.1.5.2. Optical microscopy

Using optical microscopy, a lath martensitic structure was observed (Figure 4.16), which is the typical structure of the steel with a carbon content less than 0.5 %. Also, Figures 4.17 (a) and (b) compare the microstructures of the 4340 steel specimen before and after cryogenic processing. As can be seen, no apparent difference could be seen between these two pictures. This is partly because of the traditional difficulty to distinguish between martensite and retained austenite and also the small amount of retained austenite present in this steel. This led the study in the direction of employing another method, neutron diffraction, to quantitatively analyze the phases constituting the microstructure. This was explained in detail in section 4.1.1.

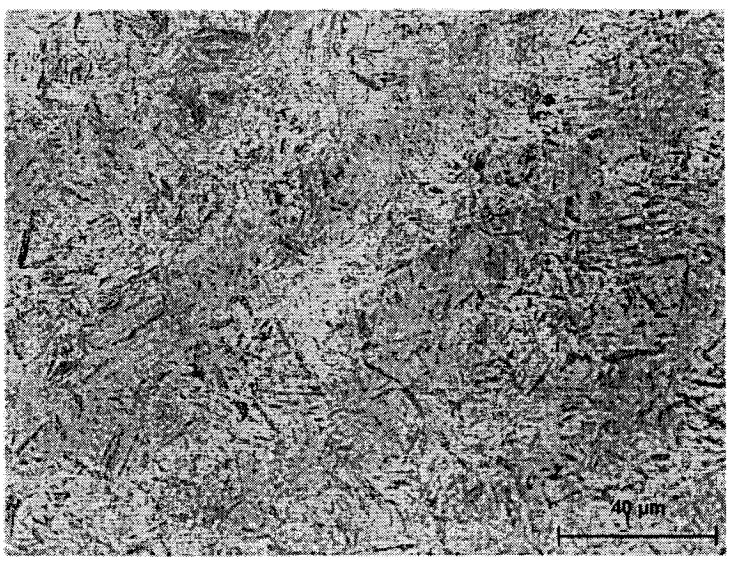

Figure 4.16 Tempered martensite of AISI 4340 steel quenched in oil from 845°C and tempered at 200°C

(a)

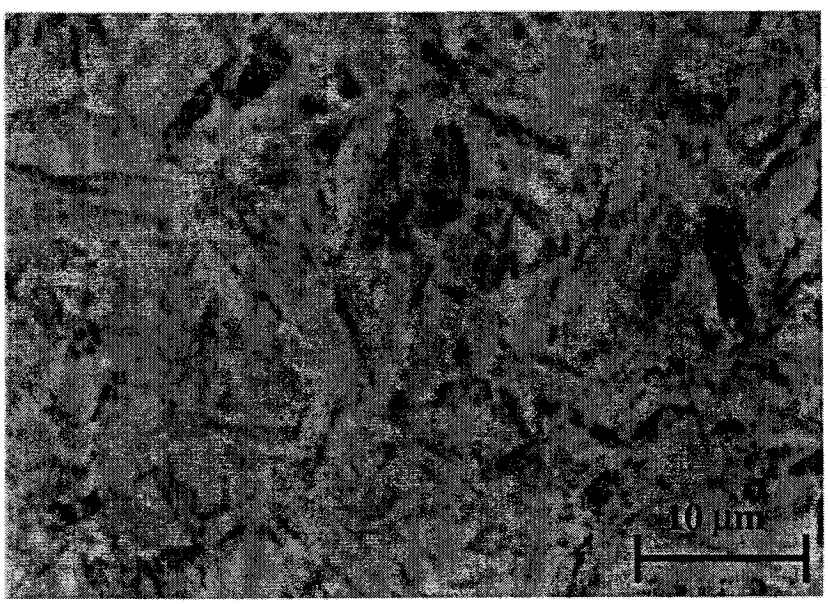

(b)

Figure 4.17 Microstructure of 4340 steel with tempering 455°C
(a) Cryogenic (b) Conventional

4.1.6. Fractography

Many types of fracture happen by a process involving crack initiation, crack propagation and fast fracture. Figure 4.18 shows the fracture surface of a fatigue test sample that is divided in to two different areas (K and M). K is the fatigue crack propagation area and M is the fast fracture area that is the remaining cross section that can no longer support the applied load. A series of locations at the outside surface were the sites for crack initiation and these then grew into one dominant crack that grew across the cross-section. These fractographs can lead to an understanding of fracture initiation and propagation, but regarding the effect of the cryogenic treatment on the fatigue behavior, no significant differences can be observed between the cryogenic and conventional samples. Figure 4.19 shows the crack propagation area of a fatigue surface of 4340 steel.

Another type of fracture surface that was examined in this work was those from the Charpy tests. Figure 4.20(a) shows the Charpy fracture surface of 4340 steel, heat treated cryogenically, which has a smaller area of shear (P region) than the specimens which underwent conventional treatment, Figure 4.20(b). As reported in Section 4.1.3, the Charpy impact results for 4340 steel cryo specimens were less than those which were treated conventionally. It has been reported [72] that a higher ratio of "P" to "S" areas is an indication of higher ductility. Therefore the conventionally treated specimen, with higher toughness, has a larger area of P than the cryo specimens. Figure 4.21 shows a higher magnification of this P area in the same specimen as shown in Figure 4.20(a).

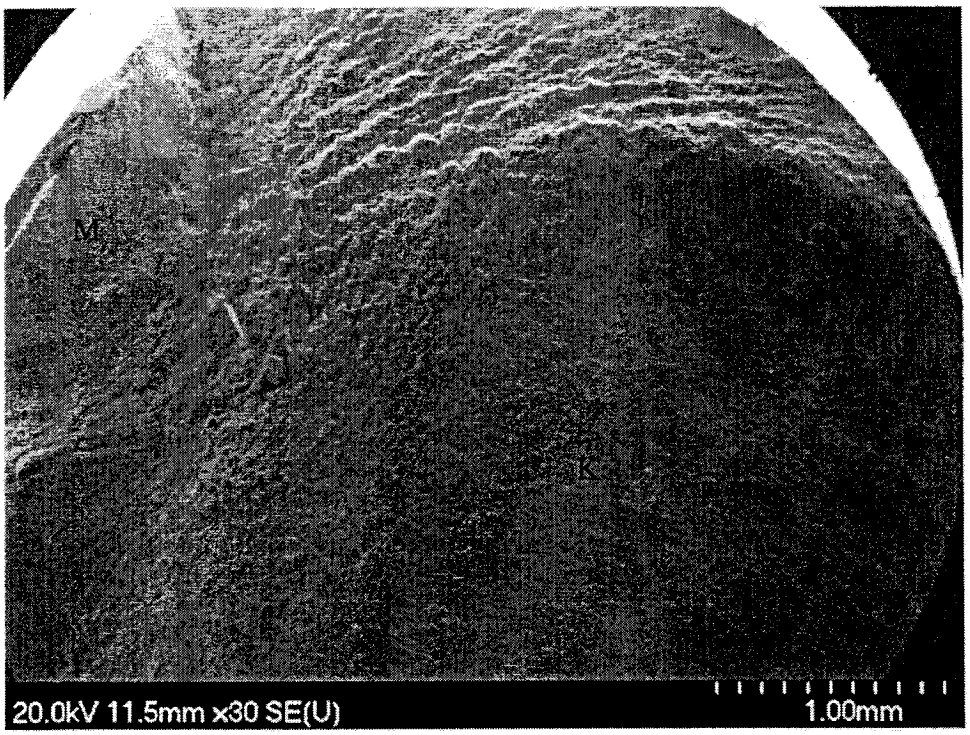

Figure 4.18 Surface of fatigue fracture of 4340 steel heat treated conventionally, the region of final fast fraction is at M and area of propagation of crack is K.

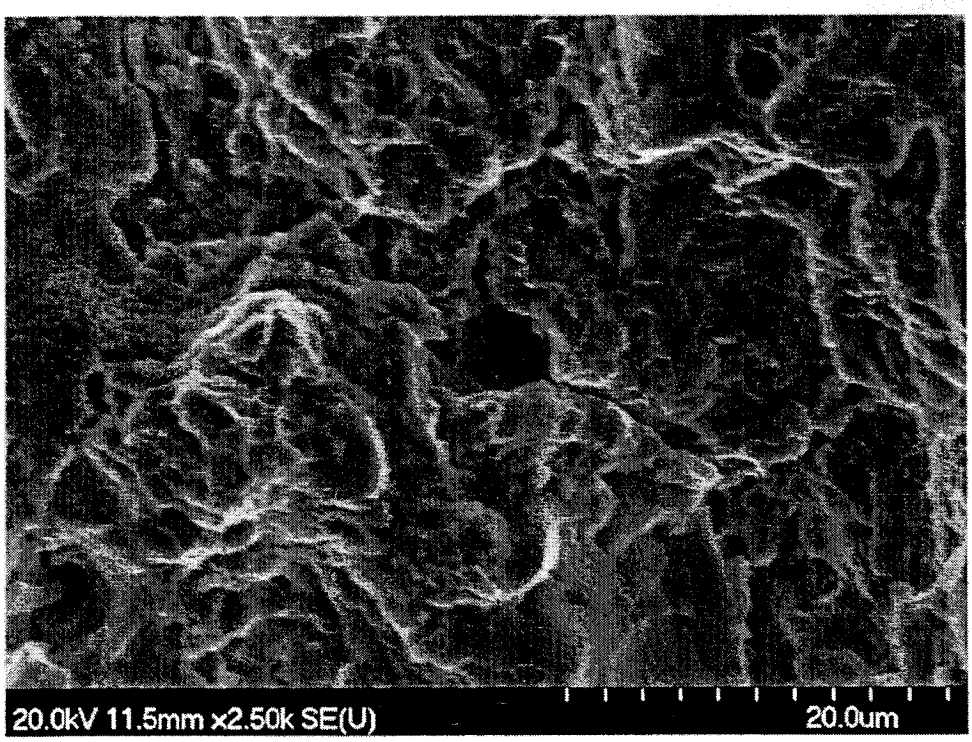

Figure 4.19 Higher magnification view of K region of the fatigue fracture surface of 4340 steel heat treated cryogenically

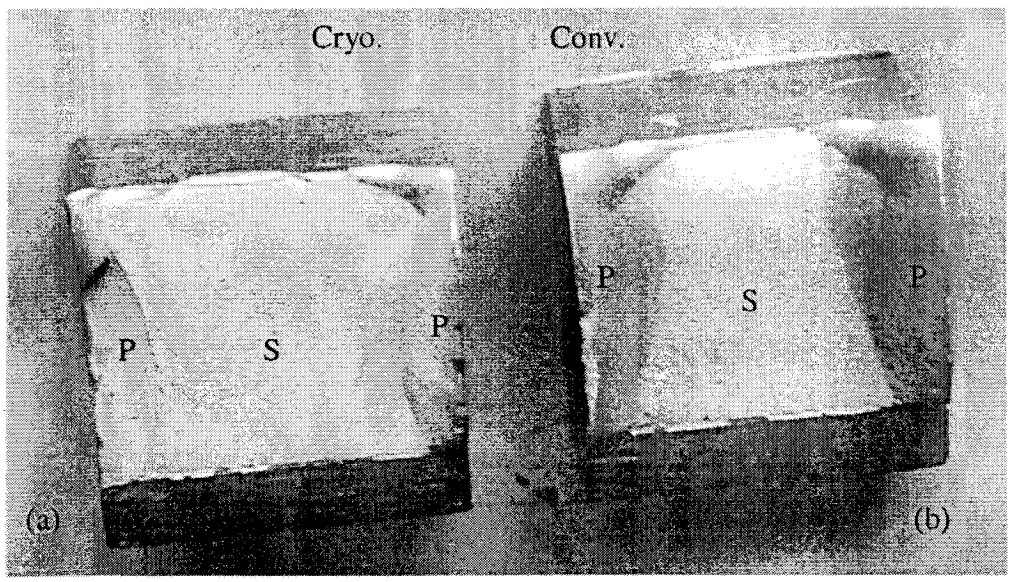

Figure 4.20 the view of Charpy fracture surface of 4340 steel heat treated (a) Cryogenically (b) Conventionally, "P" and "S" regions are shown.

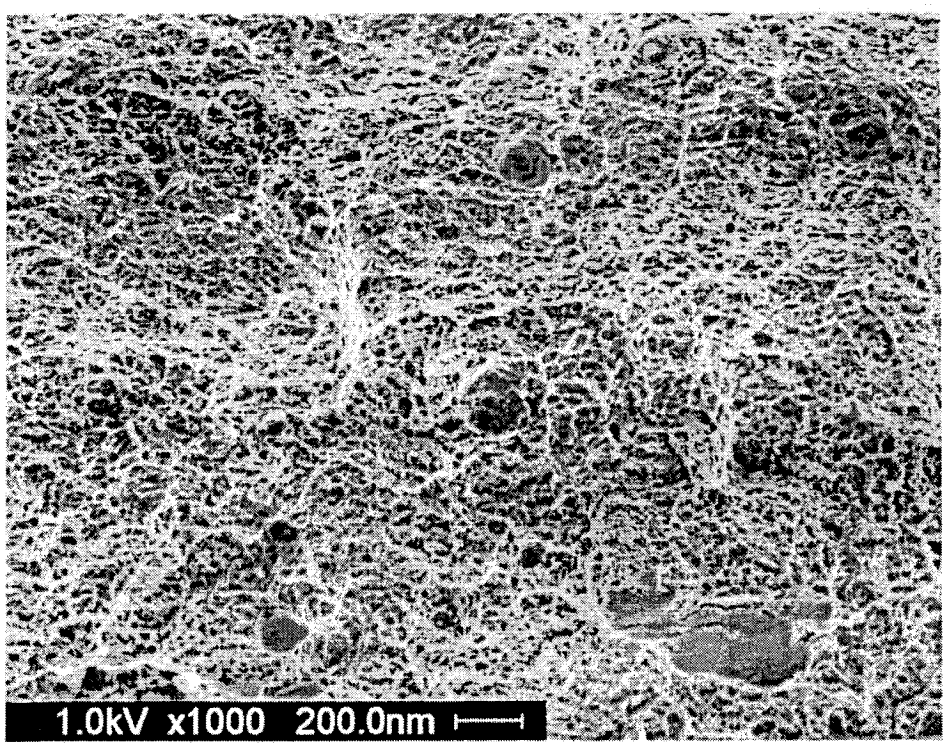

Figure 4.21 Higher magnification of Figure 4.20 at "P" area that shows large and small dimples

4.2. Aluminum alloy 7075

4.2.1. Microstructure

4.2.1.1. Optical microscopy

Comparison between the specimens that underwent the conventional T6 treatment and those that had the cryogenic treatment (sequences 1 and 2 in Section 3.5) was first performed by microstructural examination as shown in Figures 4.22 and 4.23, respectively. According to the typical microstructure of 7xxx series aluminum alloys and the primarily evaluations of the above-mentioned micrographs, the microstructure consists mainly of aluminum solid solution as the matrix. It has been shown that when the content of alloying elements exceeds the solid-solubility limit, the alloying element produces a "second phase" that may consists of either the pure alloying ingredient or an intermetallic compound phase [75]. The dark islands in the Figures will be the typical second phases existing in this type of Al alloy, such as $(Fe, Cr)_3 SiAl_{12}$, Cu_2FeAl_7, Mg_2Si, $CuMgAl_2$, Mg (Zn_2, AlCu), and $Cr_2Mg_3Al_{18}$ [76,77]. Visually comparing these two microstructures, it can be seen that the amount, as well as the distribution of the second phases, have been increased for the specimen which underwent cryogenic treatment, compared to the conventional T6 treated specimen.

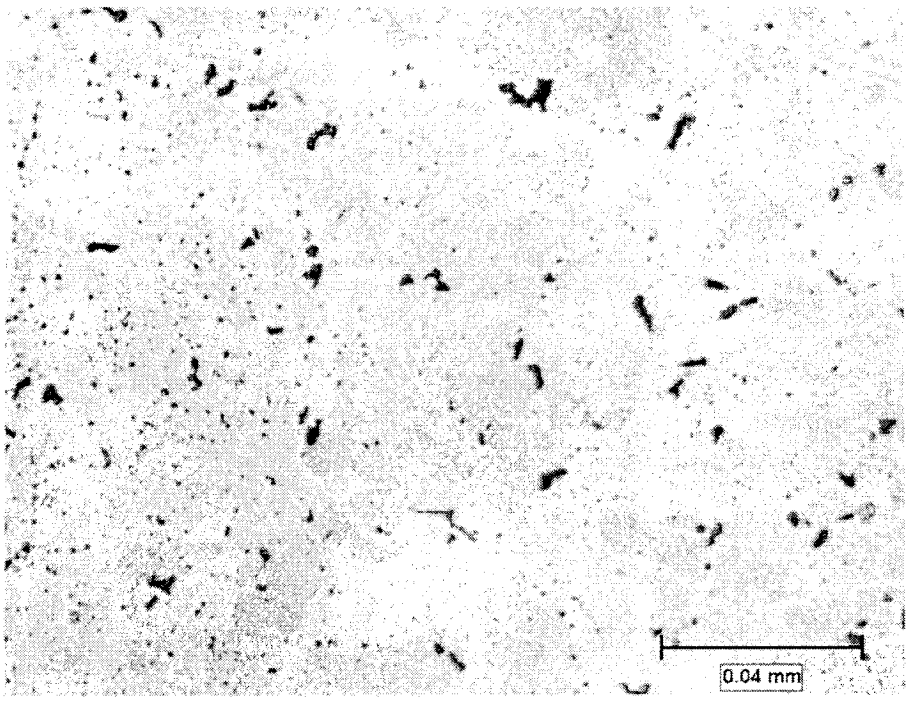

Figure 4.22 Optical micrograph of alloy 7075-T6 (Seq.1)
Precipitated fine particles (second phases) in matrix

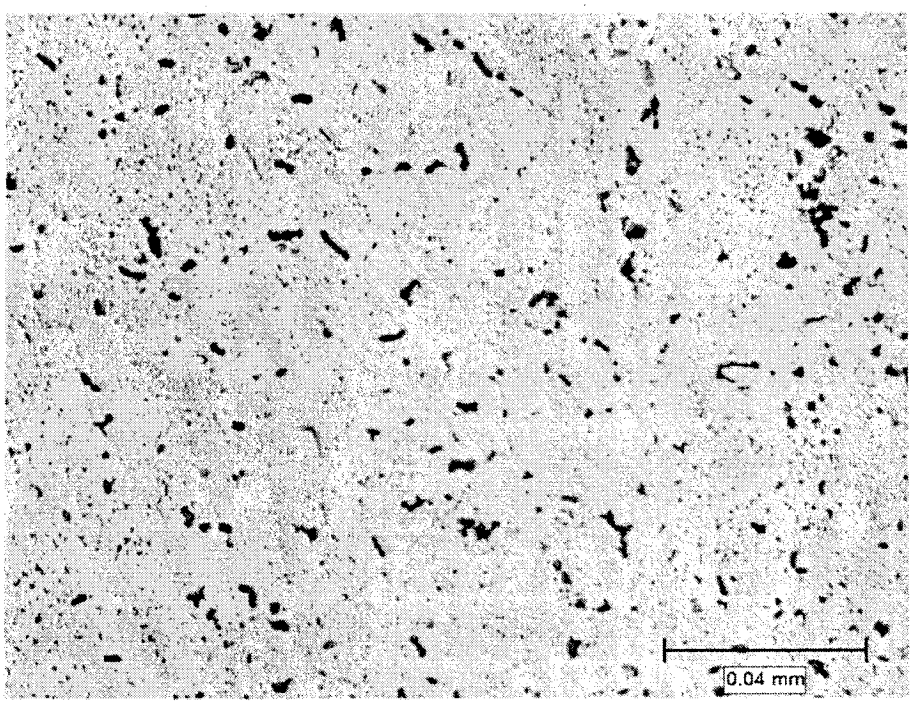

Figure 4.23 Optical micrograph of alloy 7075-Cryo (Seq.2)
Precipitated fine particles (second phases) in matrix

Further studies were performed to have a more accurate estimation of the second phases by means of image analysis as outlined in Section 3.7.1.2. The histogram in Figure 4.24, exhibits the volume fraction of the second phases for the two sequences, 1 and 2, at a magnification of 500X. It can be seen that the average volume fraction of the second phases in Seq. 2 are higher than that of Seq. 1, over the ten random selected fields.

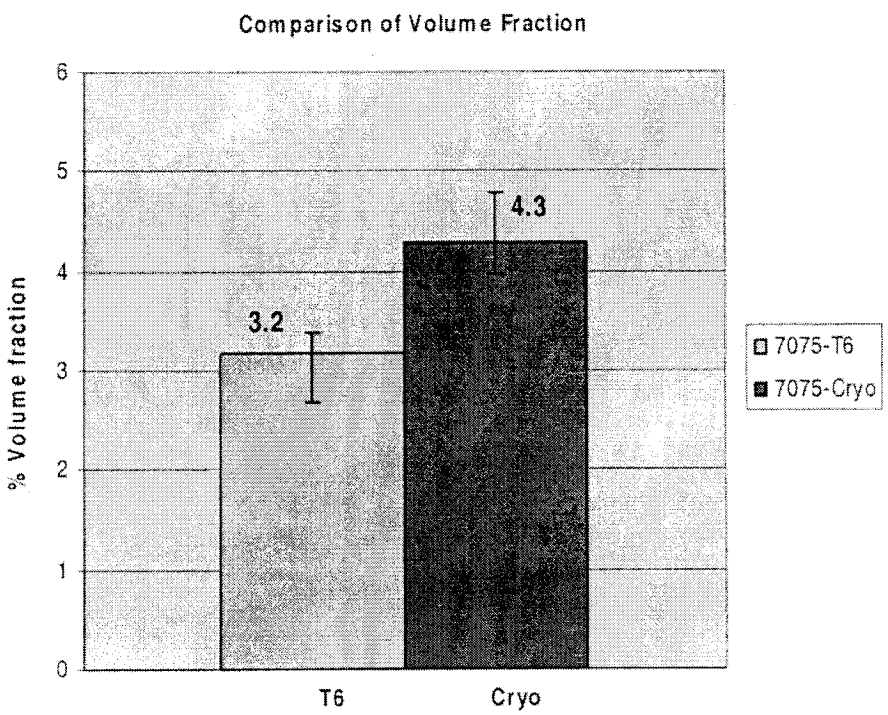

Figure 4.24 Second phase volume fraction in Aluminum alloy 7075 before and after cryogenic process

Overall, the average volume fraction of second phase in the cryo samples is 4.3 % compared to 3.2 % for the conventional material.

4.2.1.2. Backscatter Electron Spectroscopy

In order to have a better contrast between the particles and the matrix, back-scattered electron imaging (BSE) was employed. Figures 4.25 and 4.26 show the BSE pictures for two selected specimens, T6 and cryogenic treatments, respectively. It can be seen from the pictures that a particle–matrix microstructure similar to the optical microscopic pictures exists. In addition, the BSE pictures indicate that different types of particles are distributed in the matrix. These can be distinguished by the contrast between the different particles, indicating different compositions. Using higher magnification, it is also apparent that the same particle may comprise two or more phases, Figure 4.27.

4.2.1.3. Microanalysis of particles

It was deemed useful to characterize the above-mentioned particles in order to determine the effect of cryogenic treatment on the type of particles. However, it should be noted that many authors have reported that the structure of the second phases in the 7xxx series of Al alloy is very complicated and difficult to recognize [78,79].

This is due to the fact that the precipitation mechanisms in these alloys are not simple; as mentioned in the literature review, during this process several metastable phases are nucleated. There are several factors that can be chosen for analysis, and this choice will dictate the techniques used. This information includes size, volume fraction, crystallographic structure, chemistry and distribution in space. In this section, a linkage with other sections is attempted by choosing appropriate experimental techniques for characterizing second phases of aluminum alloy 7075 before and after cryogenic processing.

Electron Dispersive Spectroscopy (EDS) was used to chemically analyze the particles. Figure 4.28 shows the BSE of one of the complicated particles. The result of EDS analysis is shown in Figure 4.29, where the total elements found in this area have been determined. Elements such as Al, Zn, Mg, and Cu are the most important constituents that can be verified in this graph. Other minor elements such as Fe, Cr and Si also exist in this sample area.

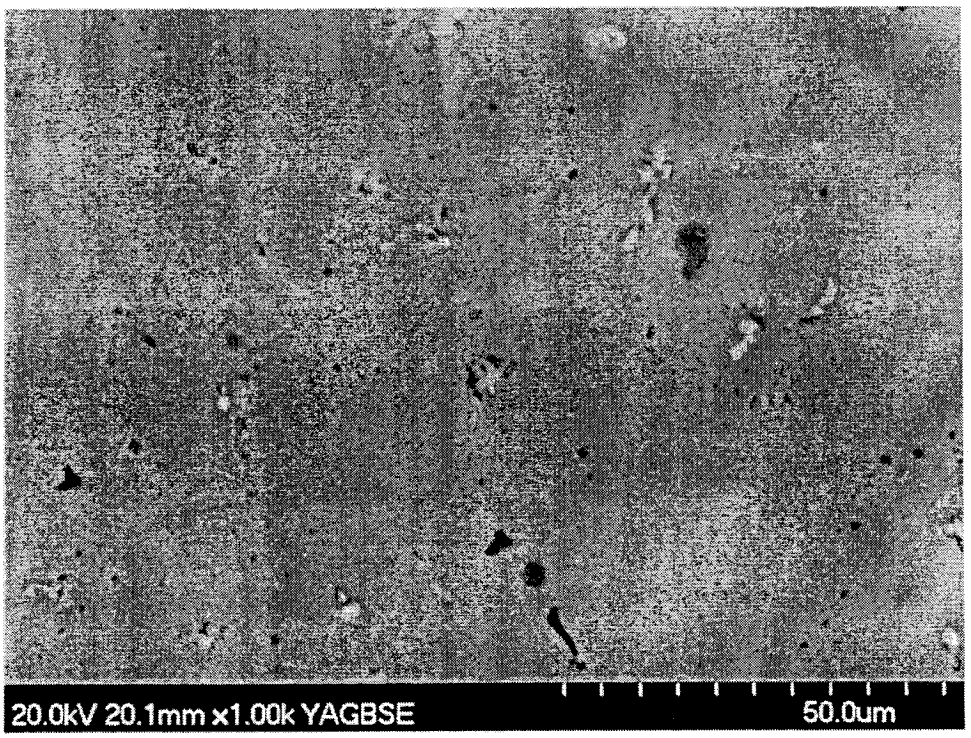

Figure 4.25 SEM backscatter micrograph of Al 7075-T6 (second phases)

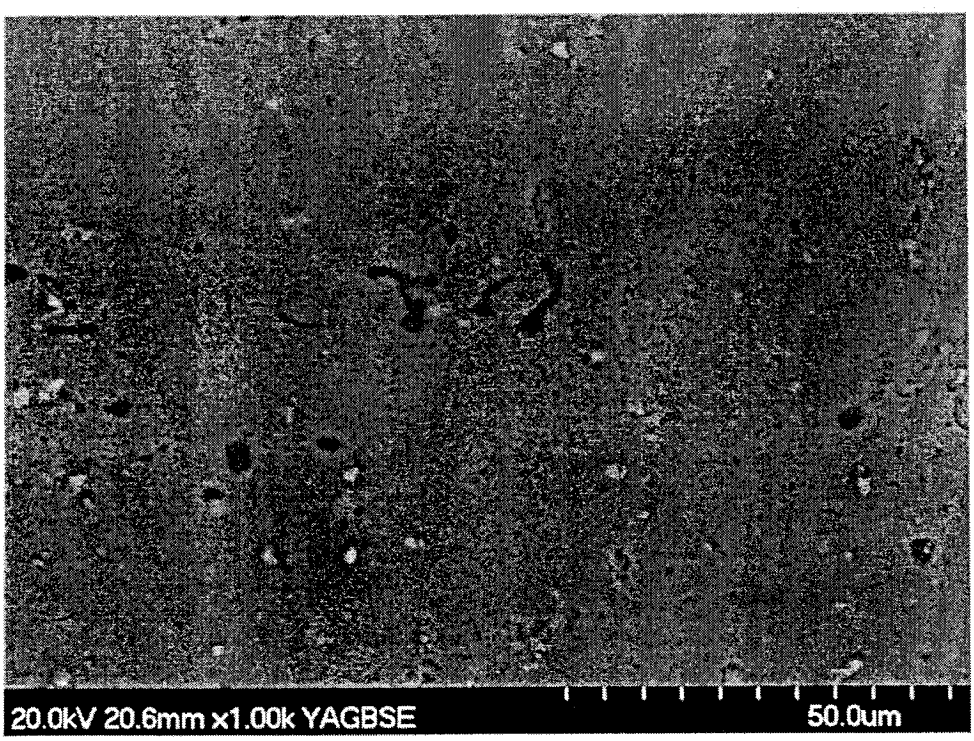

Figure 4.26 SEM backscatter micrograph of Al 7075-Cryo

It should be mentioned that these chemical analyses were carried out on some other particles with almost similar results. The various elemental maps of composition of the area shown in Figure 4.28 are exhibited in Figure 4.30. From this picture, it seems that the central part of this complex particle contains Al, Cu and Fe, Figure 4.30 (a), (b) and (g), respectively. The particle also contains Mg and Zn, Figure 4.30 (c) and (d), respectively. It should be mentioned that evaluation of all the complicated second phases in these Al alloys need more extensive studies probably by means of Transmission Electron Microscopy (TEM) accompanied by x-ray microanalysis, which was beyond the scope of work of this research. This can be continued as future work following this research.

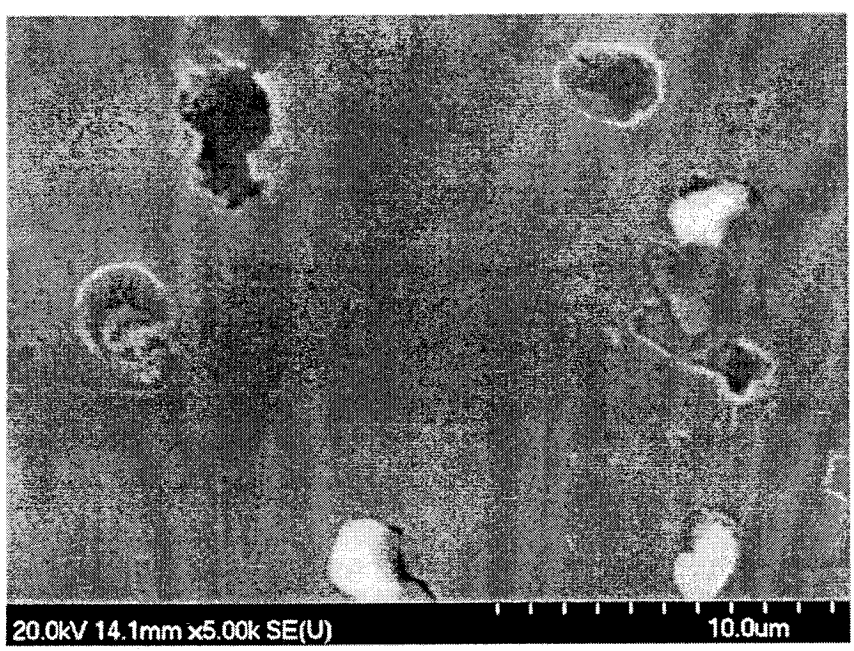

Figure 4.27 SEM backscatter micrograph of Al 7075-Cryo (diversity of second phases)

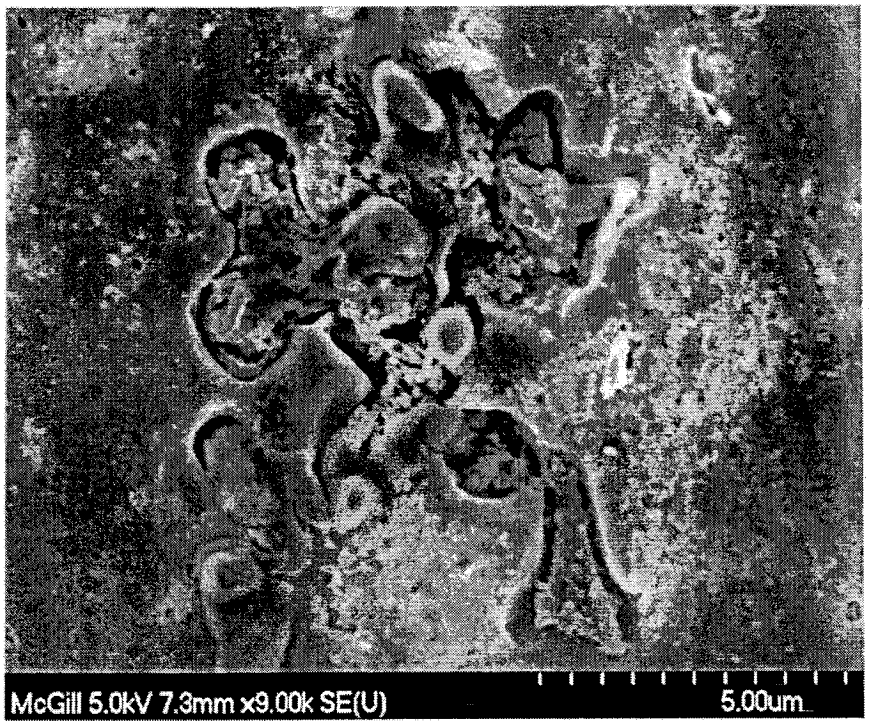

Figure 4.28 SEM backscatter micrograph of Al 7075-Cryo at higher magnification of a complex shaped second phase

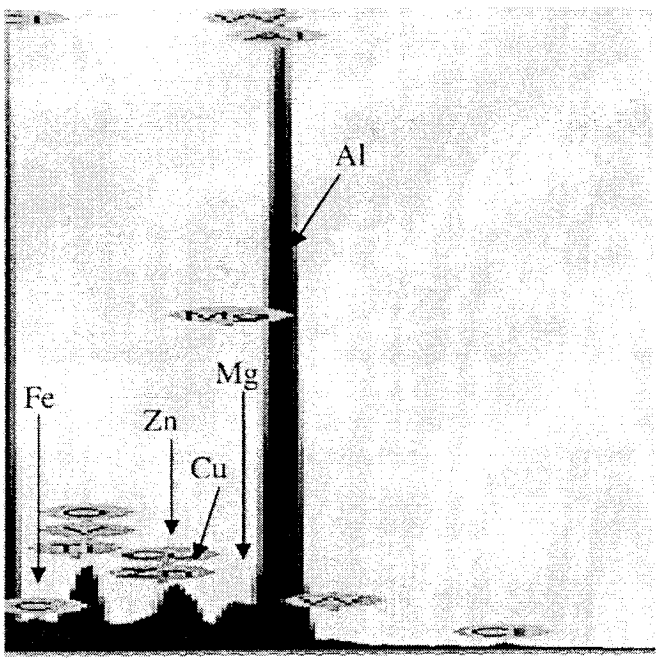

Figure 4.29 Detected peaks by microanalyzer of above second phase

However, "a qualitative analysis is often sufficient to enable the determination of the phase type, in systems where these are well known and characterized" [78]. For instance, it has been proved so far that if someone finds Fe, Cu and Al in a second phase particle in a 7xxx series Al alloy, as shown in Figure 4.30, the particle is Al_7Cu_2Fe [78]. $MgZn_2$ is other main phase that is expected to be found in this type of Al alloy [80], which is detected also in the map analysis in Figure 4.30.

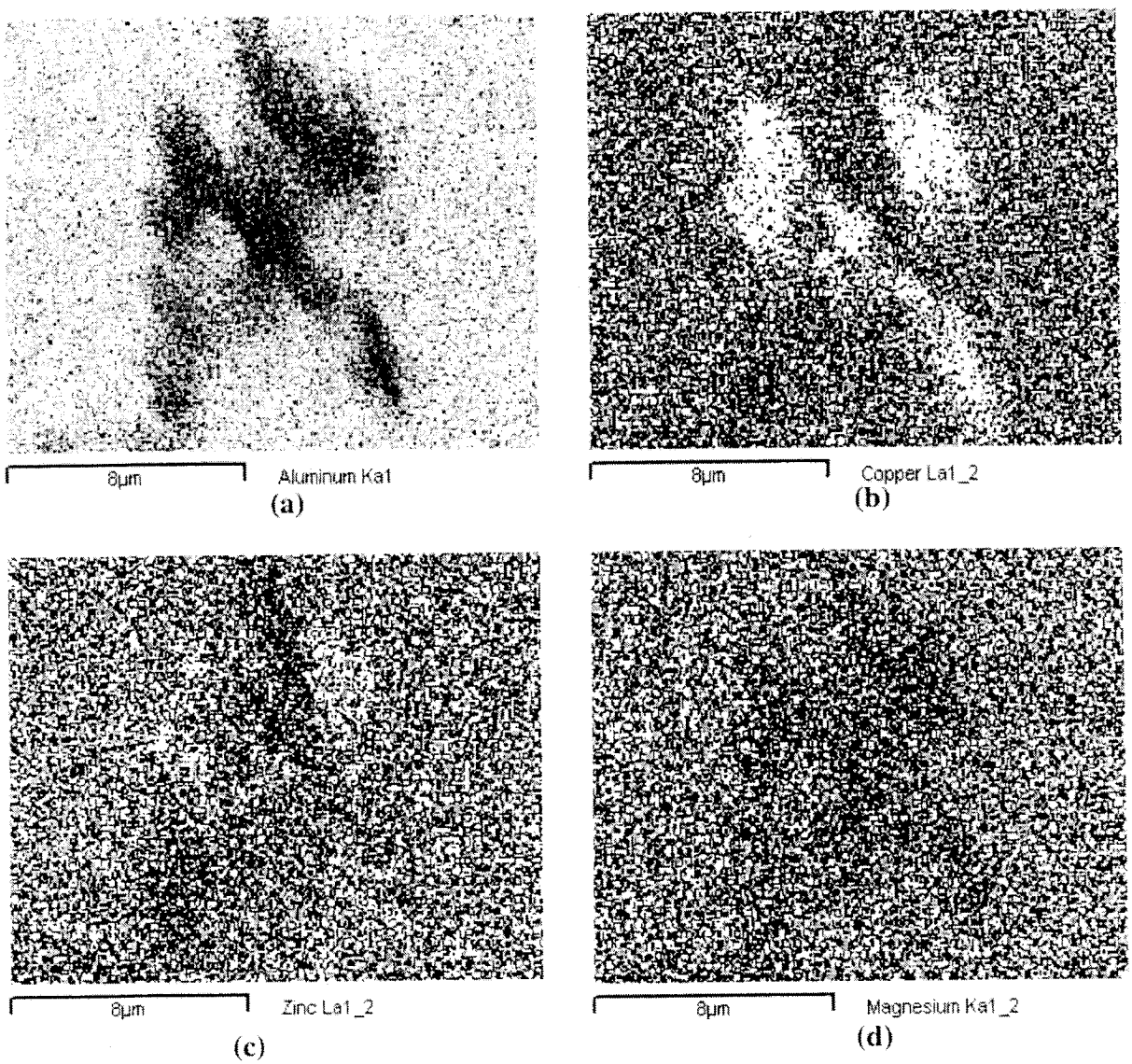

Figure 4.30 Chemical characterizations of a second phase particles in Al alloy 7075-cryo

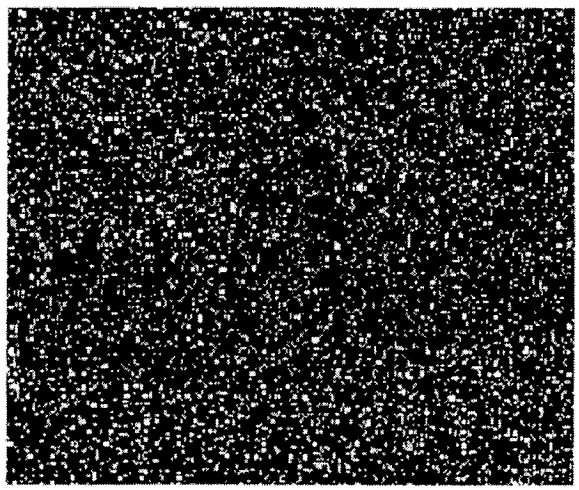

(e)

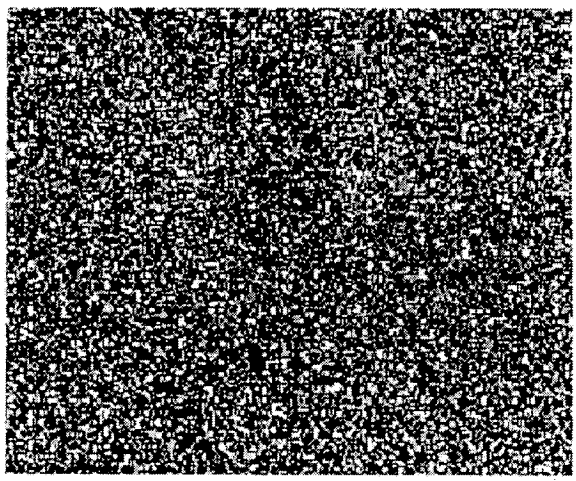

(f)

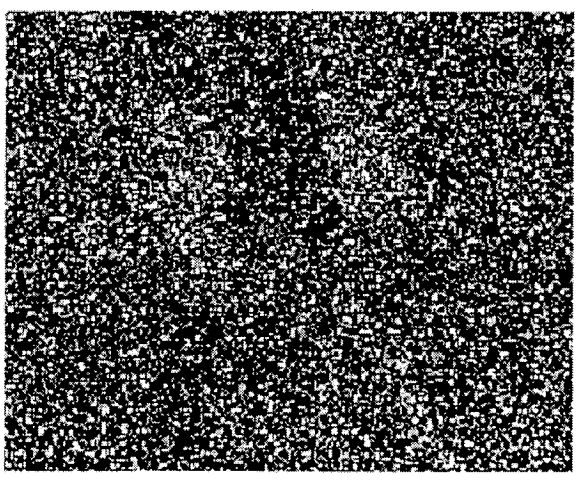

(g)

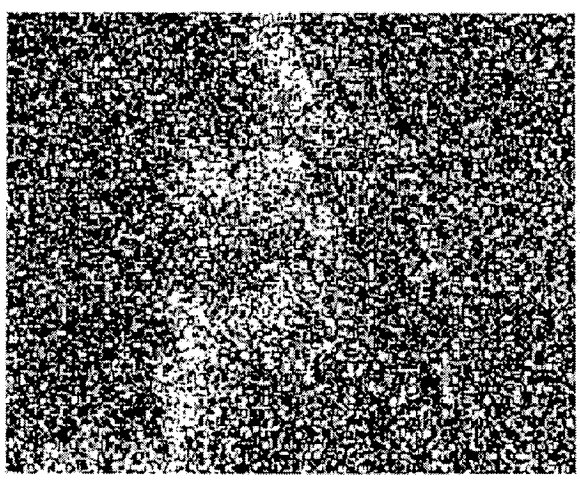

(h)

Figure 4.30 cont.

4.2.2. X-ray Diffraction (XRD)

The diffraction patterns from the XRD experiments for the specimens that underwent T6 and cryogenic treatments (Seq. 1 and 2) are shown in Figures 4.31 and 4.32. By considering the well known second phases of Al alloy 7075, as mentioned in section 4.2.1, it is possible to find space group numbers (PDF number) and lattice parameters for the second phases from main sources about compound identification such as the "Pearson Handbook" [81] and by inputting this data into programs such as GSAS and "Powder Cell" [82] it is possible to extract a pattern for each compound, which is similar to an XRD result, showing peak intensity versus 2θ. By superimposing these obtained patterns with the experimental XRD results, two major second phases, which were also indicated by the map analysis as explained in section 4.2.1 were identified. As can be seen in Figures 4.31 and 4.32, two major peaks are Aluminum and the third one, which is located at approximately 78° for 2θ, is Al_7Cu_2Fe. The intensity of this peak has been increased after cryogenic treatment. There are two more peaks which correspond to $MgZn_2$ and one of them shows a slight decrease after cryogenic treatment. There are several other well-known phases in this alloy which have been identified by other scientists before but it is difficult to recognize all of them using the XRD technique; however some of them, such as the two mentioned above, are clearly confirmed by map analysis and SEM. In this work it can be seen that cryogenic processing affects the second phase distribution in the 7075 alloy.

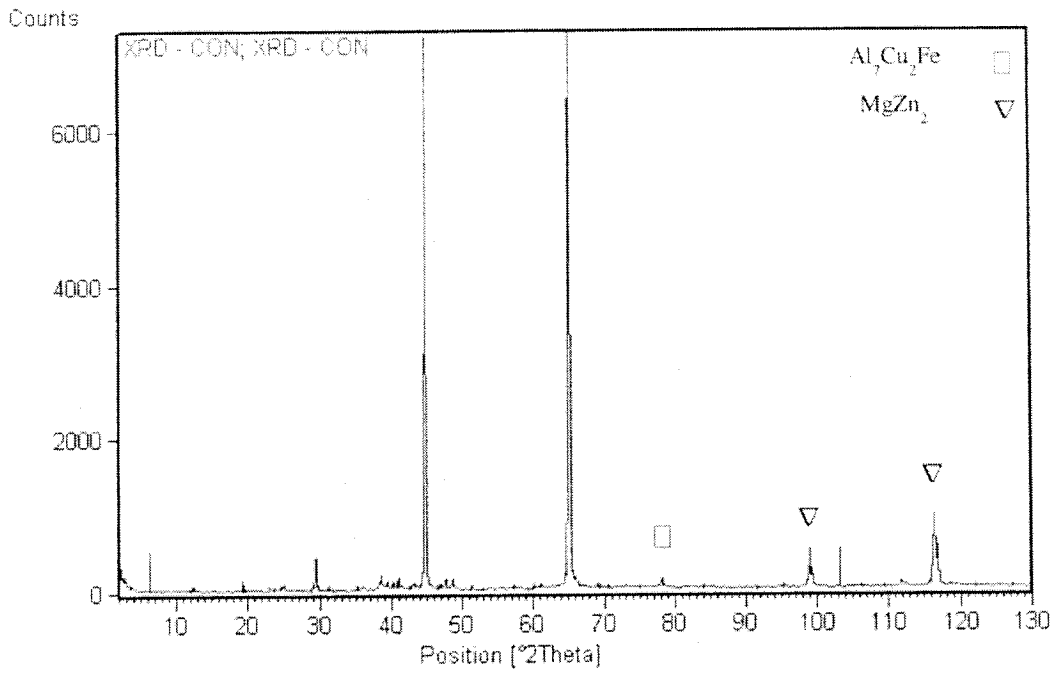

Figure 4.31 XRD experimental result of Aluminum alloy 7075-T6

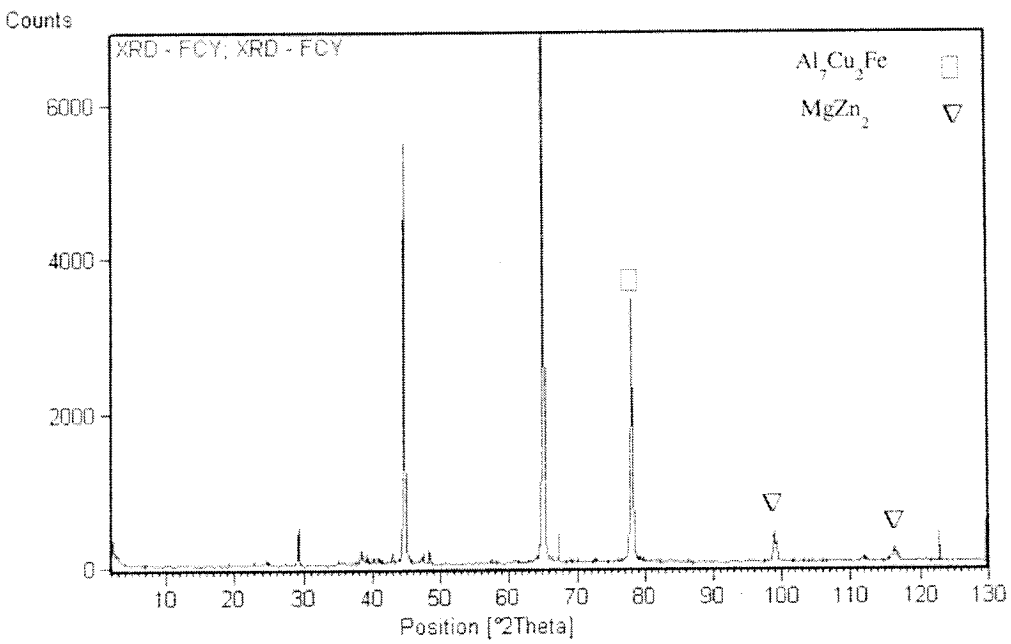

Fig. 4.32 XRD experimental result of Aluminum alloy 7075-cryo

4.2.3. Hardness

Table 4.6 shows the results of hardness measurements with and without cryogenic treatment. As can be seen, there is very little difference due to the cryogenic treatment.

Table 4.6 Hardness of Al 7075 with and without cryo treatment

Treatment	Hardness (HRB)
T6	80.2
Cryogenic	81.1

There have been some contradictions with regard to mechanical properties of cryogenically treated aluminum alloy reported by researchers. As the volume fraction of second phase was found to increase through this treatment, one would also expect an increase in hardness.

4.2.4. Impact Energy and fractography

Similar to the hardness levels of the specimens with and without cryogenic treatment, only a small change in impact toughness of the specimens was observed, as exhibited in Table 4.7.

Table 4.7 Toughness of Al before and after cryo

Treatment	Impact Energy (J)*
T6	5.3
Cryogenic	5.7

* Average of 5 tests.

Fractography of the specimens was carried out in order to study the fracture features and possible fracture mechanisms. Figures 4.33 and 4.34 show fracture surfaces of cryotreated and T6 treated specimens, respectively.

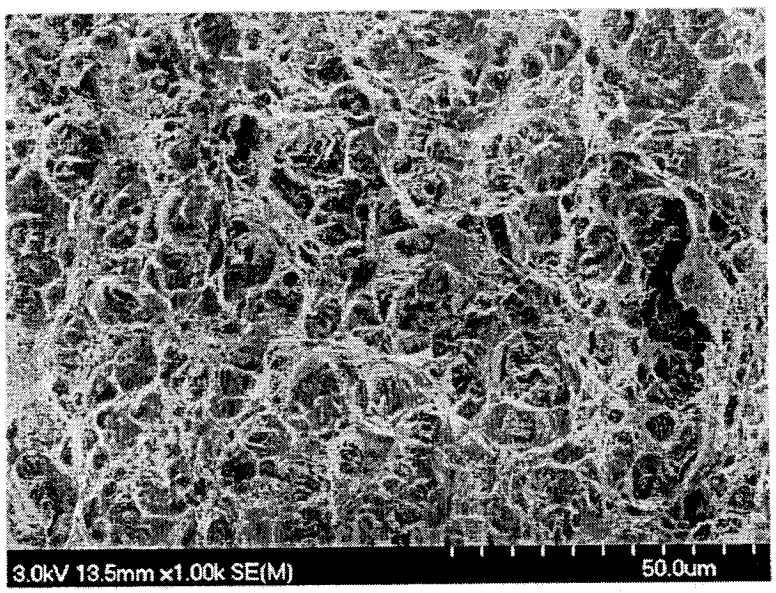

Figure 4.33 Fracture surface of charpy test of Al 7075-cryo

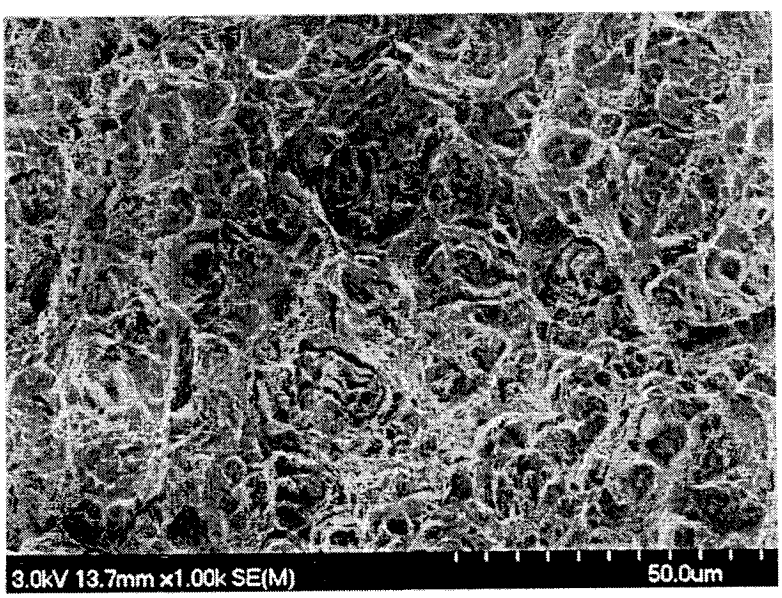

Fig. 4.34 Fracture surface of charpy test of Al 7075-T6

The fracture surface of the specimen subjected to cryogenic treatment, Figure 4.33, has smaller and more equiaxed dimples than that of the specimen without cryogenic process, Figure 4.34. It should be mentioned that this relation could be seen not only for these two areas but on the whole fracture features of the said specimens. In the microstructure section (4.2.1) it was discussed that the volume fraction of the second phase was increased after cryogenic treatment. Comparing these two Figures, it is in good agreement with the above-mentioned results; the smaller dimples being created from the higher number of second phase particles. Regarding the effect of the second phase on fracture behavior, it is well known that fracture can start with formation of microvoids at the interface with the second phase particles. Fracture then continues with connection of these voids through microvoid coalescence, until the final separation of the specimen takes place. In this condition, the higher the number of particles, the more voids are formed and the easier the microvoid coalescence takes place. This may have contributed to the slight increase of toughness of the specimens after cryogenic treatment, Table 4.7.

4.2.5. Fatigue and fractography

The S-N curve, Figure 4.35, shows the results of the fatigue tests for Al specimens under the two conditions (Seqs. 1 and 2). This graph shows that the specimens subjected to the cryogenic treatment posses slightly lower fatigue resistance compared to the conventional T6 treated samples.

It has been reported that most nonferrous alloys (e.g., aluminum, copper, magnesium) do not have a fatigue limit [72].

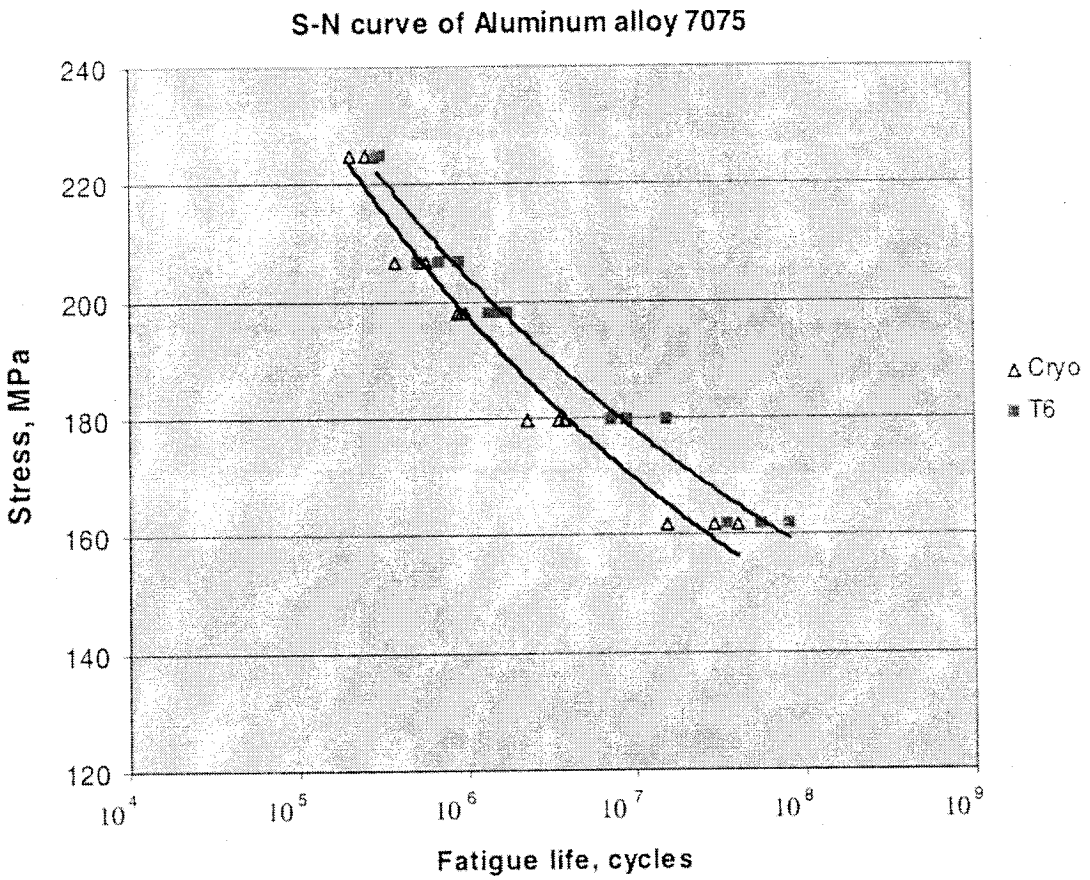

Figure 4.35 S-N curves with and without Cryogenic treatment of Al alloy 7075

The S-N curve for Al alloy 7075 was established in almost the same way as for the steel as explained before, except that the maximum applied load was 225 MPa. As mentioned in section 4.2.1.1 the cryogenic treatment increases the volume of second phases in Al alloy 7075. These second phase particles may play a role in both the initiation of fatigue cracks and the propagation of them. Hence increasing their volume fraction may negatively affect the fatigue properties of the alloy.

For more detailed investigation, the fracture surfaces of the specimens were examined by SEM. According to the fracture patterns of specimens subjected to fatigue stresses, the fracture features are composed of two main sections, the striations and fast-fracture zones. It has been shown so far that under fatigue condition, cracks often nucleate from the surface of the specimen; during the tension portion of the stress cycle the crack is pulled open and propagates forward, and on the compression portion the crack closes and is arrested. As the crack grows in size, it reaches the critical length where it becomes unstable and fast fracture takes place. Figure 4.36 indicates the striations in one of the specimens. These striations are typical of those formed in the fatigue crack propagation stage of aluminum alloys. Each step is attributed to one stress cycle in which the crack is opened and closed.

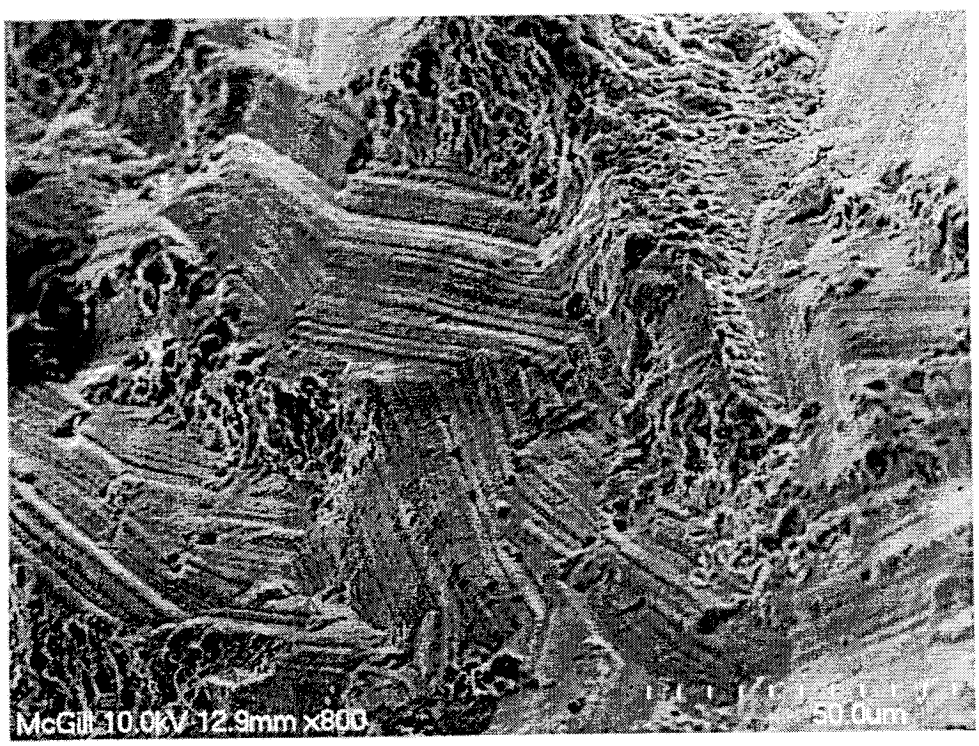

Fig. 4.36 Fatigue fracture in specimen of Al alloy 7075-cryo. The surface exhibits a pattern of fatigue striations which are visible as parallel lines.

The Final fracture portion, on the other hand, consists of the features that can show the fast fracture behavior of the specimen. This portion has been compared for two specimens, Sequences 1 and 2, in Figures 4.37 and 4.38, respectively and looks similar for both specimens. It has been proved that second phases containing iron or silicon particles limit the fatigue life of Al alloy [78].

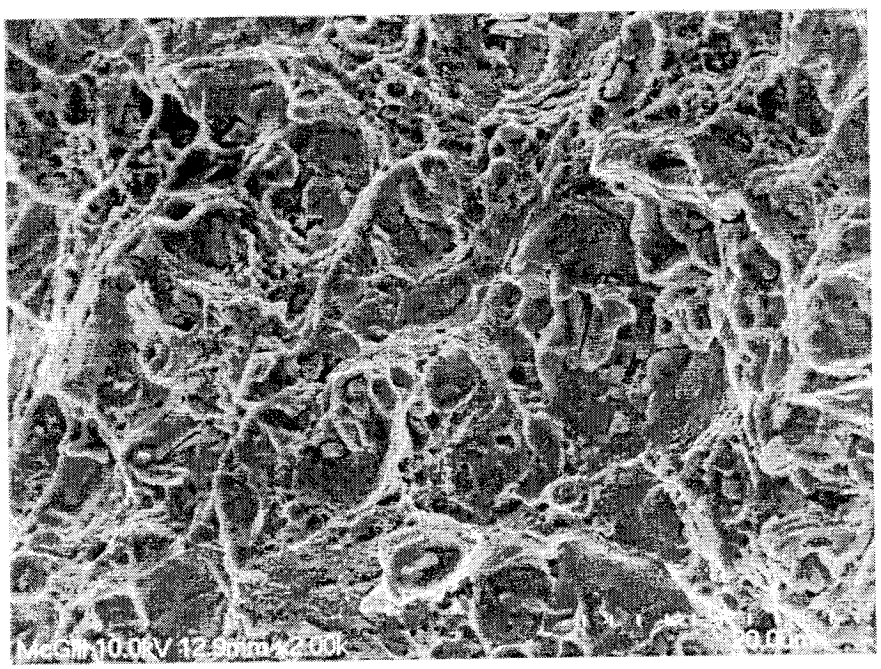

Fig. 4.37 A region of the fast fraction in fatigue test of 7075-T6

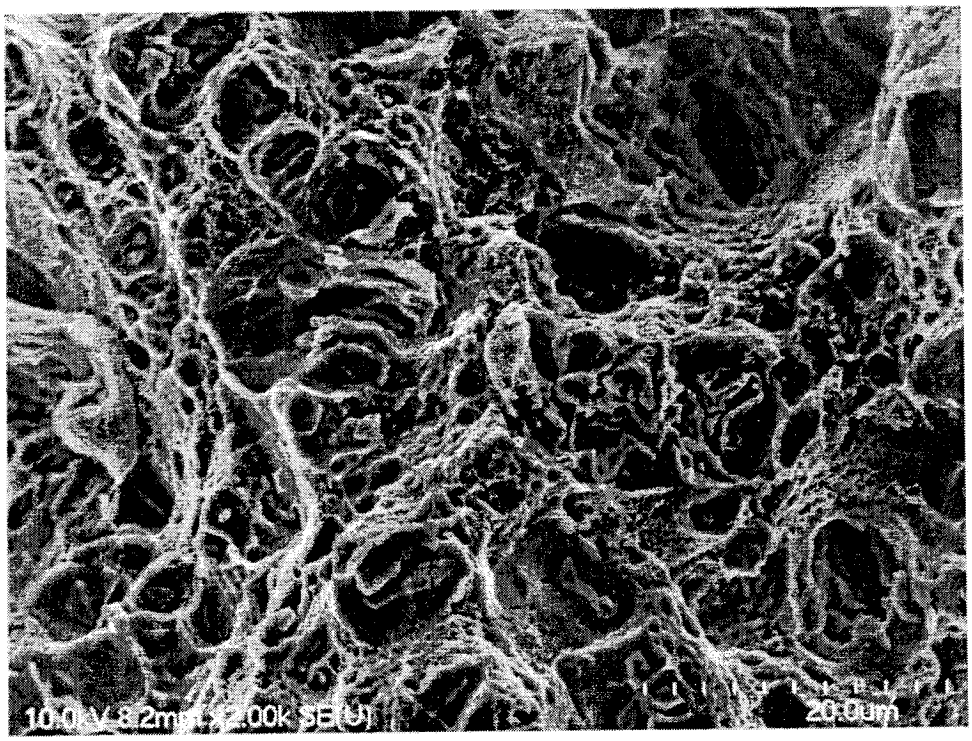

Figure 4.38 A region of the fast fraction in fatigue test of 7075-cryo

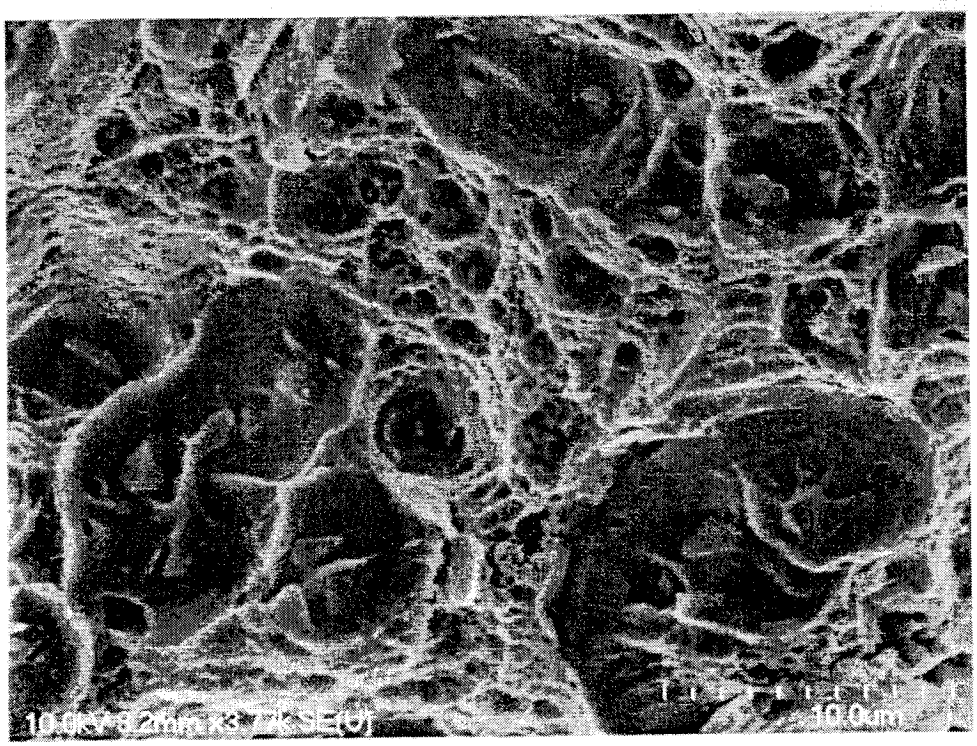

Figure 4.39 Enlarged view of above figure; many pores are visible that contained second phase particles and show dimple coalescence

These second phases can act as nucleation sites as well as crack propagation paths during failure of the specimen. This is obviously the case during the final fast fracture of the samples as shown in Figure 4.39. What could not be established conclusively however, is whether the second phase particles affected the fatigue crack propagation rate.

Chapter 5

CONCLUSIONS

The purpose of this project was proper engineering evaluation of the effect of cryogenic treatment on some properties of two high-demand alloys, AISI 4340 and 7075 Aluminum. This effect was analyzed due to conflicting reports in the open literature about the effects of cryo treatment on a range of engineering alloys. Here, it is worth to note that in this work two quite different alloys with different properties were examined in various sequences of heat treatment. As was expected, the responses of the said materials to the cryogenic treatment were different corresponding to the inherent properties of each alloy. Therefore in this section, the findings for the steel alloy are given first, followed by those for the Aluminum alloy.

- In the 4340 alloy, the main microstructural effect of the cryogenic treatment was a very small reduction in the quantity of "retained austenite". The neutron diffraction technique, a method that is accurate enough to detect small amounts of the phases (austenite and martensite), showed this increased transformation of austenite to martensite by applying the cryogenic treatment.
- This cryogenic treatment increased the hardness by a small amount (2.4 %) compared to conventional hardening in all the thermal sequences. This improvement is attributed to the smaller amount of retained austenite after cryo-treatment. Tempering the specimens at different temperatures showed

the traditional effect of tempering: the higher the temperature, the lower the hardness. In addition, at all tempering temperatures cryo-treated specimens possessed higher hardnesses.

- Employing the cryogenic treatment showed slightly detrimental effects (14.3 % decrease) on the impact energy toughness prior to tempering. This effect was carried over to all the studied tempering temperatures. This was attributed to increase in martensite volume fraction due to the cryogenic treatment. The fracture features of steel subjected to the cryogenic treatment showed less shear lips compared to the conventionally treated ones, indicating less absorbed energy.
- The fatigue limit of 4340 steel was improved after cryo-treatment and tempering. This was attributed to the higher hardness and strength of the material due to this treatment. Furthermore, the number of cycles at which the steel fractured for a given load was increased due to cryogenic treatment. This also could be related to the increase in the amount of martensite.

The following conclusions are made for cryogenic treating of Aluminum.

- In the 7075 Aluminum alloy, the increase of volume fraction of second phases was the main microstructural effect of the cryogenic treatment. This was evidenced by the results of optical microscopy, XRD, and EDS microanalysis.

- As the volume fraction of second phase was increased after cryogenic processing, the hardness of cryogenically treated aluminum alloy 7075 showed a slight increase over the one subjected to the conventional T6 treatment. There was no noticeable influence on the toughness of this alloy after cryogenic processing.
- By increasing the amount of second phase after cryo processing, the resistance of the Al alloy 7075 to fatigue is decreased, most likely by promoting the nucleation of microcracks.

The effect of cryogenic treatment on these alloys could be further studied for example; transmission electron microscopy (TEM) to analyze the possible particles formed due to sub-zero treatment, fatigue crack initiation in the case of 4340 steel and the effect of longer cryogenic treatment times on the mechanical properties. This study has shown categorically, that cryogenic treatment of 4340-type steels and 7075 aluminum alloys do not significantly enhance the hardness and toughness. This study has shown that the application of cryogenic treatment to these alloys provides some benefit in the case of 4340 steel by increasing the fatigue resistance, but a similar benefit was not observed in aluminum alloy 7075.

REFERENCES

[1] ASM, Metals Handbook, Vol.1, Tenth Edition, Medium Carbon and Low Alloy Steels, pp.432, 1990.

[2] Kent R. Van Horn, Aluminum, Vol. I. Properties, Physical Matallurgy and Phase Diagrams, 1967.

[3] Dreger, Donald R., "The promise of Cryogenic Processing," Machining Design, pp.73-78, January, 22, 1981.

[4] Pillai R. M., Pai B.C. and Satyanarayana K. G., "Deep Cryogenic of Metals," Tool Alloy Steel, pp.205-208, June, 1986.

[5] Sweeney, Jr., T.P., "Deep Cryogenics: the Great Cold Debate," Heat Treating, pp.28-32, February 1986.

[6] Alexandru I., Picos C. and Ailincai G.,"Contribution on the study of the increase of durability of the high-alloyed tool steels by thermal treatments at cryogenic temperature," Proc.2nd International Congress on Heat Treatments Of Metals, pp.573-579, Milan, Italy, 1982.

[7] Albert, M., "Cutting Tools in the Deep Freeze," Modem Machine Shop, pp.54-61, January 1992.

[8] Paulin, P., " Cold Cuts," Cutting Tool Engineering, pp.61-66, August 1992.

[9] Popandopulo A. N. and Zhukova L. T., "Transformation in High Speed Steels during Cold Treatment," Metal Science and Heat Treatment, Vol. 22, No. 10, pp.708-710, 1980.

[10] Zhmud E. S., " Improved Tool Life after Shock Cooling," Metal Science and Heat Treatment, Vol. 22, No. 10, pp.701-703, 1980.

[11] ASM, Metals Handbook, Vol. 4, Tenth Edition, Quenching of Steel, pp 67, 1991.

[12] D.A. Porter and K.E. Easterling, Phase Transformations in Metals and Alloys, Second Edition, Chapman & Hall, London, 1992.

[13] G. Dieter, Mechanical Metallurgy, Third Edition, Mc Graw-Hill, University of Maryland, 1986.

[14] Thelning, K., "Steel and its Heat Treatment", Second Edition, pp. 240-252, 1984.

[15] R.W. Cahn and P. Haasen, Physical Metallurgy, Vol. II, Fourth Edition, Elsevier Science B. V., Amsterdam, 1996.

[16] A. K. Sinha, Ferrous Physical Metallurgy, Butterworth Publishers, Stoneham, MA, 1989.

[17] R. W. K. Honeycombe, Steels: Microstructure and Properties, Edward Arnold, London,1990.

[18] ASM, Metals Handbook, Vol. 4, Tenth Edition, "Heat Treating of Steels" pp.83-84, 1991.

[19] W. D. Callister, Jr, Materials Science and Engineering, Sixth Edition, John Wiley & Sons, Inc. 2003.

[20] ASM, Metals Handbook, Vol. 4, Tenth Edition, Tempering of Steel, pp.121-124, 1991.

[21] R.E. Reed Hill, Physical Metallurgy Principles, Princeton, New Jersey, USA, 1973.

[22] S.H. Avner, Introduction to Physical Metallurgy, Second Edition, Mc Graw-Hill, New York, 1974.

[23] ASM ,Metals Handbook, Vol. 4, Tenth Edition, Heat treatment of Nonferrous Alloys, pp832-836, 1991.

[24] Handbook of Aluminum, Aluminum Company of Canada, LTD., 1957.

[25] ASM, Metals Handbook, Vol. 4, Tenth Edition, Heat Treating of Aluminum Alloy, pp. 841-864, 1991.

[26] Timmerhaus, K.D. and Flynn, T. M., Cryogenic Process Engineering, Plenum, 1989.

[27] ASM, Metals Handbook, Vol.4, Tenth Edition, Heat Treating of Steel, pp.203-206, 1991.

[28] Schiradelly R. and Diekman F.J., Cryogenics, Heat Treating Process, pp43-49, Nov, 2001.

[29] Kamody D. J. "Using Deep Cryogenics to Advantage", Advanced Materials and Processes , Vol. 154, pp215-218, Oct, 1998.

[30] Kamody D. J. "Cryogenics Process Update", Advanced Materials and Processes , H67-69, June, 1999.

[31] Collins. D.N. Deep Cryogenic Treatment of Tool Steels; a Review. Heat Treatment of Metals, Vol. 23, pp40-42, 1990.

[32] Meng F., Tagashira K. and Sohma H. "Wear Resistance and Microstructure of Cryogenic Treated Fe-1.4Cr-1C Bearing Steel", Scripta Metallurgicaet Materialia, Vol. 3L, pp865-868, 1994.

[33] Meng F., Tagashira, K. Azume R. and Sohma H. "Role of Eta-carbide Precipitation in the Wear Resistance Improvements of Fe-12Cr-Mo-V-1.4C Tool Steel" by Cryogenic Treatment, ISIJ International, Vol. 34, 205-210, 1994.

[34] Yun D., XiaopIng L and Hongshen X. "Deep Cryogenic Treatment of High-Speed Steel and its Mechanism", Heat Treatment of Metals, Vol. 25, pp55-59, 1998.

[35] Mohan Lal D., Renganarayanan S. "Cryogenic Treatment to Augment Wear Resistance of Tool and Die Steels", Cryogenics, 41, pp149-155, May 2001.

[36] Chen Ding, Li W , "Cryogenic of Al and Al alloys," Chinese Journal of Nonferrous, Vol. 10 No.6, pp891-895, 2000.

[37] Chen G., Chen Ding, "Effect of Cryogenic on Al-Fe-V-Si Alloy," Jinshu Rechuli (Chinese) Vol. 27(10), pp26-27, 2002.

[38] Chen Ding, Li W., "Grain Preferred Orientation of Al and Al Alloys through Cryogenic Treatment," Dept. Material Science Engineering, Central South Univ. Changsha, (Chinese) 410083, China, Vol. 31(6), pp544-547, 2000.

[39] Wang Q., Ke Y.,"Relief of Residual Stresses in 7050 Aluminum Alloy by Deep Cryogenic Treatment," Zhejiang Univ., Hangzhou, 310027, China, Vol. 37(6), pp748-751, 2003.

[40] Lulay K. E., Khan K., Chaaya D., "The effect of Cryogenic Treatments on 7075 Aluminum Alloy," Materials Engineering and Performance, Short Communications, Vol. 11(5) -479, October 2002.

[41] Chen P., Malone T., Bond R., Torres P., "Effects of Cryogenic Treatment on the Residual Stress and Mechanical Properties of an Aerospace Aluminum alloy," George C. Marshall Space Flight Center, NASA, A 2000.

[42] E. A. Smol'nikov and Kossovich G. A. " Cold Treatment of Cutting Tools," Metal Science and Heat Treatment, Vol.22, No. 10, pp.704-705, 1980.

[43] Mahmudi R., Faraji H.R. "Effect of Cryogenic Treatments on the Mechanical Properties and Wear Behavior of High-Speed Steel M2", Heat Treatment of Metals, Vol.27, pp69-72, 2000.

[44] Collins D.N. and Dormer J. "Deep Cryogenic Treatment of a D2 Cold-Work Tool Steel," Heat Treatment of Metals, Vol. 24, pp71-74, 1997.

[45] Barron R.F. and Mulhern C.R.,"Cryogenic Treatment of AISI-T8 and C1045 Steels," Advanced in Cryogenic Engineering Materials, Vol.26, Plenum Press, pp.171-179, 1980.

[46] Marchenko V. G. and Tsuprun A. Yu., " Effect of Liquid-Nitrigen Treatment On the Properties Of Steel 9KhS Tool," Metal Science and Heat Treatment, Vol. 31, No. 3, pp162-164, 1989.

[47] Zablotskii, V. K., Kiets Y. N., Sharban N. D. and Guarev V. V., "Structure and Properties of High Speed Steels after Cold Treatment," Metal Science and Heat Treatment, Vol.22, No.10, pp711-714, 1980.

[48] Kelkar R., Nash P.,"The Mechanism of Property Enhancement in M2 Tool Steel by Cryogenic Treatment," Thermal Processing Technology Centre, IIT Chicago, IL. MS&T, 45th MWSP Conference Proceeding, Vol. XLI.pp.13-19, 2003.

[49] Hayakawa M., Tanigami M. and Oka M., "Low Temperature Aging of the Freshly Formed martensite in an Fe-Ni-C Alloy,:Metallurgical Transactions, Section A, Vol.16A, No.10, pp.1745-1750, 1985.

[50] DeGaspari J., "The Big Chill" , Mechanical Engineering, The American Society of Mechanical Engineers, 2000.

[51] Huang J.Y., Zhu Y.T., Liao X.Z., Beyerlein I.J., Bourke M.A., Mitchell T.E., "Microstructure of Cryogenic Treated M2 Tool Steel" Material Science and Engineering, A339, pp241-244, 2003.

[52] Moore K., Collins D.N., "Cryogenics Treatment of Three Heat-Treated Tool Steels" Key Engineering Materials, Dublin, Ireland, Vol. 86-87, pp.47-54, 1993.

[53] Molinari A., Pellizzari M., Gialanella S., Straffelini G., Stiansy K.H., "Effect of Cryogenic Treatment on the Mechanical Properties of Tool Steels," Journal of Materials processing technology, 118, pp350-355, 2001.

[54] Barron R.F.,"Cryogenic Treatment of Metals to Improve Wear Resistance," Cryogenics, pp409-414, August 1982.

[55] Barron R.F. and Thompson R.H., "Effect Of Cryogenic Treatment On Corrosion Resistance" Advanced in Cryogenic Engineering, Vol.36Plenum Press, New York, pp.1375-1379, 1990.

[56] ASM, Metals Handbook, ASM Vol. 10, Eight Edition, Park, Ohio, 1985.

[57] Cullity B.D., "Elements of X-ray Diffraction," Addison-Wesley Publishing Co. Inc., pp173-194, 1978.

[58] G.E. Bacon, Neutron Diffraction, Third Edition, Oxford University Press, Great Britain, 1975.

[59] Jatczak, Chester F., Larson, John A., and Shin, Steve W., "Retained Austenite and Its Measurements by X-Ray Diffraction," SP-453, Society of Automotive Engineers, Inc., 1980.

[60] ASTM E 975-89, "X-ray Determination of Retained Austenite in Steel Near Random Crystallographic Orientation"

[61] Levine J., "Cryoprocessing Equipment", Heat Treating Progress, Applied Cryogenic Inc. Waltham, Massachusetts, pp.42-44, Dec 2002.

[62] Raj K. and Moskowitz R.," Commercial Applications of Ferrofluids", Journal of Magnetism and Magnetic Materials 85, pp.233-242, 1990.

[63] Gray R., "Magnetic Etching", Applied Metallography, ed. G. Vander Voort, New York, Van Nostrand Reinhold Co., pp.53-60, 1986.

[64] Marcelino P. et al, "Effect of a Shot Peening Treatment on the Fatigue Behaviour of Hard Chromium on Electroless Nickel Interlayer Coated AISI 4340 Aeronautical Steel" Material Research, Vol.5 no.2, June, 2002.

[65] ASTM E23 "Standard Test Methods for Notched Bar Impact Testing of Metallic Materials"

[66] ASTM E 1049, ASTM E 912-83a and ASTM E 466-82, "Standard Practice for Fatigue Tests of Metallic Materials" and "Fatigue Loading"

[67] Marder A.R. Benscoter A.O. "Microcracking in Fe-C Acicular Martensite" Transactions of the ASM, Vol. 61, pp.293-299, 1968.

[68] R. E. Little, E. H. Jebe, Statistical Design of Fatigue Experiments, The University of Michigan, Chapter 13, pp236-243, 1975.

[69] Instruction Manual Model RBF-200 Rotating Beam Fatigue Testing Machine With Supplementary Manuals For Accessory Attachments, Instruments Budd Division, Phoenixville, PA.

[70] ASM, Metals Handbook, Vol. 9, Ninth Edition, "Metalography and Microstructures", American Scociety for Metals Park, Ohio, 1985.

[71] Privet Comunication "Dr. Ron Donaberger" Chalkriver, Ontario

[72] ASM, Metals Handbook, ASM Vol. 19, 10th Edition, Fatigue and fracture, 1996.

[73] ASM, Metals Handbook, Vol.1, 10th Edition, pp678, 1990.

[74] ASTM E 1077-91,"Standard Test Methods for Estimating the Depth of Decarburization of Steel Specimens"

[75] Metals Handbook, ASM Vol. 2, 10th Edition, pp37, 1990.

[76] Metals Handbook, ASM, 8th Edition, Vol. 8, pp128, 1973.

[77] Gao, Ming; Feng, C.R.; Wei, Robert P. "An Analytical Electron Microscopy Study of Constituent Particles in Commercial 7075-T6",Metallurgical and Materials Transaction, 1145-1151, 1998.

[78] G. E. Totten, D.S. Mackenzie, HandBook of Aluminum, Vol.2, pp155, 2003.

[79] L. F. Mondolfo, Aluminum Alloys: Structure and Properties, Butterworths, 1976.

[80] Metals Handbook, ASM, 8th Edition, Vol. 7, pp251, 1972.

[81] P.Villars, L.D.Calkvert "Pearson's Handbook of Crystallography Data for Intermetallic Phases", Second Edition, Material Park Ohio, ASM International, 1991.

[82] PowderCell software program, W. Kraus, and G. Nolze, BAM Berlin